การผลิตไฟฟ้าแบบกระจายตัวสูงสุดที่รับได้โดยพิจารณาถึงข้อกำหนดการทำงานผ่านช่วง
การลัดวงจรและระบบป้องกันของการไฟฟ้า

นายดาว วาน ตู

วิทยานิพนธ์นี้เป็นส่วนหนึ่งของการศึกษาตามหลักสูตรปริญญาวิศวกรรมศาสตรดุษฎีบัณฑิต
สาขาวิชาวิศวกรรมไฟฟ้า   ภาควิชาวิศวกรรมไฟฟ้า
คณะวิศวกรรมศาสตร์ จุฬาลงกรณ์มหาวิทยาลัย
ปีการศึกษา 2555
ลิขสิทธิ์ของจุฬาลงกรณ์มหาวิทยาลัย

MAXIMUM ALLOWABLE DISTRIBUTED GENERATION WITH CONSIDERATION OF FAULT RIDE THROUGH REQUIREMENT AND UTILITY PROTECTION SYSTEM

Mister Dao Van Tu

A Dissertation Submitted in Partial Fulfillment of the Requirements

for the Degree of Doctor of Philosophy Program in Electrical Engineering

Department of Electrical Engineering

Faculty of Engineering

Chulalongkorn University

Academic Year 2012

งานทะเบียนและประมวลผล ฝ่ายวิชาการ คณะวิศวกรรมศาสตร์
แบบขอแก้ไขชื่อหัวข้อวิทยานิพนธ์ (กรณีที่นิสิตสอบวิทยานิพนธ์แล้ว)

เรื่อง   ขอแก้ไขชื่อหัวข้อวิทยานิพนธ์ ภาคการศึกษา ....2........................ ปีการศึกษา ....2012.........................

เรียน   ท่านคณบดี คณะวิศวกรรมศาสตร์

              ด้วยภาควิชา ....ELECTRICAL ENGINEERING................................ มีความประสงค์จะขอแก้ไขชื่อหัวข้อวิทยานิพนธ์

ของ นาย,นาง,นางสาว ....DAO VAN TU. .... เลขประจำตัว ....537 181 90 21.......................

นิสิตระดับ ◯ ปริญญามหาบัณฑิต ◯ ปริญญาดุษฎีบัณฑิต เรียนในหลักสูตร ◯ ปกติ ◯ ภาคนอกเวลาราชการ

ซึ่งนิสิตได้ทำการสอบวิทยานิพนธ์เรียบร้อยแล้ว คณะกรรมการสอบวิทยานิพนธ์

ได้มีมติให้ทำการแก้ไขชื่อหัวข้อวิทยานิพนธ์เพื่อความเหมาะสมและสอดคล้องกับเนื้อหา ดังนี้

              **ชื่อหัวข้อวิทยานิพนธ์เดิม ที่ได้รับอนุมัติในการสอบวิทยานิพนธ์ เมื่อวันที่ ....25/4/2013..

ภาษาไทย   (ใช้ตัวพิมพ์ดีดเท่านั้น)   ......

              การผลิตไฟฟ้ากระจายตัวสูงสุดที่รับได้โดยพิจารณาถึงความสามารถการทำงานผ่านช่วงแรงดันต่ำขณะเกิ

ดการลัดวงจรและระบบป้องกันของการไฟฟ้า..

ภาษาอังกฤษ (ใช้ตัวพิมพ์ใหญ่เท่านั้น) ..... MAXIMUM ALLOWABLE DISTRIBUTED GENERATION WITH CONSIDERATON

OF LOW VOLTAGE FAULT RIDE THROUGH CAPABILITY AND UTILITY PROTECTION SYSTEM..................................

              ชื่อหัวข้อวิทยานิพนธ์ใหม่ ที่ได้รับการแก้ไขหลังจากสอบวิทยานิพนธ์เรียบร้อยแล้ว ผลการสอบที่ได้คือ ....

ภาษาไทย   (ใช้ตัวพิมพ์ดีดเท่านั้น)...

การผลิตไฟฟ้าแบบกระจายตัวสูงสุดที่รับได้โดยพิจารณาถึงข้อกำหนดการทำงานผ่านช่วงการลัดวงจรและระบบป้องกันของการไฟฟ้า ....

ภาษาอังกฤษ (ใช้ตัวพิมพ์ใหญ่เท่านั้น) MAXIMUM ALLOWABLE DISTRIBUTED GENERATION WITH CONSIDERATION OF FAULT

RIDE THROUGH REQUIREMENT AND UTILITY PROTECTION SYSTEM ....

              จึงเรียนมาเพื่อโปรดทราบและดำเนินการต่อไปด้วย

                                        (ลงชื่อ) ....
                                                   ประธานกรรมการสอบวิทยานิพนธ์
                                                   ..../......................./.............

ความเห็นของหัวหน้าภาควิชาฯ / ประธานกรรมการบริหารหลักสูตร	เรียน คณบดีบัณฑิตวิทยาลัย
.... (ลงนาม) .... (...) ..../................./............	เพื่อโปรดทราบ (ลงนาม) .... (ผู้ช่วยศาสตราจารย์ ดร.อรรถสิทธิ์ สุรฤกษ์) นายทะเบียนคณะฯ ปฏิบัติการแทนคณบดี ..../........................./............

(สำเนาแจ้งสำนักงานการทะเบียนและประมวลผลทราบ)

Thesis Title   MAXIMUM ALLOWABLE DISTRIBUTED GENERATION WITH CONSIDERATION OF LOW VOLTAGE FAULT RIDE THROUGH CAPABILITY AND UTILITY PROTECTION SYSTEM

By   Mr. Dao Van Tu

Field of Study   Electrical Engineering

Thesis Advisor   Surachai Chaitusaney, Ph.D.

Thesis Co-advisor   Professor Akihiko Yokoyama, Ph.D.

Accepted by the Faculty of Engineering, Chulalongkorn University in Partial Fulfillment of the Requirements for the Doctoral Degree

…………………………………….. Dean of the Faculty of Engineering

(Associate Professor Dr. Boonsom Lerdhirunwong)

THESIS COMMITTEE

…………………………………….. Chairman

(Professor Bundhit Eua-arporn, Ph.D.)

………………………………….……. Thesis Advisor

(Surachai Chaitusaney, Ph.D.)

………………………………………….. Thesis Co-advisor

(Professor Akihiko Yokoyama, Ph.D.)

…………………………………….. Examiner

(Assistant Professor Somboon Sangwongwanich, Ph.D.)

…………………………………….. Examiner

(Assistant Professor Naebboon Hoonchareon, Ph.D.)

…………………………………….. External Examiner

(Pradit Fuangfoo, Ph.D.)

iv

ดาว วาน ตู :
การผลิตไฟฟ้าแบบกระจายตัวสูงสุดที่รับได้โดยพิจารณาถึงข้อกำหนดการทำงานผ่านช่วงการลัดวงจรและระบบป้องกันของการไฟฟ้า (MAXIMUM ALLOWABLE DISTRIBUTED GENERATION WITH CONSIDERATON OF FAULT RIDE THROUGH REQUIREMENT AND UTILITY PROTECTION SYSTEM)

อ. ที่ปรึกษาวิทยานิพนธ์หลัก: อ.ดร. สุรชัย ชัยทัศนีย์, 138 หน้า

อ. ที่ปรึกษาวิทยานิพนธ์ร่วม: ศ. ดร. อะคิฮิโกะ โยโกยาม่า

ในปัจจุบันระบบจำหน่ายไฟฟ้าได้เปลี่ยนโครงสร้างจากเดิมที่มีแหล่งจ่ายไฟฟ้าเพียง หนึ่งแหล่งจ่ายไฟให้กับผู้ใช้ไฟฟ้าเป็นการจ่ายไฟร่วมกับเครื่องกำเนิดไฟฟ้าแบบกระจายตัวโดยเฉพาะอย่างยิ่งเครื่องกำเนิดไฟฟ้าแบบกระจายตัวจากแหล่งพลังงานหมุนเวียน ซึ่งจำนวนการใช้งานของเครื่องกำเนิดไฟฟ้าพลังงานหมุนเวียนที่มากขึ้น นี้ ทำให้การใช้งานเครื่องกำเนิดไฟฟ้าพลังงานหมุนเวียนมีบทบาทอย่างมากในระบบไฟฟ้า กำลัง โดยตัวอย่างการใช้งานได้แก่เครื่องกำเนิดไฟฟ้าประเภท เหนี่ยวนำ ร่วมกับอินเวอเตอร์ ซึ่งเรียกรวมเป็นเครื่องกำเนิดไฟฟ้าแบบอินเวอร์เต อร์ นอกจากนี้เครื่องกำเนิดไฟฟ้าประเภทความร้อนร่วมโดยใช้เครื่องกำเนิดไฟฟ้าประเภทซิงโครนัสก็มีการใช้งานอย่างแพร่หลาย เช่นกัน โดยในมุมมองของผู้ผลิตไฟฟ้า เห็น ควร ให้ ใช้พลังงานหมุนเวียนในการผลิตไฟฟ้าเพื่อประโยชน์สูงสุดด้วยเหตุนี้กำลังกา รผลิตที่ติดตั้งควรเป็นค่าสูงสุดเท่าที่จะสามารถเป็นไปได้

อย่างไรก็ตามการติดตั้งเครื่องกำเนิดไฟฟ้าแบบกระจายตัว มีโอกาสทำให้เกิดการละเมิดเงื่อนไขการทำงานของระบบไฟฟ้า เช่น ค่าพิกัดของสถานีไฟฟ้าและสายไฟฟ้า พิกัดของแรงดัน และ ยังเป็นสาเหตุให้เกิดการทำงานที่ผิดพลาดของอุปกรณ์ป้องกันในระบบไฟฟ้า

วิทยานิพนธ์ฉบับนี้ ได้พิจารณาปัญหา การคำนวณต่างๆ เช่น ด้านการลดลงของขอบเขตการป้องกันระบบไฟฟ้า Reach reductionและ ด้าน การทำงานผ่านช่วงแรงดันต่ำขณะเกิดการลัดวงจร เพื่อทำให้กำลังการผลิตของเครื่องกำเนิดไฟฟ้าแบบกระจายตัวมีค่าสูงสุด โดยคุณลักษณะกระแสลัดวงจรของเครื่องกำเนิดไฟฟ้าแบบอินเวอร์เตอร์ ที่ส่งผลไปยังกระแสลัดวงจรของระบบไฟฟ้านั้น จะพิจารณาถึง การทำงานผ่านช่วงแรงดันต่ำขณะเกิดกา รลัดวงจร ที่ต้องการ จากผู้ปฏิบัติการในระบบจำหน่ายด้วย จากคุณลักษณะ ดังกล่าวมานี้เอง วิทยานิพนธ์นี้ได้นำเสนอแบบจำลองของเครื่องกำเนิดไฟฟ้าแบบอินเวอร์เตอร์เพื่อการคำนวณกระแสลัดวงจรแบบประยุกต์ซึ่งสามารถประมาณค่ากระแสลัดวงจรในระบบได้เพื่อใช้ในการกำหนดและตรวจสอบการทำงานของระบบป้องกัน โดยวิธีการในการคำนวณกระแสลัดวงจรนี้ได้ใช้ร่วมกับวิธีการในการหาค่าสูงสุดของเครื่องกำเนิดไฟฟ้าแบบกระจายตัว ในการทดสอบประสิทธิภาพขอ งวิธีการที่นำเสนอเพื่อหาค่ากำลังไฟฟ้าสูงสุดที่ติดตั้งของเครื่องกำเนิดไฟฟ้าแบบกระจายตัว วิทยานิพนธ์ฉบับนี้ได้ทดสอบกับระบบทดสอบ IEEE 34 บัส

ภาควิชา	วิศวกรรมไฟฟ้า	ลายมือชื่อนิสิต	
สาขาวิชา	วิศวกรรมไฟฟ้า	ลายมือชื่อ อ.ที่ปรึกษาวิทยานิพนธ์หลัก	
ปีการศึกษา	2555	ลายมือชื่อ อ.ที่ปรึกษาวิทยานิพนธ์ร่วม	

5371819021 : MAJOR   ELECTRICAL ENGINEERING

DAO VAN TU: MAXIMUM ALLOWABLE DISTRIBUTED GENERATION WITH CONSIDERATION OF FAULT RIDE THROUGH REQUIREMENT AND UTILITY PROTECTION SYSTEM. ADVISOR: SURACHAI CHAITUSANEY, PH.D., CO-ADVISOR: PROF. AKIHIKO YOKOYAMA, PH.D.

Distribution systems are changing from one-source supplying structure into multi-source supplying structure with participations of distributed generations. The strong increase in number of renewable-based generating plants, with the advanced control technology, impulses their role in power systems. Using a package of an asynchronous generator along with an inverter to synchronize the output with the power system is an upward tendency for generating units in these plants. Such generating unit is known as an inverter-based distributed generation. Besides, many combined heat and power plants using synchronous generators are still used in power systems and named synchronous machine-based distributed generation. From distributed generation's owner perspectives, the renewable energy should be exploited; hence, the installation capacity of the distributed generation is expected to be as large as possible. However, the installation of distributed generation may violate system operating limits such as substation and line capacities, voltage limits and causes other impacts dealing with protection system operation.

This thesis considers typical problems such as system operating limits, reach reduction of utility relay, and fault ride through requirement from distribution system operators in order to maximize distributed generation's installation. Fault responses of the inverter-based distributed generation to a fault in the network are characterized with consideration of fault ride through requirement of the distribution system operators. Based on the obtained characteristics, a new model of the inverter-based distributed generation is proposed. This model is convenient for an adaptive fault calculation algorithm which is to estimate fault currents in the system for setting and checking the operation of protection system. This fault calculation algorithm is then employed by an algorithm proposed for maximizing distributed generation. The IEEE 34 Node Test Feeder is then used to illustrate the effectiveness of the algorithm in determining the maximum distributed generation installed in this system.

Department   : Electrical Engineering   Student's Signature

Field of Study : Electrical Engineering   Advisor's Signature

Academic Year : 2012   Co-advisor's Signature

ACKNOWLEDGEMENTS

Contents

List of Tables

List of Figures

List of Abbreviations

3F	Three-phase fault
COG	Coefficient of grounding
DFIG	Doubly-fed induction generator
DG	Distributed generation
DLGF	Double line-to-ground fault
DSO	Distribution system operator
ETO	Emitter turn-off thyristor
FRT	Fault ride through
GOF	Ground overcurrent function
GTO	Gate turn-off thyristor
IBDG	Inverter-based distributed generation
IGBT	Insulated gate bipolar transistor
LLF	Line-to-line fault
LVRT	Low voltage ride through
NRF	Natural reference frame
PCC	Point of common coupling
PI	Proportional-Integral
PLL	Phase-locked loop
POF	Phase overcurrent function
PR	Proportional-resonant
PV	Photovoltaic
PWM	Pulse-width modulation
SBDG	Synchronous machine-based distributed generation
SLGF	Single line-to-ground fault
SRF	Synchronous reference frame
SVPW	Space vector pulse-width modulation
TOV	Temporary overvoltage

CHAPTER I

INTRODUCTION

This chapter starts with identifying the problem to solve in the thesis. Then, research objectives, scopes, and methodologies are announced as a thesis direction. Lastly, thesis organization is introduced with a brief overview of all chapters.

1.1 Problem Identification

The term *distributed generation* (DG) indicates all small electric power generators ranging in capacity from 15 to 10,000 kW, connected to power systems to provide electric power to electrical consumers [1]. Obviously, a DG is small in size compared to a conventional generator, whose size is about hundreds of megawatts, in power systems. Furthermore, a DG is distributed in electrical grids because the use of renewable energy resources is difficult for centrally dispatching and planning. Thus, DGs are usually connected to medium or low voltage systems which cover a huge load area and directly supply to customers.

From DG's owner perspectives, the renewable energy should be mostly exploited; hence, DG capacity is generally expected to be as large as possible. However, a new DG installation brings about difficulties to the utility under a technical view. When a DG is planned to be installed, the distribution network, to which the DG is connected, was designed already. In addition, the network is conventionally in a one-source supplying topology. As a result, a DG interconnection changes the existing network topology at which operation and protection schemes are originally compatible. This incompatibility produces technical resistances for DG implementation. In order to overcome these resistances, the first task is to evaluate the impacts of DG on the present network to which it is connected. Solutions to resolve the detrimental impacts resulted from DG connection are then required. So far, many evaluated impacts and solutions have been relevant to voltage regulation, protection operation, and system reconfiguration [2], [3]. A typical protection impact is relay reach reduction which always occurs at any DG capacity. This problem has been analyzed in [4], [5] considering the participation of synchronous machine-based distributed generation (SBDG) in distribution networks. Maximization of SBDG with consideration of system operating limits and reach reduction of relays was discussed in [6]. Nevertheless, there has been less concern about inverter-based distributed generation (IBDG). This motivates DG maximization in this paper thesis to be considered with

not only the system operating limits but also the relay reach reduction problem caused by the installation of both SBDG and IBDG.

In order to evaluate the reach reduction of utility relay, fault currents through that relay should be estimated; and hence, fault calculation is needed. Unfortunately, the conventional fault calculation technique is no longer used for this purpose due to the difference in modeling an IBDG from an SBDG. Some researches negotiate this problem by neglecting the fault current from the IBDG with an assumption that the IBDG current is very small compared with the SBDG current and the IBDG is isolated very fast after the fault occurrence [2], [3]. In fact, the response of an IBDG to a fault occurring in the utility system, which contributes in the total fault current, is influenced by the inverter control system. In addition, this control system is designed to comply with the requirement of Distribution System Operators (DSOs). Recent grid codes require DGs to remain connected to the network and to support the voltage during fault, usually named Fault Ride Through (FRT) requirement. It is therefore reasonable to discuss FRT for analyzing impacts of DG on relay reach. A new technique for calculating fault current in a distribution system with both SBDG and IBDG is an auxiliary solution moving forward to resolving advanced problems of DG's installation.

From the above discussion, this thesis considers typical problems including system operating limits, reach reduction of utility relay, and FRT requirement in order to maximize DG's installation in a distribution network.

1.2 Scopes

Scopes of this thesis are:

- − Characterization of the behavior of distribution networks with IBDG's participation in a fault event.
- − Fault calculation in distribution networks with IBDG
- − The paper only considers the protection of the main feeder of the distribution network
- − Maximization of DG installation under the condition of predefined DG location.

1.3 Objectives

There are three objectives expected to be achieved as follows.

- − To propose an adaptive fault calculation algorithm for a distribution network with SBDG and IBDG.

  − To analyze impacts of SBDG and IBDG on utility relay reach.
  − To propose an algorithm for maximization of DG installation in distribution network.

1.4 Methodology

Research in this thesis employs simulation and comparison techniques as follows.

1.4.1 Simulation Technique

This thesis contains three simulations performed in Matlab environment [7] with integration of MATPOWER program [8].

The first simulation is to simulate the operation of a grid-connected IBDG under system fault condition. A typical control system is selected for the IBDG in this simulation. The Simulink Tool in Matlab/Simulink is then employed to capture the time-variant fault responses of the IBDG. The responses are then characterized so as to model the IBDG for fault calculation.

The second simulation is to illustrate the operation of an adaptive fault calculation algorithm. This algorithm is based on a power flow technique which determines line power flows, bus voltages and line currents in a sequence network connection. Results obtained from this algorithm are utilized to check the operation of relays and bus voltage limits during faults.

The last simulation is to illustrate the operation of DG maximization algorithm. This simulation is performed on the IEEE 34 Node Test Feeder with DGs. Results from the second simulation are utilized by this algorithm.

1.4.2 Comparison Technique

Comparison technique is used to validate the proposed algorithms. For validating the adaptive fault calculation algorithm, two comparisons are performed: the first one is between results from the proposed calculation algorithm and the conventional fault calculation in a reference textbook; the second one is between results from a Simulink simulation and the proposed fault calculation algorithm. In order to validate the DG maximization algorithm, its result is compared with the result from a sensitivity-based algorithm that is robust and reliable.

1.5 Thesis Structure

The rest of the thesis is organized into the following chapters.

Chapter 2 starts with a literature review on using renewable energy resources in power systems and classification of DGs with a focus on the IBDG. Then, a literature of DG impacts on the operation of the protection system is reviewed with a focus on the reach reduction problem. Some grid codes for interconnecting DG to power systems are then briefly presented. At the end of this chapter, previous researches on DG maximization are summarized to clarify the novelty of the solution in this thesis.

Chapter 3 shows more details in the control system of the IBDG including the insight of its transformation, computation and control blocks. Fault response of the IBDG is analyzed and characterized so as to build an IBDG model compatible with fault calculation for setting protective devices. The IBDG model is then employed by an adaptive algorithm to calculate the fault currents in a system with IBDGs.

Chapter 4 proposes algorithms to maximize DG with consideration of FRT requirement and utility relay reach reduction. Sensitivity-based and Tabu search methods are the fundamental of these algorithms.

Chapter 5 validates the proposed fault calculation algorithm in Chapter 3 by comparing fault currents from the conventional fault calculation with respective currents from the proposed algorithm in a system without IBDGs. The time-variant currents obtained from a Matlab/Simulink simulation are then used to validate the proposed algorithm in a system with IBDGs.

Chapter 6 presents applications of the DG maximization algorithms in Chapter 4.Three case studies are performed to illustrate the effectiveness of each algorithm. Then, a comparison between these two algorithms is the basis to determine which one is better to suggest utility and DG developers.

Chapter 7 concludes the thesis, states the thesis's contributions, and outlines recommendations.

CHAPTER II

INTEGRATION OF RENEWABLE ENERGY RESOURCES INTO POWER SYSTEMS

This chapter is a summary on using renewable energy resources in power systems, classification of DGs with the focus on the IBDG, and impacts of DG on the operation of the protection system. A brief review of connection requirements from some recent grid codes for interconnecting DG to power systems is also presented. The end of this chapter is a literature review of DG maximization in distribution systems.

2.1 Usage of Renewable Energy in Power Systems

Renewable energy comes from the sun, wind, hydro, tide, etc. Even that there are some problems in using these energies such as high cost and intermittent output, they are attractive and tend to be expanded in the scale of use. This is because the increase in electrical demand and the accelerated scramble for energy resources have caused the hike in fossil prices. Some facts and figures are summarized in this section.

2.1.1 Solar Energy

Most common modern type of solar conversion is implemented in solar farms which have millions of connected solar cells. The grid-connected centralized applica-
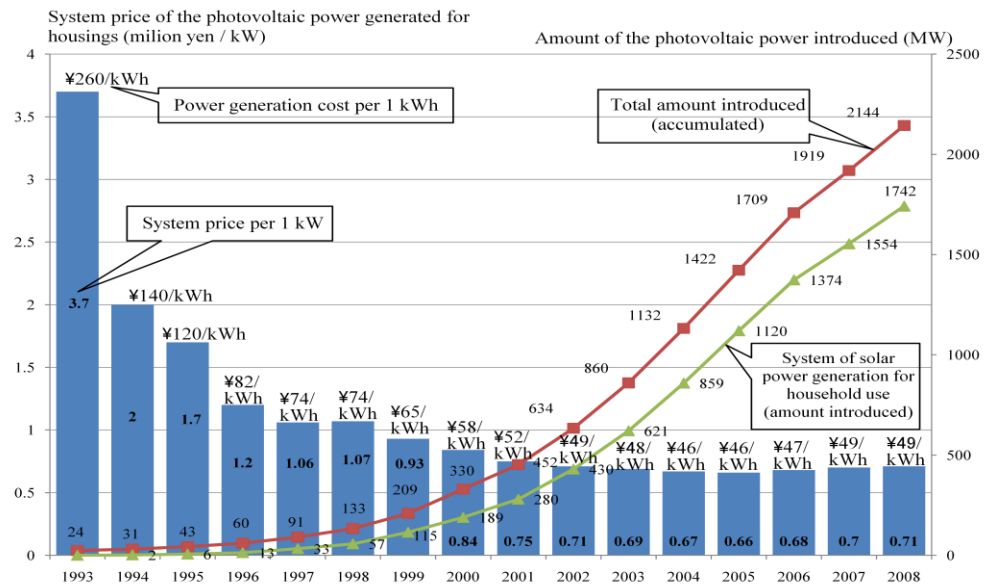
Figure 2.1 Changes in the amount of photovoltaic power generation penetration, system prices and the cost of power generation in Japan [9]

tions grew to comprise 35% of the grid-connected cumulative installed capacity in 2008 [9]. This is the reflection of the development market for utility-scale PV power systems in a number of countries. Solar cost has fallen with the rapid increase in photovoltaic power generations and advances in introduction as illustrated in Figure 2.1. The international comparison of photovoltaic power generation in 2008 is shown in Table 2.1.

Table 2.1 International comparison of photovoltaic power generation [10]

Number	Country	Capacity of the facility	
		MW	%
1	Germany	5,340	39.8
2	Spain	3,354	25.0
3	Japan	2,144	16.0
4	US	1,169	8.7
5	Italy	458	3.4
6	South Korea	358	2.7
7	France	180	1.3
8	Australia	105	0.8
9	Portugal	68	0.5
10	Netherlands	57	0.4
11	Switzerland	48	0.4
12	Canada	33	0.2
13	Austria	32	0.2
14	UK	23	0.2
15	Mexico	22	0.2
16	Malaysia	9	0.1
17	Norway	8	0.1
18	Sweden	8	0.1
19	Turkey	4	0.0
20	Denmark	3	0.0
21	Israel	3	0.0
World total		13,426	100

2.1.2 Wind Energy

Wind power is produced much in the US, Germany, and Spain. Figure 2.2 illustrates the international comparison of the amount of wind power introduced as of the end of 2008. In Japan, a production amount of 1,880 MW of wind power had been introduced at the end of 2008, ranked no.13 in the world with 1.6% [10]. However, after Fukushima disaster in 2011, the energy policy of Japan has been expected to focus on renewable energy. Besides, better conditions are necessary to decrease the cost of wind and solar production.
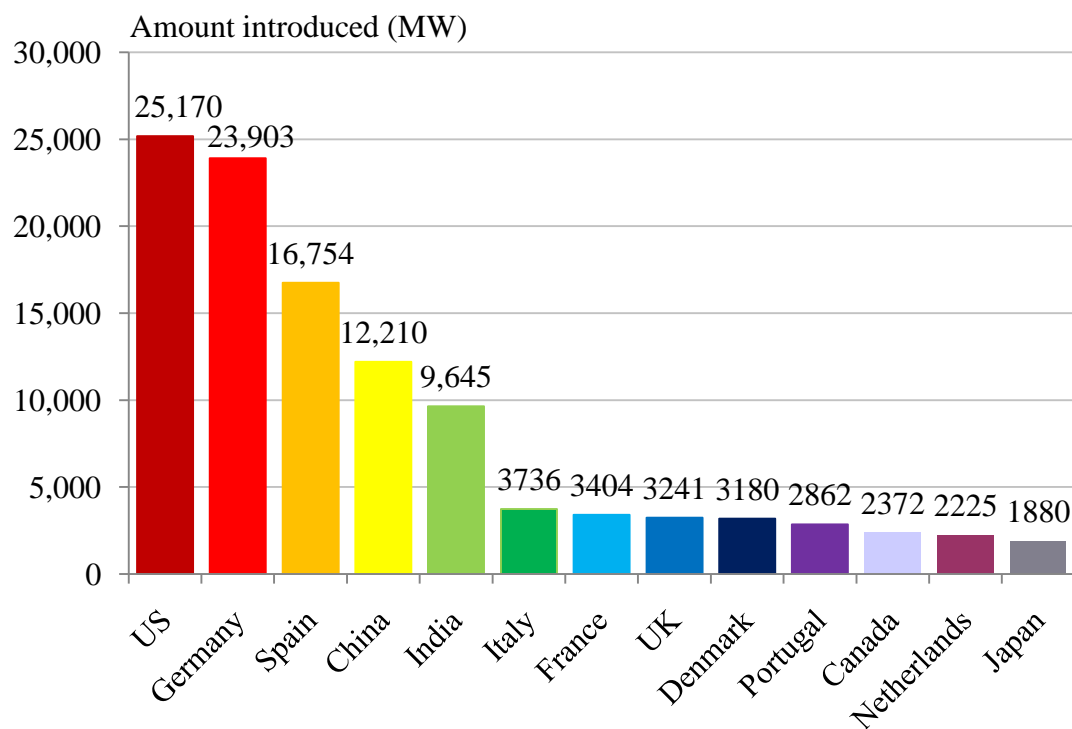
Figure 2.2 International comparison of the amount of introduced wind power [10]

2.1.3 Other Renewable Energy

Other renewable energies such as tidal power, geothermal energy, biomass, and ocean wave energy have been developed but the utilized amount has been limited in power systems. The barrier includes high installation cost compared to solar and wind energies or comes from the electric cycle demand difference. That is, maximum potential output sometimes coincides with peak demand but at other times minimum output does [3].

Machines used to convert the aforementioned energy into electrical energy are usually distributed generations. These generators are based on various technologies

including rotating machines and power electronic converters, which are summarized in the following section.

2.2 Distributed Generation Technologies

Because of the constraints in geographical availability of the renewable resources, generators powered from these sources (except large scale hydro and large offshore and onshore wind farms) are typically much smaller than the fossil fueled and nuclear powered generators dominating in the current power systems. Practically, small generators are usually connected to medium and low voltage networks. Such generation is known as distributed or dispersed generation.

2.2.1 Definition and Classification

A DG is known as a small-scale electric generator, typically smaller than 10 MVA, located next to or connected to the load being served either with or without an electric grid interconnection [1], [3].

In order to evaluate the impacts of DG on fault currents, the DG technologies can be categorized clearly into four types [11]:

- Synchronous generators
- Induction generators
- Doubly-fed induction generators
- Inverters and Static power converters

Their structures and operations are discussed in more details with the focus on the inverter and static power converters as follows.

2.2.2 Synchronous Generators

A DG which is based on a synchronous generator is known as an SBDG. An SBDG is excited by a field excitation system, which is supplied by a separate generator set. Therefore, an SBDG can run either stand-alone or interconnected to power systems. Additionally, such generator supplies high sustained current to a near fault.

Primary energy of an SBDG may come from various types. SBDGs most often use some forms of fossil fuel with a reciprocating piston engine, a gas turbine, or a steam turbine. However, fossil fuel is not renewable. In a renewable-based generating plant, some forms of primary energy resources require to be burnt before feeding an SBDG. They may be garbage, animal waste (methane) and biomass. An SBDG may be employed in a solar thermal power generation where solar thermal energy is used to

transform water into steam to drive a steam turbine. SBDGs may be applied in wind-powered generation but it is not popular. The largest constraint here is that synchronous generators require very constant rotational speed, which is difficult to meet for wind turbines.

2.2.3 Induction Generators

An induction generator, a type of asynchronous machine, requires an external source to provide the magnetizing current to establish the magnetic field across the air gap between the rotor and the stator. An induction generator always operates in parallel with a power system. Generally, when a fault occurs in the power system, causing low voltage at the generator terminal, an induction generator cannot supply electric power. Hence, the contributed current drops down dramatically after the fault.

Induction generators are used in micro hydro and wind power plants. The former is due to advantages such as availability, low cost, and robustness at varying rotor speed. The latter is because induction generators can be easily installed on the gearbox and operated at varying rotor speed. In such application, the generator is driven by wind turbines and not governed directly by the synchronous frequency rotational speed. In order to synchronize with the connected power system, a static power converter system may be interposed between the generator and the power system.

2.2.4 Doubly-fed Induction Generators

A Doubly-fed Induction Generator (DFIG) is an induction generator with a multiphase wound rotor and a multiphase slip ring assembly with brushes for accessing to the rotor windings.

DFIGs are mostly used in wind power plants because these generators can operate well with various wind speed range. The rotor currents are controlled by power converters instead of simply induced by the stator magnetic field, as being the case of a simple induction generator. The rotor current is controlled so that the sum of the apparent rotation of the rotor magnetic field, with respect to the rotor, plus the physical speed is always at the synchronous speed of the power system frequency. The physical rotational speed of the generator can be varied over a wide range – both faster and slower than the synchronous speed. When the rotor rotates faster than the synchronous speed, the direction of real power flow is out of the rotor, into the rotor side converter, through the dc link, and through the line-side converter to the power system. When it rotates at a speed less than the synchronous speed, the direction of real power flow is back into the rotor.

2.2.5 Inverter-based Distributed Generations

There are many generators that do not generate the synchronous voltage with the power system to which they are connected. Their outputs may be dc (PV cells, storage batteries, dc generator) or non-synchronous ac (asynchronous generators and synchronous generators running at non-synchronous speed). To synchronize with the power system, an inverter or a static power converter is used to convert those outputs into voltage and current compatible with the power system.

Packages consisting of generators and inverters or static power converters are known as IBDGs. They are more and more widely used for exploiting renewable energy in power systems due to many advantages as follows.

- Energy conversion by power electronic devices such as diodes, transistors, and thyristors has higher efficiency and reliability compared with the one by rotating machinery.
- An IBDG has fast response because it has almost no inertia. The power factor of this generator can be controlled ranging from -1 to 1.
- The fast computation afforded by microprocessors in IBDG packages is convenient for measurements, communications and protection coordinations.
- The current output is easily limited by the control system.

The main disadvantage of IBDG is relevant to semiconductor devices such as Gate Turn-off Thyristor (GTO), Emitter Turn-off Thyristor (ETO), and Insulated Gate Bipolar Transistor (IGBT) in the power converter section. These devices possess a limited flowing current because of the thermal limit. In addition, these devices are expensive.

The advantage of limiting current ability may be useful for some cases of fault in the power system. However, it turns to be a disadvantage for the associated protective device to detect and clear faults because the difference between fault current contributed by the inverter in fault cases and the full load current is not a large amount. This is one of the problems causing the difficulty in IBDG application.

Recently, advancements in power electronic technologies have created new opportunities in the design of inverters. Most of them use Pulse-Width Modulation (PWM) for controlling the firing angle of IGBTs. This type of inverter is known as PWM switched inverter. For more advanced control systems, the Space Vector Pulse-

Width Modulation (SVPWM) is employed instead of the PWM [12]. A simulation of the operation of this inverter type will be performed in Chapter 3.

A typical structure of an IBDG is depicted in Figure 2.3. It consists of a control system, whose inputs require voltages and currents at the inverter terminal and the PCC, a modulation generator, an inverter, and a filter circuit [13]-[15]. The primary energy is converted into the electrical energy in the fashion of dc voltage directly by PV cells, storage batteries, or indirectly by a package of power generators and converters. All primary energy sources are assumed to be represented by an equivalent dc source. An inverter converts the dc voltage of this source into an ac voltage at the appropriate frequency and magnitude, as specified by the power system. The inverter is controlled by signals from a PWM or SVPWM generator. The reference signal for this generator is produced by a controller.
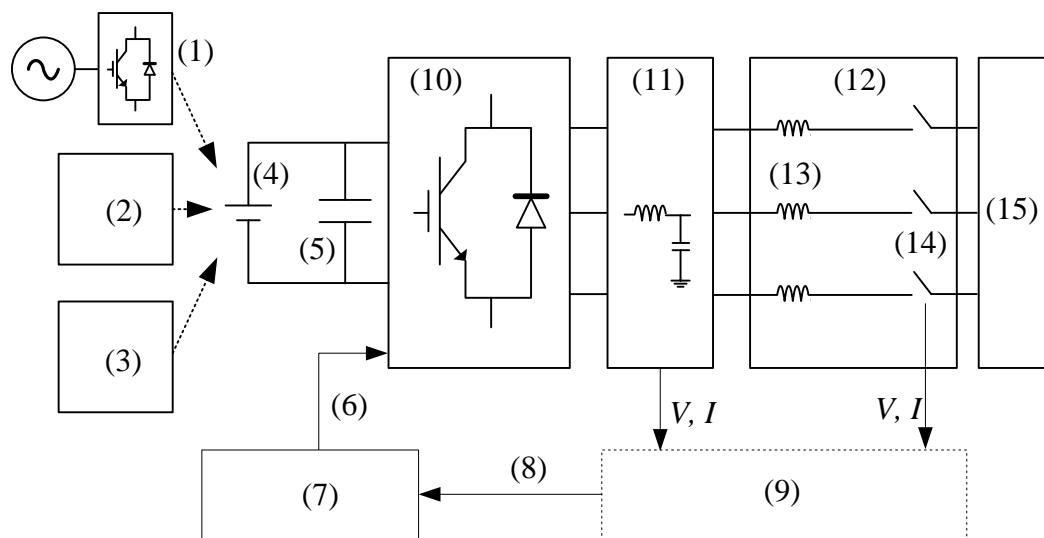
(1)-Power generators and converters   (9)-Controller

(2)-PV cells   (10)-Inverter

(3)-Storage batteries   (11)-Filter

(4)-Equivalent DC source   (12)-Interconnection system

(5)-Input capacitor   (13)-Coupling reactance

(6)-Gate signals   (14)-PCC

(7)-PWM/SVPWM generator   (15)-Power system

(8)-Reference signals

Figure 2.3 A typical IBDG structure

The control system inputs include voltages and currents at the inverter terminal, dc voltage of inverter, voltage at the PCC, and reference values. Generally, the control system generates reference signals to the input of the PWM/SVPWM generator. In some cases, it also controls the dc voltage input of the inverter.

2.3 Problems of Utility Protection System with DG Interconnection

The presence of DG on a feeder affects the existing protection system by introducing new fault current from the DG source. It causes the fault current through protective devices to not only flow in bi-direction but also increase in its level. Impacts of DG on protection system are reviewed in this section.

2.3.1 Impact Review [4], [16]-[19]

The installation of DGs causes the fault currents in the whole system to be changed. Particularly, this installation reduces the current flowing from the substation through the protective device in comparison with the case before installing DG. This is a source of the reach reduction problem of relays due to DG penetration. Other impacts that may occur in protection systems deal with reclosing, protection coordination, and false tripping of protective devices.

2.3.1.1 Reach Reduction

As shown in Figure 2.4, utility breaker and recloser are set to "see" a certain distance down the radial feeder. This is sometimes referred to as the "reach" of the device. The reach is determined by the minimum fault current that the device can detect. As an example, when a DG is present between the recloser and the fault as shown in Figure 2.4, fault currents at the relaying points (both the utility and recloser sides) will decrease in comparison with the fault currents before adding DG. Therefore, both relays will react as if the fault is further down the feeder, outside their protection zones, and consequently they will not operate. This problem is defined as the reach reduction of relay, and will be discussed in more details in Chapter 4.

(1)-Utility breaker

(2)-Recloser
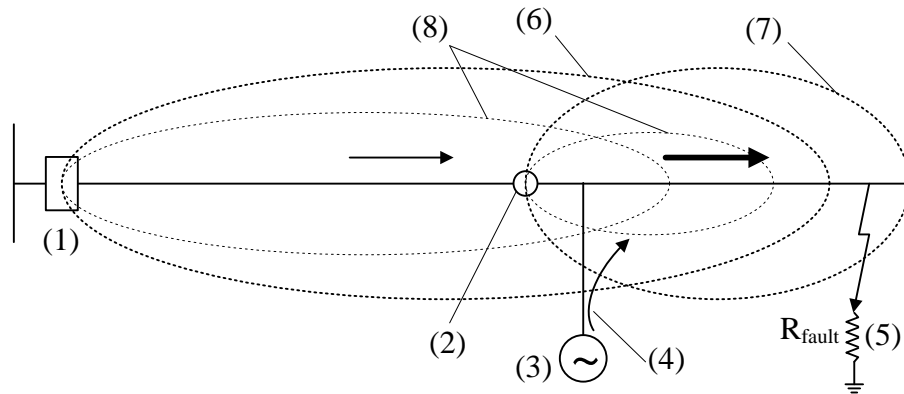
(3)-Distributed generation

(4)-DG infeed

(5)-Fault resistance R_{fault}

(6)-Normal reach of utility breaker relay

(7)-Normal reach of recloser relay

(8)-Reduce reach due to DG infeed

Figure 2.4 Representation of protection reach reduction

2.3.1.2 Protection Coordination

Another impact of DG is about the protection coordination. Figure 2.5 presents the case that the recloser-fuse may face the coordination problem in the fuse saving scheme. Operating characteristics of the recloser and the fuse are typically set in the fashion as shown in Figure 2.6. Inside the range between the minimum and the maximum current, the fast curve of recloser (recloser F) lies below the fuse minimum melting (fuse MM) and the slow curve of recloser (recloser S) lies above the total clearing curve of fuse (fuse TC).
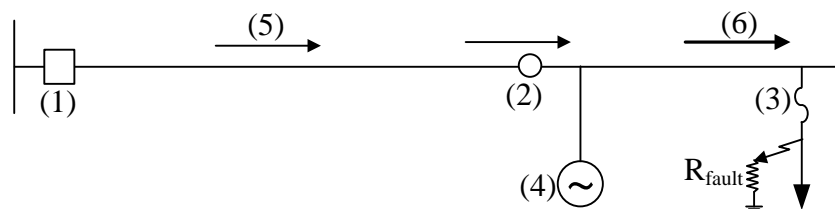
(1)-Utility breaker

(2)-Recloser

(3)-Fuse

(4)-Distributed generation

(5)-Recloser current

(6)-Fuse current

Figure 2.5 Fault currents with DG infeed
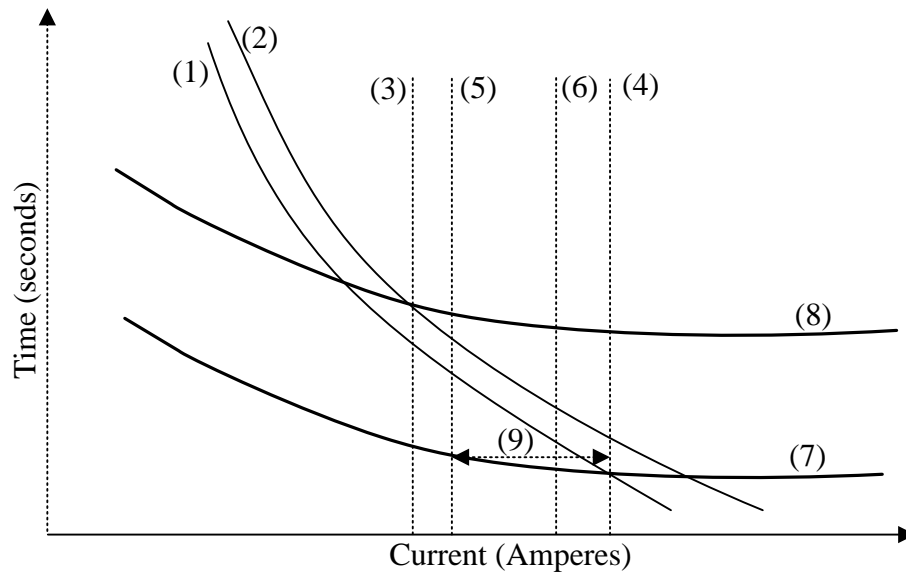
(1)-Fuse MM	(4)-Maximum current	(7)-Recloser F
(2)-Fuse TC	(5)-Recloser current	(8)-Recloser S
(3)-Minimum current	(6)-Fuse current	(9)-Margin

Figure 2.6 Impact of DG on Recloser – Fuse coordination

Before installing DG in the system, the current flowing through the recloser and the fuse are nearly the same for a fault occurring behind the fuse. The recloser-fuse coordination is set so that this fault current is always between the minimum and maximum current as shown in Figure 2.6. Thus, the recloser will open first with the fast curve (Recloser F) and then reclose after a preset time. If the fault is not temporary, the fuse will melt to de-energize the fault with the back-up of recloser using the slow curve (Recloser S). However, with the penetration of DG, the fault current through the fuse in this case is larger than the recloser current. If the fuse current is out of the margin in Figure 2.5, the coordination will be lost.

2.3.1.3 False Tripping

The presence of DG as the second source in the system, which is primarily designed for only one source supply (the utility source), brings the possibility for bi-directional fault currents. This can cause the false tripping as illustrated in Figure 2.7. For a fault occurring in the feeder protected by the utility breaker 2, only this breaker should operate to separate the faulted feeder. Nevertheless, the DG infeed may trigger the utility breaker 1 to operate, causing the unfaulted feeder to be cut off from the system source.
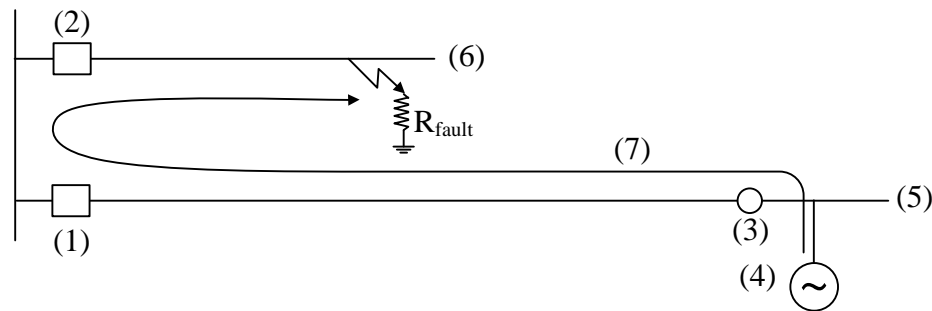
(1)-Utility breaker 1   (4)-Distributed generation   (7)-DG infeed

(2)-Utility breaker 2   (5)-Unfaulted feeder

(3)-Recloser   (6)-Faulted feeder

Figure 2.7 False tripping due to DG infeed

2.3.1.4 Reclosing

The last impact reviewed here is the utility reclosing. Utility reclosing and DG are fundamentally incompatible. There must be sufficient time between shots of the recloser or reclosing function device for the fault arc to dissipate and clear. This means that any DG on the system must detect the presence of the fault and be disconnected early in the reclosing interval. Otherwise, the fault continues as indicated. If DG cannot be disconnected due to any reasons, the unsynchronization problem may cause DG or the utility to be damaged when the recloser energizes the feeder again.

2.3.2 Discussion on Interconnection Transformer [20]-[22]

There are various transformer winding connections to fulfill various needs such as handling single phase loads, simplifying ground relaying, saving the insulation cost, and minimizing ferroresonance and harmonic problems [20]. To interconnect DG to utility systems, many transformer connection types have been proposed [21], [22]. Each of them has advantages and disadvantages. However, it is accepted that a connection type can be used extensively for interconnecting DG, if its disadvantages can be eliminated or mitigated. For instance, the grounded wye (utility)-delta (DG) transformer as depicted in Figure 2.8 is one of the applicable types. Its advantages and eliminable disadvantages are analyzed as follows.
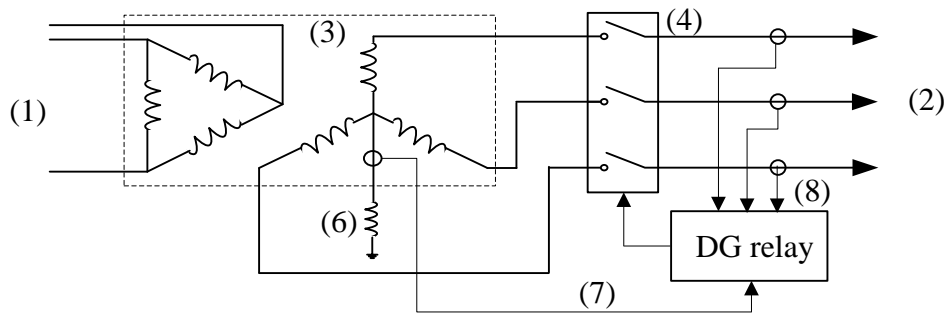
(1)-Distributed generation   (4)-DG breaker   (7)-Residual current I_{res}

(2)-Utility systems   (5)-DG relay   (8)-Current input I_{abc}

(3)-Transformer   (6)-Grounding reactance

Figure 2.8 Grounded wye-delta transformer for connecting the DG to utility system

Advantages:

- The delta winding blocks triplen harmonics from the generator and prevents the sensing of utility relay in response to an internal generator ground fault.
- Protection at the DG side can detect ground faults on the utility system side.
- The effectively grounded system condition may be provided during the unintentional islanding modes.

Disadvantages:

- The transformer is considered as a grounded source. Thus, the ground fault current through the utility relay may be reduced that causes the relay's sensitivity to be degraded. Furthermore, the transformer may encounter high fault currents due to the bolted ground faults.
- Although triplen harmonic currents in the utility system from harmonic sources cannot pass through the transformer, they tend to circulate through the wye winding with the grounded neutral point, contributing to transformer heating.

A reactor is normally added in the neutral point of the grounded wye winding so as to eliminate these disadvantages. This reactor can limit ground fault currents, unbalanced currents, and harmonic currents. If its reactance is sized properly, the corresponding transformer can provide an effectively grounded source. However, the ground overcurrent function of DG relay should be maintained to enable the ability of detecting ground faults on the utility side. Thus, a careful analysis on the proper size of grounding reactance along with the increase of DG size is performed in Chapter 4.

2.4 Network Connection Requirements

A document about the description of connection condition for a power plant or a load is usually announced by a country in the world and known as the grid code. Before going to summarize some grid codes, a connection standard published by the IEEE committee is analyzed as an international grid code. Then, grid codes from Vietnam, Denmark, Ireland, and Germany are summarized in order to bring the research closer to the industrial applications.

2.4.1 General Requirements

2.4.1.1 IEEE Standard 1547^{TM}-2003 [11]

IEEE Std.1547^{TM}-2003 establishes criteria and requirements for interconnection of distributed resources to electric power systems. It provides a uniform standard and requirements relevant to the performance, operation, testing, safety considerations, and maintenance of the interconnection. This standard covers all DG technologies with aggregate capacity of 10 MVA or less at the PCC. Some clauses in this standard relevant to this thesis are as follows.

- The grounding scheme of the interconnection shall not cause overvoltages that exceed the rating of the equipment connected to the power system and shall not disrupt the coordination of the ground fault protection on that system. This clause will be followed in Chapter 4 according to which the grounding scheme is discussed and the maximization of DG considers the operation of the ground fault protection.

- The DG unit shall cease to energize the power system for faults on the system circuit to which it is connected. In case of reclosing coordination, the cessation is performed prior to reclosure by the system. If the island is not planned (unintentional island), the DG shall detect the island and cease to energize the power system within 2 seconds of the formation of an island. This is the reason why the fault detection of DG should detect all faults in the system as fast as possible as discussed in Chapter 4.

- The protection functions of the interconnection system shall detect the effective (rms) or fundamental frequency value of each phase-to-phase voltage, except where the transformer connecting the local system to the utility system is a grounded wye-wye configuration, or single-phase installation, the phase-to-neutral voltage shall be detected.

IEEE Std.1547[TM]-2003 requires voltage protection of the interconnection system to protect the utility system from faults (undervoltage protection) and potentially damaging overvoltage that can occur in an unintentional island. This requirement should be used for DG which is in current-limited control mode such as IBDG as discussed later. The response of interconnection system to abnormal voltages is detailed in Table 2.2.

Table 2.2 Interconnection system response to abnormal voltages [11]

Voltage range (% of the nominal system voltage)	Clearing time (s)
V < 50	0.16
50 ≤ V < 0.88	2.00
110 < V < 120	1.00
V ≥ 120	0.16

2.4.1.2 Vietnam Circular [24]

The Ministry of Industry and Trade of Vietnam issued Circular No. 32 / 2010/TT-BCT on electricity distribution systems. The circular states regulations for developing and operating the distribution systems, requirements and procedures for interconnecting a load or a source to the distribution system. The requirements for measuring at the PCC are also stated. Here, some clauses relevant to the DG interconnection requirements are summarized. Most of them are stated in Chapter 5 of this circular. Clause 43 in this chapter states the particular requirements for an interconnected DG.

- The grounding scheme of the DG interconnection system is required to follow the scheme of the utility system to which it is connected.
- Under normal operation conditions of the system less than 110 kV, the negative-sequence voltage at the PCC is required to be less than 5% of the nominal voltage.
- The circuit breaker of the interconnection system is required to coordinate with the recloser of the utility system to ensure that the DG must be isolated at least after the utility recloser opens at the first time. The isolation state must be maintained until the utility system is restored successfully.

2.4.2 Fault Ride Through Requirement

Until recently, most DGs installed in the system were small in size and are connected at medium voltage networks. The proportion of DG capacity to the total amount of system generation capacity was still small. As a result, technical requirements for connection in most countries are simple so that they do require the DG to be disconnected from the utility system whenever a fault occurs in the utility system as introduced in Section 2.4.1. That is, the DG must retain separated until the utility system is restored successfully.

The situation has started to change with the strong increase in the number of renewable-based generating plants and the advanced control technology. The renewable-based DG should make a contribution to network support in not only normal operation but also transient conditions. Therefore, these generating plants must stay connected in the event of network disturbances and contribute a dynamic support to the utility system if possible. The capability of passing through the fault or other disturbances, which cause the voltage change at the PCC, without being disconnected from the network, is called the fault ride through (FRT) capability. Some documents concentrate on the voltage dips caused by disturbances and state this in more details as the low voltage ride through (LVRT) capability.

Many countries have added the FRT requirement into national grid codes such as Germany, Denmark, Scotland, Spain, Ireland, UK, Canada and USA. Some national grid codes, e.g. Denmark, German, and Ireland have specific FRT requirement for distribution networks as well as transmission ones while the others have focus only on the transmission level. Up to now, most FRT requirements have been stated for wind turbines because of their high proportion capacity to the total system generation capacity. These requirements are possible to be extended to cover other generating plants if their capacity increases so that the effect on the system stability is significant. In fact, the technical requirement of Germany for generating plants' connection to and parallel operation with the medium voltage networks [29] covers all renewable-based generating plants. For instance, they include wind energy, hydro power, co-generation units, and PV plants. The requirements for non-synchronous machine-based generators receive more concerns because the characteristics of these generators are complicated and different from those of synchronous machines, which are well understood by system operators. The FRT requirement includes two subrequirements: (1) remaining connected requirement following a voltage-time characteristic and (2) supporting network voltage during fault. They are summarized as follows.

2.4.2.1 Voltage time characteristic

Danish Grid Code [25]

According to the specifications stated in Danish grid code for wind turbines connected to grids with voltages below 100 kV, the wind turbines must remain connected during grid faults as shown in Figure 2.9. Wind turbines must not be disconnected from the grid during voltage dips that is not less than 0.2 p.u. for the first 100 ms after the fault. With a linear time axis, the curve section between 0.1 and 0.75 seconds is a straight line.

Some special situations in which the wind turbines must not be disconnected from the grid are:

- Case of 3-phase short-circuit: Must not be disconnected if the short-circuit lasts less than 100 ms.
- Case of 2-phase short-circuit with/without earth fault: Must not be disconnected if the short-circuit lasts less than 100 ms and followed by a new short-circuit from 300 ms to 500 ms later, also lasting 100 ms.
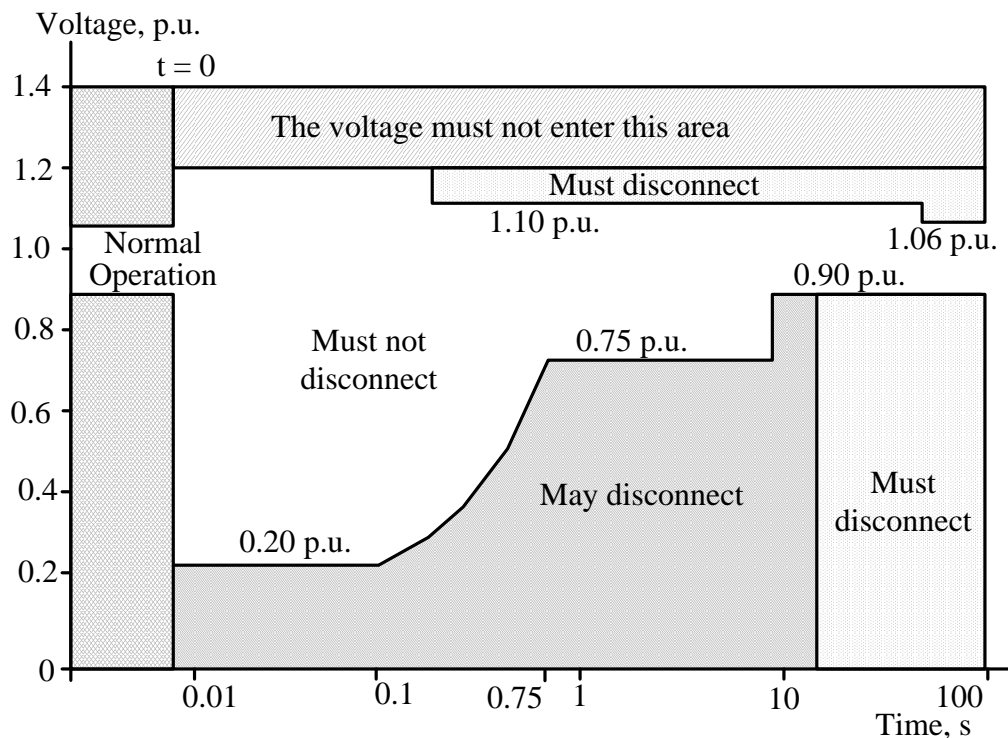
Figure 2.9 Danish requirement concerning disconnection in the event of voltage dips

[25]

Irish Grid Code [26]

Wind farm power stations in Ireland are categorized into five types based on their connection types and the voltage level as shown in Figure 2.10 and explained in more details in Table 2.3.
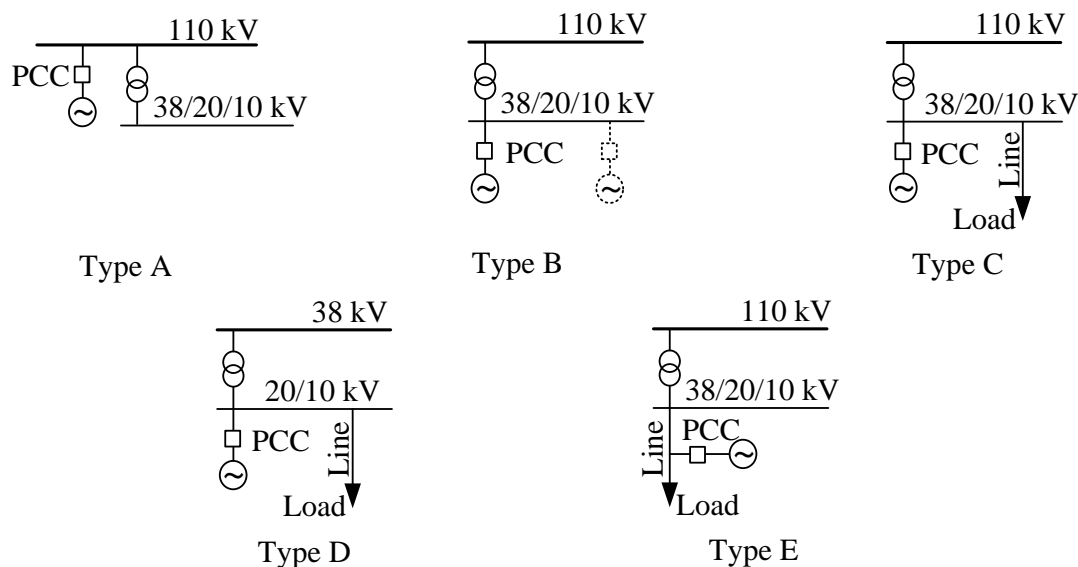
Figure 2.10 Irish connection type classifications for wind farms [26]

Table 2.3 Description of Irish connection type classifications for wind farm [26]

Type	Specifications
A	The connection is performed at 110kV to a DSO operated 110kV bus bar.
B	The connection is performed at a distribution system voltage ($\leq$ 38 kV) to a dedicated Wind Farm Power Station(s) transmission station. There are no load customers connected to the DSO operated 38/20/10 kV busbar.
C	The connection to the distribution system is performed via a dedicated feeder, into an existing 110kV station.
D	The connection to the distribution system is performed via a dedicated 38kV, 20kV, or 10kV feeder into an existing 38kV distribution station.
E	The connection is performed at an existing distribution line with load.

Types B, C, D, and E Wind Farm Power Stations shall remain connected to the Distribution System for voltage dips on any or all phases, where the distribution

system phase voltage measured at the PCC remains above the heavy black line in Figure 2.11.

Type A Wind Farm Power Stations shall remain connected to the distribution system for voltage dips on any or all phases, where the distribution system phase voltage measured at the PCC remains above the heavy black line in Figure 2.12.
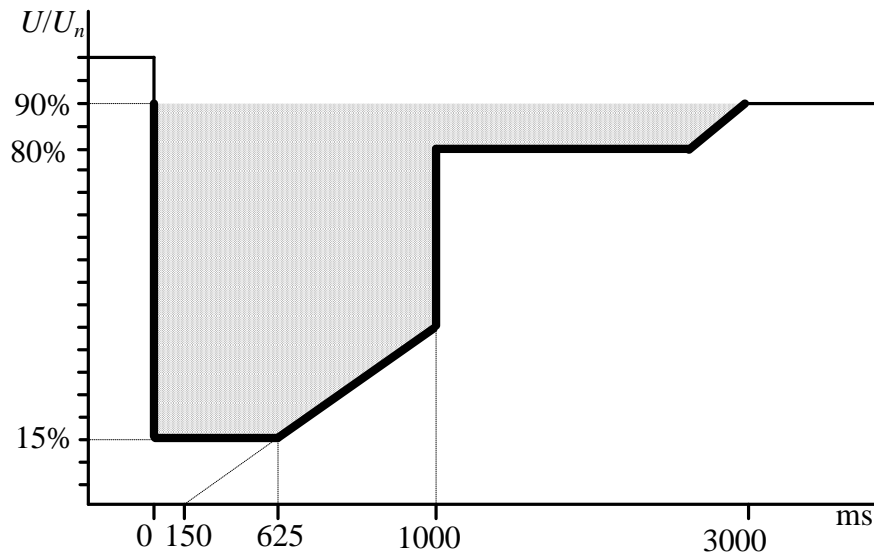
Figure 2.11 Irish FRT requirements for Type B, C, D, E wind farms [26]
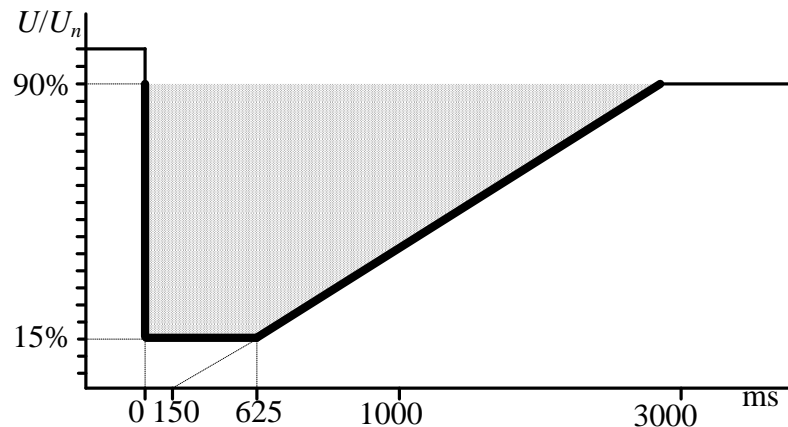
Figure 2.12 Irish FRT requirements for Type A wind farms [26]

German Grid Code [27]-[29]

In Germany, based on the Transmission Code 2007 [27] and the Grid code for extra high voltage [28], similar requirements concerning the grid-supporting electrical behavior of distributed generators have been transferred to the medium voltage network [29]. General requirements are as the following technical terms.

- not to be disconnected from the network in the event of network faults
- to support the network voltage during a network fault by feeding a reactive current into the network
- not to extract from the medium voltage network after fault clearance more inductive reactive power than prior to the occurrence of the fault

These requirements apply to all types of short-circuits (i.e. single-phase, two-phase and three-phase short-circuits). The objective here is to prevent large power system collapse when a sudden power loss challenges the limited primary reserve for frequency stabilization.

Due to the different characteristic of fault current contribution, a distinction is made between type-1 and type-2 generating plants. A type-1 generating unit exists if a synchronous generator is directly (only through the generator transformer) connected to the network. The others are type-2 generating units.

Concerning type-1 plants, they must remain connected to the network if the voltage drops at the value above the borderline in Figure 2.13.
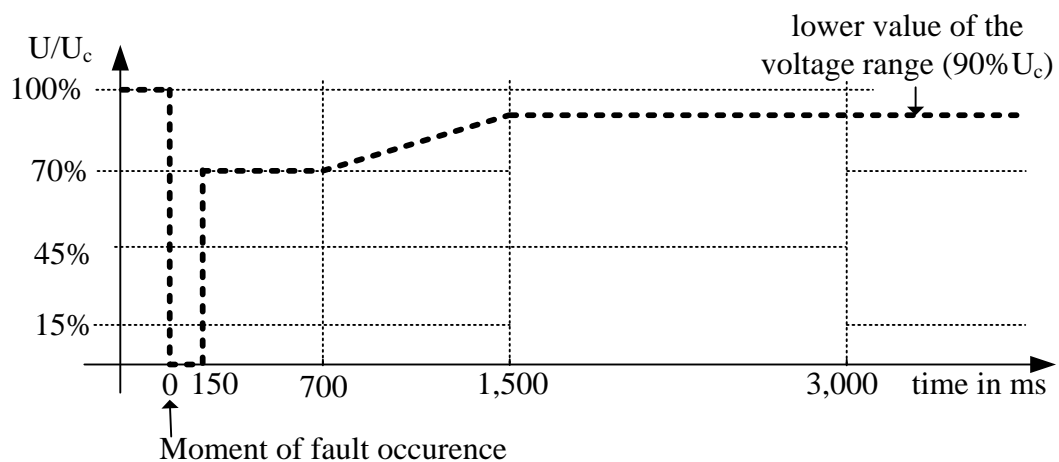
Figure 2.13 Borderline of the voltage profile at the PCC of a type-1 generating plant [29]

For type-2 generating plants, the voltage profile in Figure 2.14 is applied to the requirement of dynamic network support as the following technical terms.

- Generating units must not disconnect from the network in the event of voltage drops to 0 % U_c of a duration ≤ 150 ms.
- If the voltage drops at values below 30% of U_c, there are no requirements addressing that generating plants have to remain connected to the network.

- Any short-circuits or voltage drops due to disturbances must not lead to instability or to a disconnection of the generating facility from the network above the borderline 1 in Figure 2.14.

- If the voltage drops at values above the borderline 2 and below the borderline 1, generating units shall pass through the fault without disconnecting from the network. Feed-in of a short-circuit current during that time is to be agreed with the network operator. In consultation with the network operator, it is permissible to shift the borderline 2 if the generating plant's connection concept requires doing so. Also in consultation with the network operator, a short-time disconnection from the network is permissible if the generating plant can be resynchronized in 2 seconds, at the latest, after the beginning of the short-time disconnection. After resynchronization, the active power must be increased with a gradient of at least 10% of the nominal capacity per second.

- Below the borderline 2, a short-time disconnection of the generating plant may be carried out in any case. Prolonged resynchronization times and lower gradients of the active power increase after resynchronization as compared to those admissible above the borderline 2 are permitted if they are agreed with the network operator.
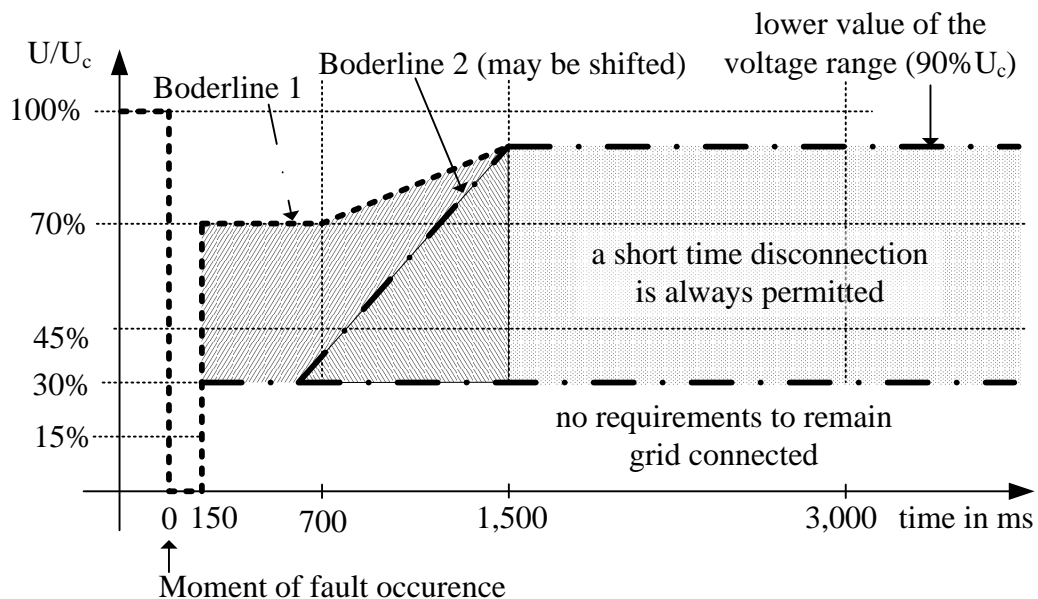
Figure 2.14 Borderline of the voltage profile at the PCC of a type-2 generating plant [29]

2.4.2.2 Dynamic network support

After the fault identification, the generating plant may be required to provide the network support by providing reactive power. The required reactive power is defined by a function of voltage drop. Generally, this support is expected to be maximum allowed by the plant's technology.

The Irish grid code requires wind farms a current defined as follows.

- Active power is provided in proportion to retained voltage.
- Reactive current is maximized but not exceeding wind farm limits.
- The maximization of reactive current shall continue for at least 600ms or until the distribution system voltage recovers to within the normal operational range of the distribution system.

The wind farm power station shall provide at least 90% of its maximum available active power as quickly as the technology allows and in any event within 1 second of the distribution system voltage recovering to the normal operating range.

The German grid code requires the dynamic voltage support clearer than the Irish one. The generating facilities must support the network voltage during a voltage drop by means of additional reactive current (of the positive sequence of the fundamental). To this end, voltage control according to Figure 2.15 shall be activated in the event of a voltage drop of more than 10% of the effective value of the generator voltage. This voltage control must ensure the supply of a reactive current at the low-voltage side of the generator transformer with a contribution of at least 2% of the rated current per percent of the voltage drop ($k \geq 2$). The facility must be capable of feeding the required reactive current within 20 ms into the network (control response time). If required, it must be possible to supply reactive current of at least 100% of the rated current. After the return of the voltage to the dead band range, voltage control must be maintained at least over additional 500 ms according to the given characteristic.
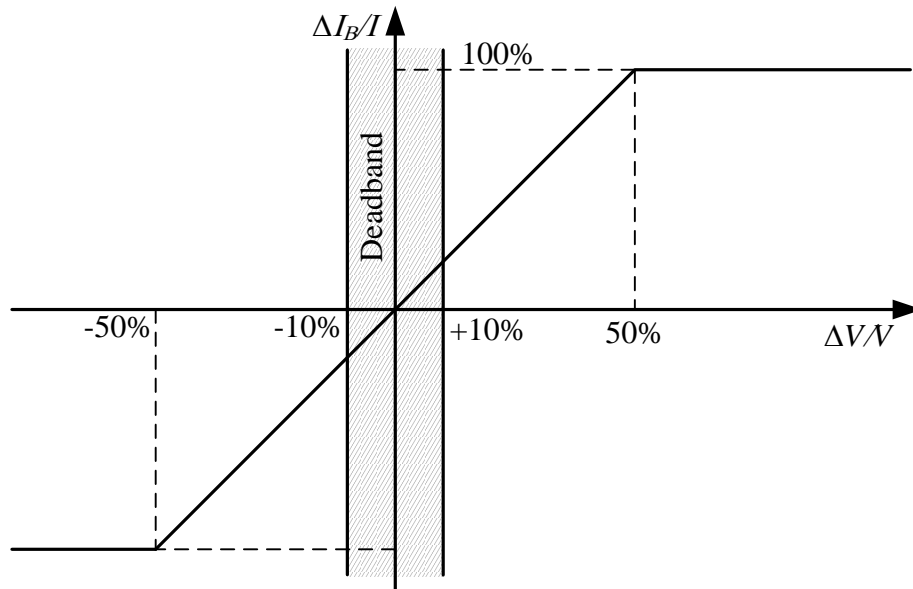
Figure 2.15 Required reactive current [29]

$$k = \frac{\Delta I_B / I_N}{\Delta V / V_N} \geq 2 \qquad (2.1)$$

where $\Delta I_B = I_B - I_0$ and $\Delta V = V - V_0$

Explanations:

V_N: nominal voltage $\qquad\qquad\qquad\qquad$ V_0: voltage prior to disturbance

V: instantaneous voltage (during the disturbance) $\quad$ I_N: nominal current

I_{B0}: reactive current prior to disturbance $\qquad\qquad$ I_B: reactive current

It can be seen that the function range to meet the requirements of the grid code causes the renewable-based generating plants to be adapted in sizing, controlling, and protecting. Besides that, the occurrence of the additionally reactive current ranging from 0 to 100 percent of the rated current (may be larger if possible) is a challenge for calculating the short-circuit current in the system during the fault. This problem will be solved in Chapter 3 by an adaptive fault calculation algorithm.

2.5 Maximization of DG in Distribution Systems

Many researches which discuss about optimal planning and operation of DG have been published. This section reviews some significant publications on maximization

of DG in distribution systems. A synthesis is then revealed to be a premise for the problem formulation in the following chapters.

Loss reduction and system cost are usually the objectives of the optimization problem. The location and capacity of DG are optimized in [30]-[33]. An implementation of Tabu Search to optimally allocate the DG is illustrated in [30] where the authors minimize the power loss under conditions of predefined number of DGs and their total capacity. The authors in [31] consider the trade-off between loss minimization and DG capacity maximization. In this research, an ordinal optimization method is used to specify the locations and capacities of DG; whereas, voltage and branch flow limits are set as constraints. The preference of DSOs for sitting and sizing of DG installation is analyzed in [32]. The authors examine the effect of network regulations on the optimal connection of new DG with consideration of voltage and line capacity limits. The optimal DG unit's size, power factor, and location is determined in [33] by employing an artificial bee colony algorithm with an objective function of loss minimization subject to voltage and line limits. The optimum of DG capacity is also discussed in [34]-[38]. The effect of energy resources categories are taken into account in [34] and [35] by considering the load factor of each DG, meaning that the available DG capacity is allocated based on the amount of energy that is delivered. Another approach of single/multiple objective optimal power flow is used in [36] and [37]. The authors in [36] simulate how the incentives of the DSOs and DG developers affect their choice of DG capacity within the limits of the existing network. The limits include costs of DG connection, losses, and network deferral. The optimal accommodation of DG is determined in [37] with a multi-period AC power flow. The connection cost and the availability of energy resource are also considered in [38] where the authors present a methodology which maximizes the amount of energy that may be reaped from a given area. A synthesis of these works is that the objective function is about loss reduction or system cost and the constraints consider simple system parameters including voltage and line capacity limits. In addition, all DGs models are embedded in a cost function and load factor is used to draw the difference among DG technologies. DG models and constraints of these works may lack the information of DG installation's impacts which have been reviewed in Section 2.3.

Researches in [39]-[42] focus on technical aspects of DG's installation. The authors in [39] propose analytical methods to predict allowable distributed generation resources on a radial distribution feeder before voltage harmonic limits are exceeded. The final result is a determination of allowable penetration levels of distributed

generation resources for a range of distribution feeders. The harmonic problem is combined with the protection coordination limits in [40] to determine the maximum DG penetration level. The authors consider both SBDG and IBDG so that the objective function is proposed to maximize DG penetration level from both types of DG units, taking into account power balance constraints, bus voltage limits, total and individual harmonic distortion limits specified by the standard, over-current relay operating time limits, and protection coordination constraints. Besides, a method to find the threshold value of the DG capacity, beyond which recloser-fuse coordination is lost, is proposed in [41] to prevent the reliability degradation. In addition, the maximum amount of DG that may be installed without requiring major changes in the existing electric power system is determined in [42]. The authors show that conductor's ampacity and voltage rises are limiting factors that manifest themselves under different conditions. It can be seen that although these researches focus on the technical impacts of DG on the network, the important impact of relay reach reduction is not concerned and most of concerned impacts are evaluated with the SBDG.

The above shortcomings are taken into consideration in this thesis in order to determine the maximum allowable DG. Besides, recent network requirements in Section 2.4 are necessary to be updated to the research. Particularly, Chapter 3 takes the FRT requirement into an adaptive fault calculation. Then, it is employed in DG maximization algorithms in Chapter 4.

2.6 Summary of Chapter 2

Involving challenges of unstable outputs, high costs and installation constraints, renewable energy has been introduced through various measures to reach a certain amount. Most common utilized renewable energies are from the sunlight and the wind. All DG technologies for energy conversion have been reviewed in this chapter. The focus is placed on the conversion of renewable energy into electrical energy using IBDGs.

This chapter shows that DG impacts on utility systems must be taken into account before connecting DG. Utility protection systems may need new settings or upgrading with proper devices. However, the investment cost may be significant. Another solution is to limit the fault current supplied by DG. This requires careful research efforts on the mentioned impacts. This thesis concentrates on the reach reduction problem since it affects all relays in the system excluding the one of DG.

The IEEE Std. 1547[TM]-2003, the Circular of electricity distribution system of Vietnam and some other national grid codes are summarized in this chapter. The new

requirement about FRT capability from European countries is considered carefully. It consists of two main requirements: riding through the fault and supporting network voltage. Taking grid codes into consideration brings the research closer to practical situations. Thus, results of the research in this thesis will be more acceptable and applicable to real works.

CHAPTER III

FAULT CURRENT CALCULATION IN DISTRIBUTION SYSTEMS WITH IBDGs

Despite being required, according to the IEEE standard [11], to physically fast disconnect IBDGs from the grid in a fault event, IBDGs are reasonably accounted in fault current calculation to catch up with the FRT requirements in some new grid codes as introduced in Chapter 2. These grid codes require an IBDG to have a capability of passing through a fault signed by voltage at the PCC. As such, the IBDG continues to feed current during a fault instead of fast shutting down and isolating itself.

There have been considerable efforts directed to the development of solution models and algorithm for synchronous, induction and doubly-fed induction generators with great success and wide application [43]-[46]. However, comparatively fewer solutions have been developed for IBDGs. In addition, most publications concerning IBDGs have not received a high unanimity. Some authors proposed a model and an algorithm to capture the fault response of IBDG during the fault period but they did not concern the control system of IBDG [47]. Such algorithm is not convenient to build a calculation tool for protective device setting that needs the flexibility for many fault cases. The fault response in the time-variant curve fashion of an IBDG has a similar limitation [48]-[50]. Some authors derived IBDG models for fault calculation with deep insight on the transfer functions of the control system [51]. Unfortunately, those models are suitable for an inverter-only microgrid instead of a grid with parallel operations of the IBDGs and the utility source. Therefore, the growing need of both DG owners and distribution utilities for more complete studies has motivated the development of solutions to calculate the fault current in the system with IBDGs.

The objective of this chapter is to propose an accurate fault current calculation method in a system with IBDGs serving for DG impact evaluation and protective device settings of both utility's and DG's protection systems. The chapter is organized as follows. Fault response of an IBDG is firstly explored in Section 3.1 in order to model this generator for a fault calculation method. Based on this model, Section 3.2 proposes an adaptive algorithm to calculate the fault current in distribution networks with IBDGs.

3.1 IBDG Model for Fault Calculation

A typical structure of an IBDG consists of a control system, whose inputs are voltages and currents at the inverter terminal and the PCC, a modulation generator, an inverter, and a filter circuit as introduced in Chapter 2. There are several modulation techniques for inverter power supply such as pulse width modulation (PWM), pulse density modulation, and pulse frequency modulation. The most successful, for the voltage source inverter case, is the PWM. Compared to other approaches, the PWM offers significant advantages, for instance in terms of ease of implementation, constant frequency inverter operation and immediate demodulation by means of simple low-pass filters [12]. The PWM technique is usually implemented by space vector modulation (SVPWM) in three phase switching converters. The inverter in this thesis is assumed to be controlled by signals from a PWM generator.

3.1.1 Control System of an IBDG

Generally, a capacitor is installed at the inverter input. This capacitor maintains the dc voltage input of the inverter during a short transient. Thus, the dc voltage is assumed to be constant throughout the fault calculation [48]. Additionally, the controller of the inverter regulates the output complex power around a desired set point. Among many control techniques [52], [53], a control system is implemented in the Natural Reference Frame (NRF) can be accepted [51], [54]-[55]. Figure 3.1 depicts a schematic diagram of an IBDG with a three-phase three-leg inverter of that control system. Details of the vector transformation are in Appendix A.
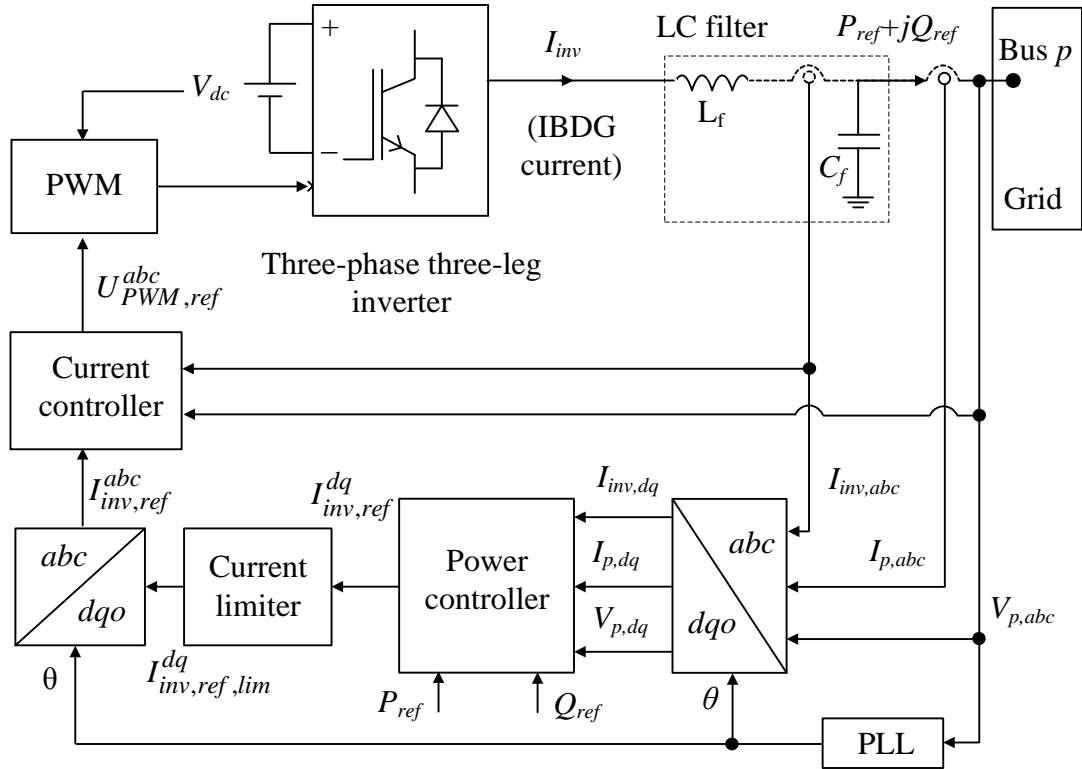
Figure 3.1 General control system of a grid-connected IBDG

The output LC filter is at the terminal of the inverter to filter out the undesired switching frequency components from the output current spectrum. The inclusion of the LC filter makes the controller design and controller parameters adjustment more difficult. However, empirical parameters are selected for the filter in this research, since the design of the LC filter is out of the scope of this research.

Assume that the IBDG is connected to Bus p of a power system. The power injected into Bus p is desired to be around a set point (P_{ref}, Q_{ref}). After transforming output currents ($I_{inv,abc}$, $I_{p,abc}$) and voltage ($V_{p,abc}$) from abc coordinates into dqo coordinates, they are used to perform the reference inverter output current $I^{dq}_{inv,ref}$ by the power controller. This current is then retransformed into abc coordinates. All transformations use the fundamental frequency generated from the voltage at the IBDG terminal by a Phase-Locked Loop (PLL) to synchronize the inverter outputs with the grid. Using ($I^{abc}_{inv,ref}$, $I_{inv,abc}$, $V_{p,abc}$), the current controller generates the reference input voltage $U^{abc}_{PWM,ref}$ for the PWM generator which controls switching signals of the inverter to create the desired output power. More details of control system components are discussed as follows.

3.1.1.1 Power Controller

The reference current given by (3.1) is computed in the Synchronous Reference Frame (SRF) by using output power set point and feedback voltage. This equation is explained in Appendix A.

$$
\begin{bmatrix} I_{p,ref}^d \\ I_{p,ref}^q \end{bmatrix} = \frac{2}{3} \frac{1}{\left(V_p^d\right)^2 + \left(V_p^q\right)^2} \begin{bmatrix} V_p^d & V_p^q \\ V_p^q & -V_p^d \end{bmatrix} \begin{bmatrix} P_{ref} \\ Q_{ref} \end{bmatrix} \tag{3.1}
$$

where V_p^d, V_p^q are the d-axis components of the phase-to-ground voltage in peak value at Bus p; $I_{p,ref}^d$ and $I_{p,ref}^q$ are components of the current in peak value injected to Bus p in corresponding to three-phase reference power (P_{ref}, Q_{ref}). Figure 3.2 represents a schematic diagram of the power controller in the SRF.

The reference value of the inverter current $I_{inv,ref}^{dq}$ is computed from the reference current injected into Bus p and the current flowing through the filter capacitor. Additionally, in order to limit the power controller bandwidth and to filter out harmonic content from the voltage and current spectrum (under unbalanced conditions), a low-pass filter is employed. The filter cut-off frequency f_c must provide both sufficient suppression of voltage harmonics and unbalance and quick enough response of power control loop [48]. Assuming the first order low-pass filter is used, the reference output of the power controller is determined by (3.2).
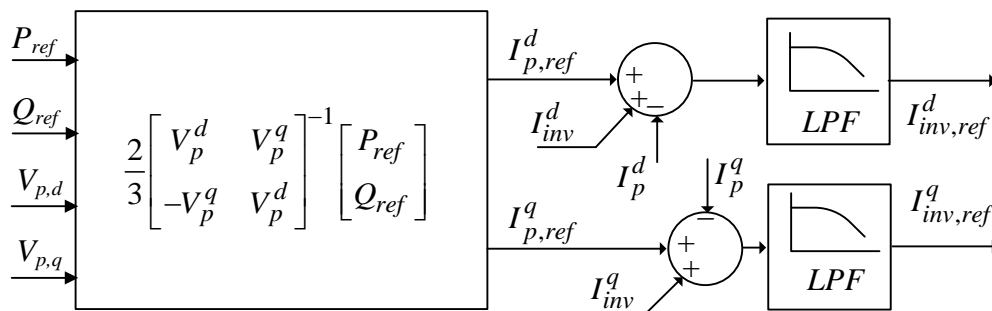
Figure 3.2 Schematic diagram of the power controller

With the selected filter, components that have frequency of 2ω in $I_{inv,ref}^{dq}$ caused by the negative-sequence are filtered out. The zero-sequence components are not considered here because a three-phase three-leg inverter is used. Thus, the output signals of the power controller are clean dc derived from positive-sequences of $V_{p,abc}$, $I_{p,abc}$, and I_{abc}^{inv}. This result is important for modeling the IBDG under an unsymmetrical fault condition as discussed later.

$$
\begin{bmatrix} I_{inv,ref}^d \\ I_{inv,ref}^q \end{bmatrix} = \frac{2\pi f_c}{s + 2\pi f_c} \left\{ \begin{bmatrix} I_{p,ref}^d \\ I_{p,ref}^q \end{bmatrix} + \begin{bmatrix} I_{inv}^d \\ I_{inv}^q \end{bmatrix} - \begin{bmatrix} I_p^d \\ I_p^q \end{bmatrix} \right\} \tag{3.2}
$$

3.1.1.2 Current Limiter

Due to the thermal limit of semiconductor devices, inverters are usually designed to supply a maximum current of typically less than twice their nominal values in the event of a network fault [2], [49], [56]-[58]. This limitation can be implemented by using the current limiter in the SRF as illustrated in Figure 3.3. Under normal conditions, the switch is closed on the normal position N. When a fault occurs, as soon as $I_{inv,ref}$ reaches the limit I_{thres} in the saturation block, the switch is closed on the limited position L by the switching signals to pass a saturated current $I_{inv,sat}$ through the switch. The switch goes back to N after the fault is cleared and the system is recovered to normal operating condition [54].
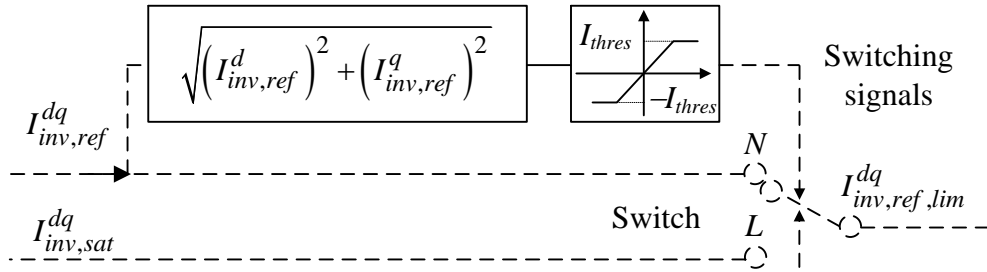
Figure 3.3 Schematic diagram of the current limiter in the SRF

The saturated current $I_{inv,sat}$ is selected so that the inverter is sufficient to supply without exceeding its capability. The simplest method is to cut off the active power P_{ref}. The IBDG supplies only reactive power to the system. The current $I_{inv,sat}$ thus can be defined by operation (3.3).

$$
I_{inv,sat} = K \angle \left(\delta_{Vp} - \theta_0 \right) \tag{3.3}
$$

where δ_{Vp} is the phase of the IBDG terminal voltage V_p and θ_0 is a constant. Equation (3.3) indicates that $I_{inv,sat}$ lags V_p by θ_0. Therefore, the IBDG injects reactive power into the system if $0 < \theta < \pi$. Magnitude K must be less than the thermal limit of inverter, i.e. 2 p.u. in IBDG rating. However, most generating plants set K to 1 p.u. that is the rated current of the IBDG. The formulation of $I_{inv,sat}$ in *abc* coordinates uses the phase obtained from a PLL and is explained later.

3.1.1.3 Current Controller

The control in the NRF is straightforward for understanding and implementing. Although the PI controller has a poor control performance with sinusoidal control signals, the zero steady-state error is still achieved in using P+Resonant (PR) regulators with k_p and k_i parameters. The transfer function of a PR regulator is defined as (3.4) [59].

$$G_{PR} = k_p + \frac{2k_i s}{s^2 + \omega^2} \tag{3.4}$$

The first term in (3.4) is a proportional gain that is in the same way as in the PI controller. The second term is a second order generalized integrator which achieves very high gain in a narrow band center around the frequency ω. Therefore, ω is usually called resonant frequency. In this paper, it is the fundamental frequency ($2\pi 50$ rad/s). The output of the PR regulator and the feed-forward voltage $V_{p,abc}$ are then summed up to form reference voltages for the SVPWM generator as depicted in Figure 3.4.
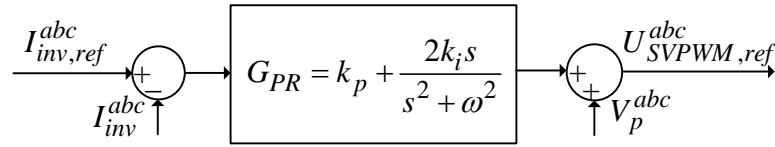
Figure 3.4 Schematic diagram of the current controller

3.1.1.4 Phase-Locked Loop (PLL)

A PLL is utilized to synchronize the inverter output with the grid. Generally, the PLL tracks the positive-sequence voltage at the connected bus (Bus p) as depicted in Figure 3.5. All transformations inside the control system refer to this voltage. As an example, the saturated current with a predefined magnitude K inside the current limiter can be generated by a circuit in Figure 3.6. The low-pass filter (LPF) is to eliminate the all high frequency signals occupying in V^{dqo}_p. The cut-off frequency is generally 5 Hz. This means, a signal with frequency higher than 5 Hz is filtered out. As a result, V^{dqo}_p after the LPF includes purely dc signals that reflect the positive-sequence component of the voltage V_p.
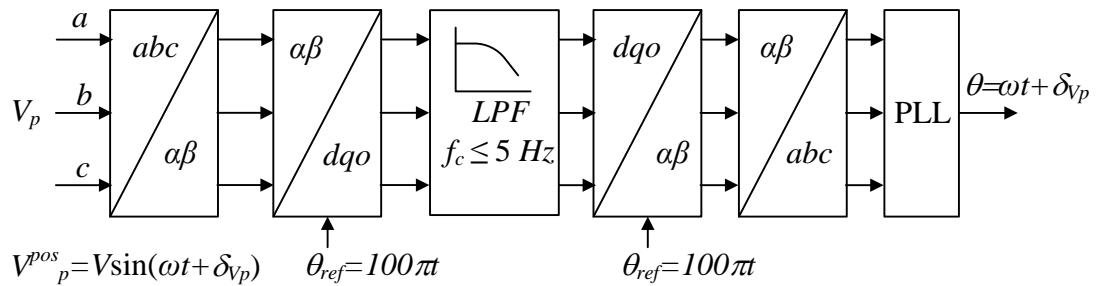
Figure 3.5 Tracking IBDG terminal voltage by PLL
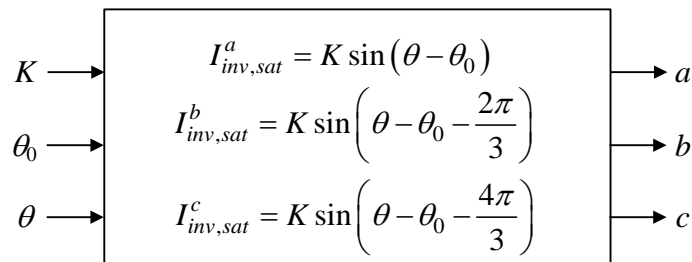
Figure 3.6 Formulation of the saturated current

In Figure 3.6, θ_0 must be from 0 to $\pi/2$ so that the voltage V_p leads $I_{inv,sat}$ and the IBDG does not absorb the active power. This formulation satisfies (3.3). If the IBDG is switched to the current source, an amount of reactive power will be injected into the grid.

3.1.2 Fault Response of an IBDG

When a fault occurs in the utility system, voltages at the faulty phases decrease. The IBDG terminal voltages changes and may be unbalanced. Thus, inverter currents are changed to maintain the desired power output. However, the IBDG control system only responds to the positive-sequence components due to the low-pass filter inside the power controller as explained in Section 3.1.1, causing the power output to be controlled around the set value based on the positive-sequence voltage and current.

Changes of the voltage at the connecting bus (Bus p in Figure 3.1) under fault condition mainly depend on the type, location, impedance of fault, and line parameters. For example, a three phase fault with high impedance is simulated to cause the phase voltages at the terminal of the IBDG to dip 11.58% compared to the prefault voltage as seen in Figure 3.7. Before the fault, the IBDG current is 0.96 p.u. that is a little lower than the rated current. After the fault, the IBDG current increases to 1.09 p.u., i.e. 12.6% instead of 11.58%. This difference can be explained by using (3.5), which is the equation of the expected current contributed from IBDG.

$$I_{inv,ref} = \frac{P_{ref} - jQ_{ref}}{V_p^*} + j\omega C_f V_p \tag{3.5}$$

where (P_{ref} + jQ_{ref}) is the reference power; V_p is the line voltage at Bus p with all variables in per unit. The last term in (3.5) is the current flowing out through the filter capacitor (capacitive current). This current depends on the voltage at Bus p. The IBDG current in Figure 3.8 increases 12.6% instead of 11.58% to compensate the capacitive current. Therefore, the output power is controlled around the set value (0.91 p.u.) as shown in Figure 3.9 where the reactive power is set to be zero.
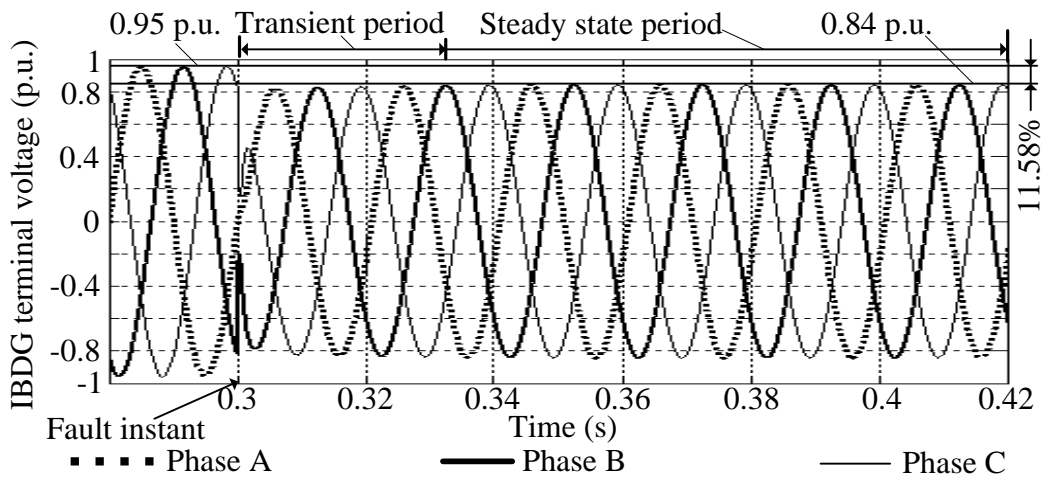
Figure 3.7 IBDG terminal voltage during a 3F-under limit
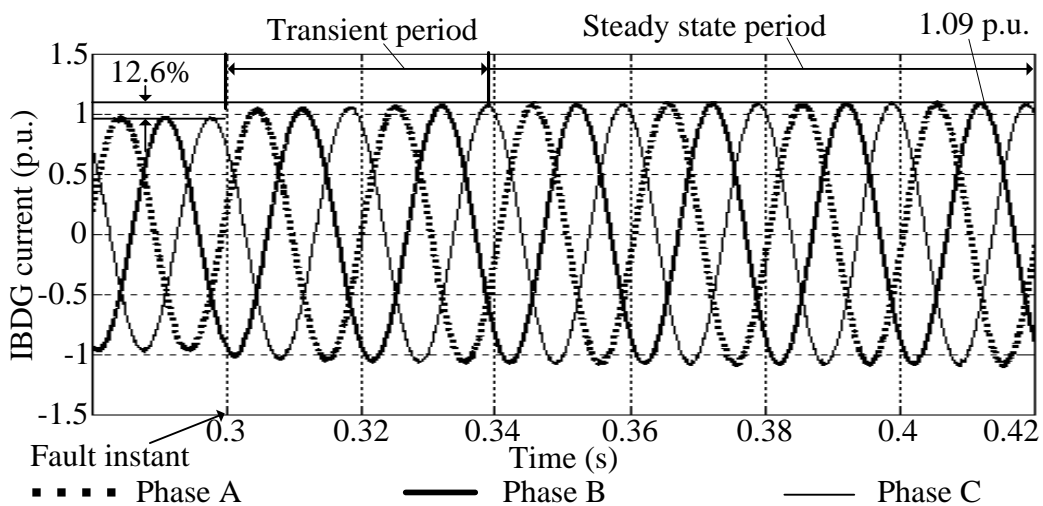
Figure 3.8 IBDG responses to a 3F-under limit
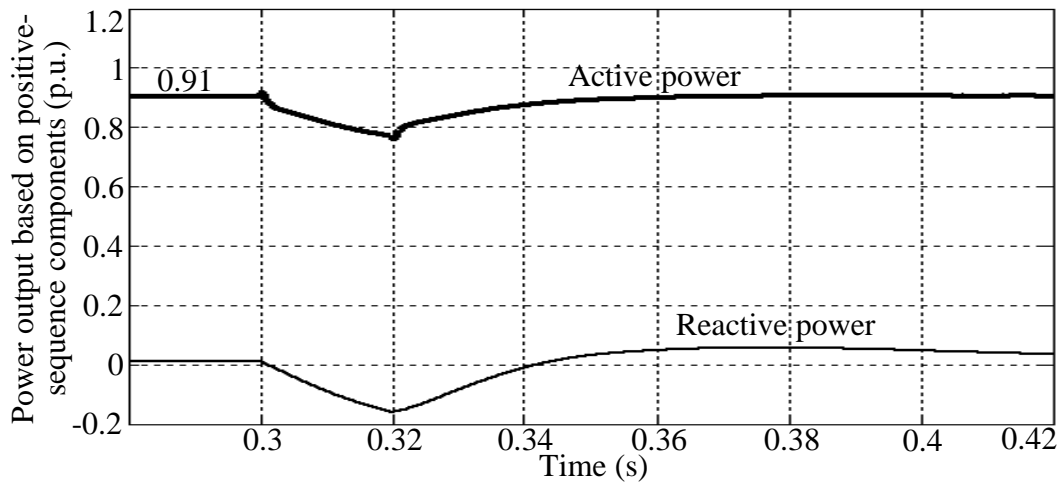
Figure 3.9 Output power of IBDG during a 3F-under limit

The IBDG current includes rich positive-sequence components resulting in well balanced phase currents despite any unsymmetrical fault in the network. Figures 3.10 and 3.11 show another example of IBDG fault responses to a SLGF. In Figure 3.10, the voltage at phase A dips 21.05%; whereas, the voltage dip of the corresponding positive-sequence voltage is smaller with 7.37% as in Figure 3.11; the IBDG phase current increases 8.33% from the prefault value as in Figure 3.12 and the corresponding positive-sequence current increases 8.33% as well.
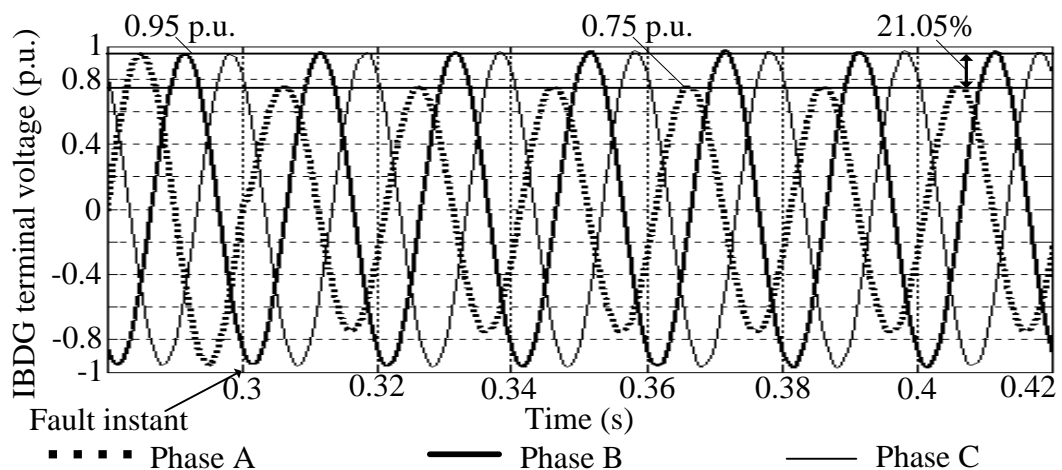
Figure 3.10 IBDG terminal voltage during a SLGF-under limit
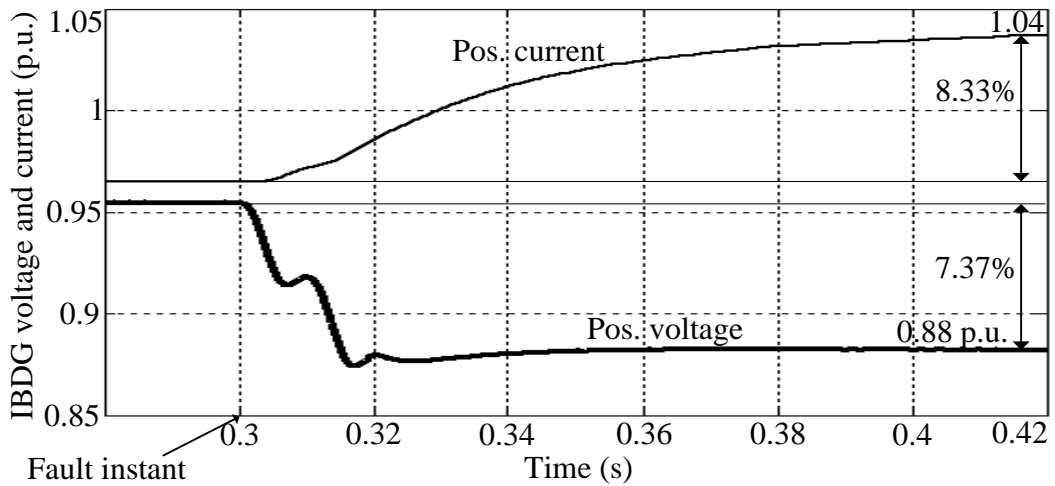
Figure 3.11 Positive-sequence voltage and current of an IBDG during a SLGF-under limit
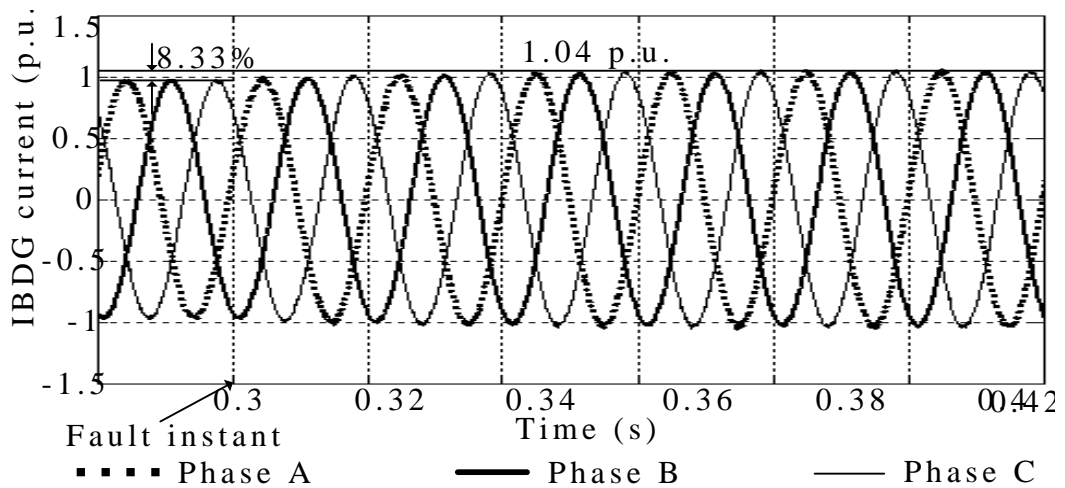
Figure 3.12 IBDG responses to a SLGF-under limit

If the changes of V_p involving high $I_{inv,ref}$ from (3.5) cause the corresponding dq components to reach the limit I_{thres} in Figure 3.3, the IBDG current will be forced to be at a predefined current even the output power is not around the set point. This case is illustrated from Figure 3.13 to 3.15. When a three-phase fault (3F) occurs with low fault impedance, the phase voltage drops. This drop causes the IBDG current to increase until it reaches the limits of I_{thres}=1.5 p.u. at time t=0.336 seconds. The IBDG is switched to the current source mode with $I_{inv,sat}$=1 p.u. (in IBDG rating) The IBDG terminal voltage is stable as of 52% of the rated voltage. Obviously, the generated active power cannot go back to the set value of 0.91 p.u. as in Figure 3.15.
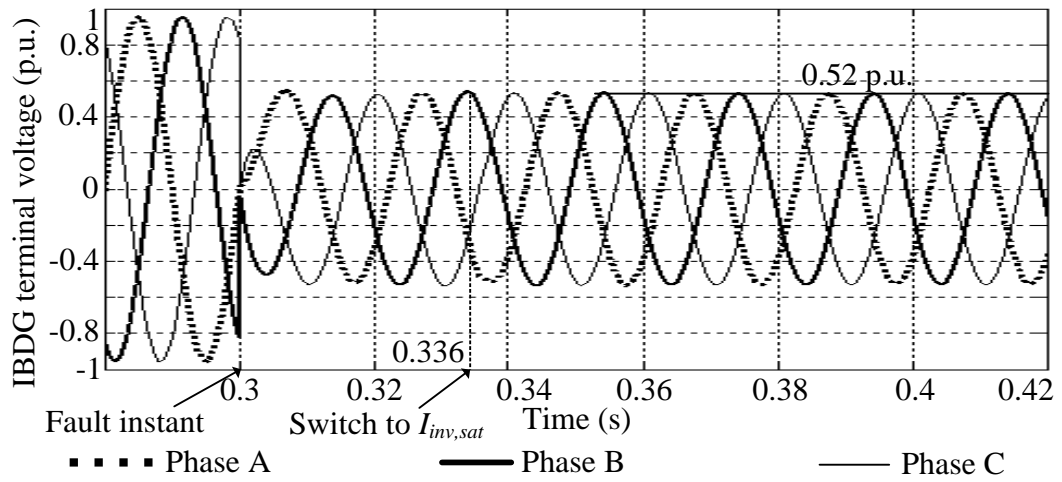
Figure 3.13 IBDG terminal voltage during a 3F-over limit
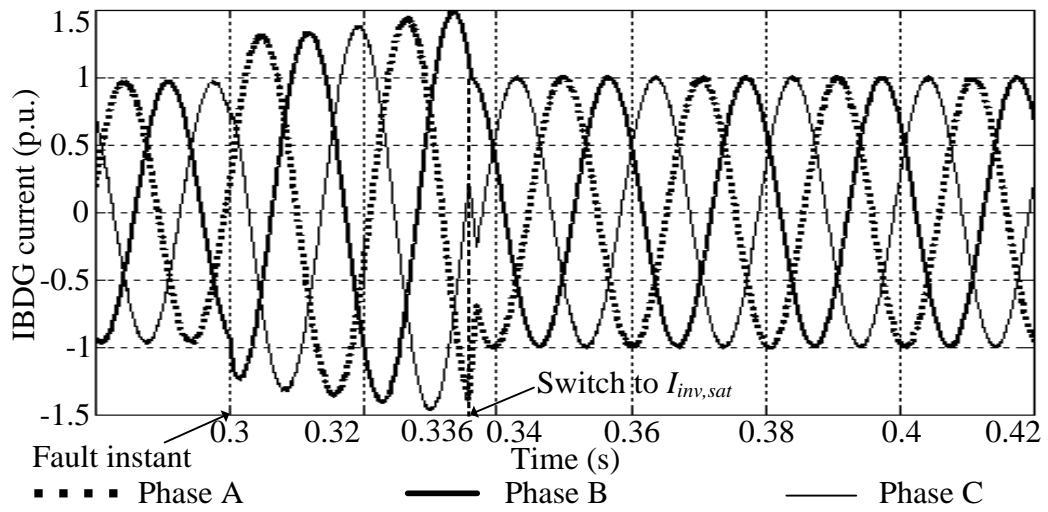
Figure 3.14 IBDG responses to a 3F-over limit
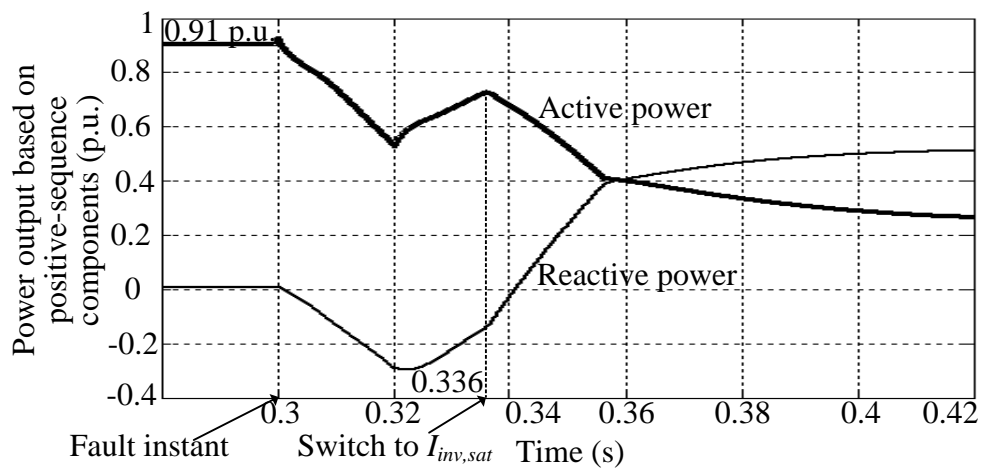
Figure 3.15 Output power of IBDG during a 3F-over limit

As discussed in Chapter 2, the dynamic voltage support is required when the IBDG rides through the fault. The saturated current $I_{inv,sat}$ can be adjusted so that it lags the terminal voltage V_p by $\pi/2$. This means, $\theta_0 = \pi/2$. In fact, the response in Figure 3.15 partly satisfies the support requirement because an amount of reactive power is injected to system after the IBDG is switched to current source of $I_{inv,sat}$. If this current is set so that $I_{inv,sat} = |I_{IBDG,rated}|\angle(\delta_{Vp}-\pi/2)$, i.e. the fully reactive current, the active power will decrease to zero. An example of fully reactive current support is illustrated in Figures 3.16. A DLGF causes the IBDG to be switched to current source that is controlled so that the current lags the terminal voltage by $\pi/2$. The reactive power increases from 0 p.u. to a stable value of 0.53 p.u.; whereas, the active power decreases from 0.91 p.u (prefault value) to zero.
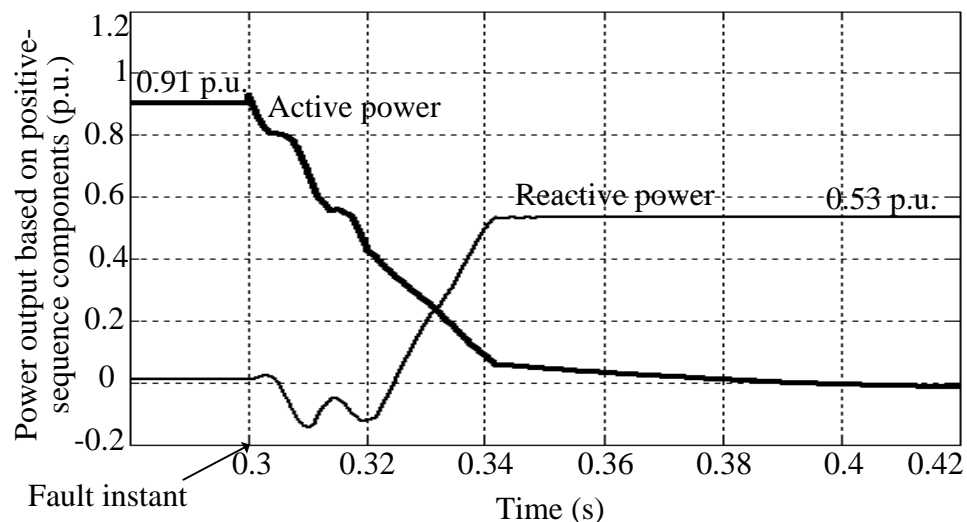
Figure 3.16 Output power of IBDG during a DLGF-fully reactive current

Some important conclusions about the fault response of the selected IBDG in this section can be listed here:

− An IBDG may remain connected to the system after a fault occurs due to the FRT requirement
− The transient period is short (3-4 cycles)
− The steady state period is established after the transient period
− Magnitudes of IBDG currents range from 0 to the limit ($\leq$ 2 p.u.)
− IBDG current includes most of positive-sequence component; components due to the harmonics can be neglected
− The IBDG current may be fully reactive to satisfy the FRT requirement

–   The output power is constant after a few cycles in both cases of the IBDG current: (1) under the limit and (2) at the limit

3.1.3 A Simple IBDG Model

From the conclusions at the end of Section 3.1.2, the short transient period can be neglected in the fault calculation for setting protective devices. Therefore, an IBDG is simply represented as a constant PQ source or a constant current source depending on the relation between $I_{inv,ref}$ and I_{thres} as illustrated in Figure 3.17. This model is explained as follows.
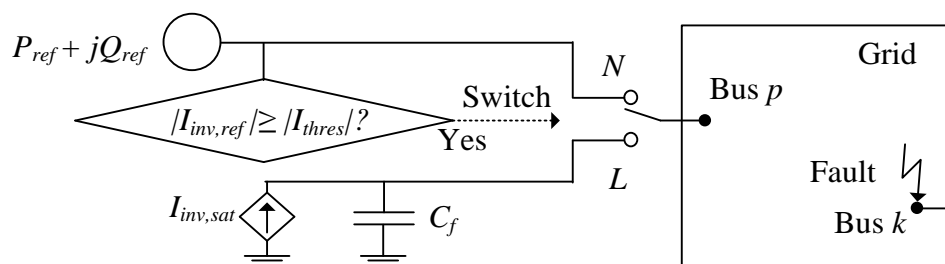
Figure 3.17 Model for IBDG under fault condition

When a fault occurs, an IBDG is modeled as a constant PQ source in the positive-sequence network (position N). The comparison between $I_{inv,ref}$ and I_{thres} in the positive-sequence values instead of phase values is acceptable because the control system filters out other components before pushing them to the current limiter as shown in Figures 3.1 and 3.2. In case of exceeding the threshold I_{thres}, the model of IBDG is switched to the position L and a constant current $I_{inv,sat}$ is injected into Bus p instead of the constant PQ. In addition, the capacitor of the filter is connected in parallel with the constant current source $I_{inv,sat}$.

Providing that the dynamic network support requirement is considered, the IBDG is controlled to inject a fully reactive current $I_{inv,sat}$ into the utility system to satisfy the DSOs requirement. Consequently, the IBDG is only modeled by the dependant current source in parallel with the filter capacitor C_f. The saturated current can be defined by (3.6).

$$I_{inv,sat} = \left| I_{IBDG,rated} \right| \angle \left(\delta_{Vp} - \theta_0 \right) \tag{3.6}$$

where $0 \leq \theta_0 \leq \pi/2$; $I_{IBDG,rated}$ is the rated current of the IBDG. In case of fully reactive support, $\theta_0 = \pi/2$.

Although the FRT requirement requires the reactive current injected to Bus p, the current controlled before the capacitor C_f as in Figure 3.17 can be acceptable. This is because the difference between current before and after the C_f is small. The inclusion of C_f in the model is to reflect more accurately the operation of the IBDG.

3.2 An Adaptive Algorithm for Fault Calculation

This section proposes an adaptive algorithm to calculate fault currents in a power system with IBDGs. The algorithm is based on the philosophy of the conventional fault calculation which uses the Thevenin's theorem and the bus impedance matrix [43]-[45]. It should be repeated that an IBDG is not modeled as a circuit of an independent constant voltage source in series with an impedance that has represented a synchronous generator conventionally. The Thevenin's theorem and the superposition method thus cannot be applied on the positive-sequence network [60]. However, they can be used in the negative and zero-sequence networks because the selected IBDG does not support these sequence currents as concluded in Section 3.1.2.

Similarly to the conventional fault calculation technique, the adaptive algorithm is demonstrated firstly with a three-phase balanced fault calculation. The calculation technique for an unbalanced fault is then developed by using the concepts of symmetrical components and the technique for the three-phase balanced fault calculation.

3.2.1 Algorithm for Three-phase Balanced Fault Calculation

The conventional fault calculation uses the Thevenin's theorem with the assumption that all voltage sources are independent. The superposition method can be applied to determine the fault voltage from the prefault voltage and the change in the network voltage caused by the current through the added branch (fault impedance). Nevertheless, a constant PQ source as a model of an IBDG is not an independent current or voltage source, causing the above method to be no longer to be applied and some adaptations are necessary here.

The proposed algorithm is performed on conventional system representations except the IBDG model. The faulty power system is represented in per-phase model as shown in Figure 3.18. Section 3.1.2 concluded that the steady-state period of the IBDG fault response was established very fast after the fault instant for all cases. In addition, the power balanced state was also established during the fault.
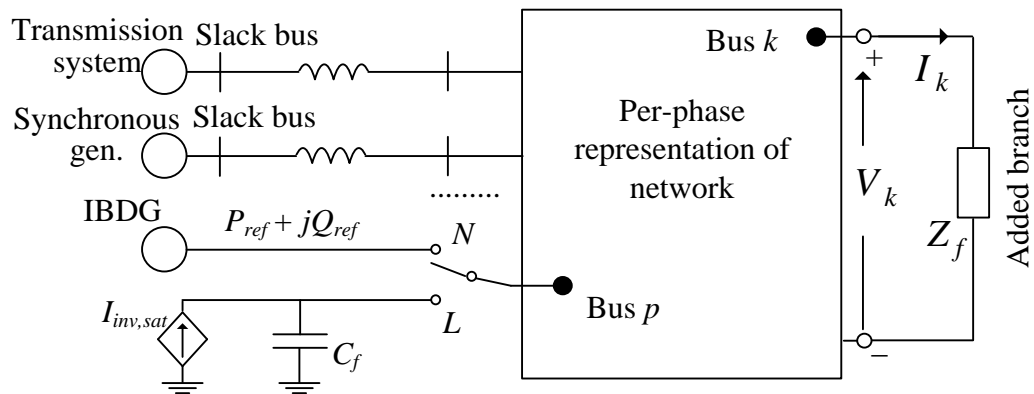
Figure 3.18 Network representations for 3F calculation

Applying Kirchhoff Current Law, the current entering Bus p (p = 1, ..., n) is equal to the sum of all currents from other buses in the system as given by (3.7) where Y_{pq} is the element of the bus admittance matrix.

$$I_p = \sum_{q=1}^{n} Y_{pq} V_q \qquad (3.7)$$

On the other hand, the entering current is specified by the total power entering to Bus p and the voltage at Bus p can be estimated by (3.8) where subscript (*) denotes the conjugate operator.

$$I_p = \frac{P_p - jQ_p}{V_p^*} \qquad (3.8)$$

Expressing (3.7) in polar form and substituting for I_p in (3.8) to form (3.9) where $Y_{pq} \angle \theta_{pq}$ is the polar form of an element of the bus admittance matrix Y_{bus}.

$$P_p - jQ_p = |V_p| \angle -\delta_p \sum_{q=1}^{n} |V_q| |Y_{pq}| \angle \left(\theta_{pq} + \delta_q \right) \qquad (3.9)$$

The active and reactive power entering to Bus p can be obtained by separating the real and imaginary parts of (3.9). They are expressed by (3.10) and (3.11).

$$P_p = \sum_{q=1}^{n} |V_p| |V_q| |Y_{pq}| \cos \left(\theta_{pq} - \delta_p + \delta_q \right) \qquad (3.10)$$

$$Q_p = -\sum_{q=1}^{n} |V_p||V_q||Y_{pq}| \sin\left(\theta_{pq} - \delta_p + \delta_q\right) \tag{3.11}$$

Nonlinear equations (3.10) and (3.11) can be solved by using iterative techniques such as Gauss-Seidel and Newton-Raphson. Because of the quadratic convergence, Newton-Raphson method is mathematically superior to the Gauss-Seidel method and is less prone to divergence with ill-conditioned problems. The equations are therefore represented in a form to be solved by using Newton-Raphson method (power flow-based technique).

Mathematically, (3.10) and (3.11) comprise $2n$ independent nonlinear equations for an n-bus system. Each bus has four variables: P_p, Q_p, $|V_p|$, and δ_p. Thus, there are $4n$ variables in $2n$ independent equations. In order to make these equations resolvable, the number of variables for each bus should be reduced to two. Practically, a bus in any power systems falls into one of the three types: load bus (P and Q are known), voltage-controlled bus (P and $|V|$ are known), and slack bus ($|V|$ and δ are known). The slack bus physically makes up the difference between the scheduled loads and generated power that are caused by losses in the network. Generally, there is only one slack bus needed in a power system. If the system has more than one slack bus, the power flow solution can be still reached because the number of variables is still equal to the number of equations ($2n$). This situation occurs in this research when an SBDG is modeled as a constant voltage source (including both magnitude and angle) and an impedance. Thus, the bus between the voltage source and the impedance is treated as one slack bus exclusive of another one from the transmission system source representation.

Expanding (3.10) and (3.11) in Taylor's series around the initial estimate $[\delta(0), V(0)]$ and neglecting all higher order terms result in a set of linear equations. The partial derivatives of (3.10) and (3.11) evaluated at $\Delta\delta_p(k)$ and $\Delta|V_p(k)|$ form elements of Jacobian matrix $J = [J_1, J_2; J_3, J_4]$ as given by (3.12). Elements of submatrices J_1, J_2, J_3, and J_4 can be found in any power systems textbooks.

$$\begin{bmatrix} \Delta P & \Delta Q \end{bmatrix}^T = J \begin{bmatrix} \Delta\delta & \Delta|V| \end{bmatrix}^T \tag{3.12}$$

For slack buses, both voltage magnitudes and voltage angles are known. As a result, the equations involving (ΔP, $\Delta\delta$), (ΔQ, ΔV), and the corresponding columns of the Jacobian matrix are eliminated. For voltage-controlled buses, the voltage magnitudes are known and the corresponding rows and columns are eliminated as

well. Therefore, if there are *s* slack buses and *m* voltage-controlled buses in the systems, there are ($n \times s$) active power constraints and ($n \times s \times m$) reactive power constraints.

An IBDG bus is treated as a PQ bus during fault if the reference current of the inverter does not exceed the threshold current. The entering power can be estimated by using (3.10)-(3.11). For exceeding situation, the IBDG is switched to a current source of $I_p^{inv,sat}$ with constant magnitude. The phase of this current depends on the phase of the terminal voltage so that the reactive power of the IBDG must be injected into the system. In practice, the phase of $I_p^{inv,sat}$ is adjusted by the control system until $I_p^{inv,sat}$ lags the terminal voltage by an expected angle, i.e. θ_0 in Section 3.1. However, in the algorithm being proposed here, the process is simpler as follows.

The phase α_p of $I_p^{inv,sat}$ is assumed to satisfy the reactive current requirement so that $\alpha_p = \delta_p - \theta_{0p}$ where δ_p is the phase of the terminal voltage V_p and θ_{0p} is the leading angle. Equation (3.8) can be rewritten as (3.13) where the generated power of the IBDG is no longer included in the entering power ($P_p + jQ_p$) in the first term.

$$I_p = \frac{P_p - jQ_p}{\left|V_p\right| \angle -\delta_p} + \left|I_p^{inv,sat}\right| \angle \alpha_p \tag{3.13}$$

Equation (3.13) is updated to (3.10) with $I_p^{inv,sat}$ to form (3.14).

$$P_p - jQ_p = \left|V_p\right| \angle -\delta_p \sum_{q=1}^{n} \left|V_q\right|\left|Y_{pq}\right| \angle \left(\theta_{pq} + \delta_q\right) - \left|V_p\right|\left|I_p^{inv,sat}\right| \angle \left(\alpha_p - \delta_p\right) \tag{3.14}$$

Substituting $\alpha_p = \delta_p - \theta_{0p}$ in (3.14) to obtain (3.15),

$$P_p - jQ_p = \left|V_p\right| \angle -\delta_p \sum_{q=1}^{n} \left|V_q\right|\left|Y_{pq}\right| \angle \left(\theta_{pq} + \delta_q\right) - \left|V_p\right|\left|I_p^{inv,sat}\right| \angle -\theta_{0p} \tag{3.15}$$

The entering power at Bus *p* is estimated by (3.16)-(3.17) by separating the real and imaginary parts of (3.15).

$$P_p = \sum_{q=1}^{n} \left|V_p\right|\left|V_q\right|\left|Y_{pq}\right| \cos\left(\theta_{pq} - \delta_p + \delta_q\right) - \left|V_p\right|\left|I_p^{inv,sat}\right| \cos\theta_{0p} \tag{3.16}$$

$$Q_p = -\sum_{q=1}^{n} |V_p||V_q||Y_{pq}|\sin\left(\theta_{pq} - \delta_p + \delta_q\right) - |V_p||I_p^{inv,sat}|\sin\theta_{0p} \qquad (3.17)$$

Obviously, the IBDG representation as a current source causes the diagonal elements of submatrices J_2 and J_4 to be changed as shown in (3.18)-(3.19).

Diagonal elements of the submatrix J_2:

$$\frac{\partial P_p}{\partial |V_p|} = 2|V_p||Y_{pp}|\cos\theta_{pp} + \sum_{q\neq p}^{n}|V_q||Y_{pq}|\cos\left(\theta_{pq} - \delta_p + \delta_q\right) - |I_p^{inv,sat}|\cos\theta_{0p}$$

$$(3.18)$$

Diagonal elements of the submatrix J_4:

$$\frac{\partial Q_p}{\partial |V_p|} = -2V_p|Y_{pp}|\sin\theta_{pp} - \sum_{q\neq p}^{n}|V_q||Y_{pq}|\sin\left(\theta_{pq} - \delta_p + \delta_q\right) - |I_p^{inv,sat}|\sin\theta_{0p} \quad (3.19)$$

The power mismatches $\Delta P_p(k)$ and $\Delta Q_p(k)$ are the algebraic differences between the scheduled power comprising the scheduled generated and load power and the estimated values obtained from (3.10)-(3.11) or (3.16)-(3.17). If the maximum power mismatch is less than a specified accuracy ε, voltage vector $V(k)$ is the expected solution. If not, the linear simultaneous equation (3.12) is now solved directly to obtain the corrections of the voltage magnitude $\Delta|V_p(k)|$ and the angle $\Delta\delta_p(k)$. The bus voltages are updated by these corrections. Note that these updates are not applied to slack buses for both voltage magnitudes and angles and voltage-controlled buses for the voltage magnitudes. Then, a new iteration is performed with $V_p(k+1)$ starting from (3.10)-(3.11) and (3.16)-(3.17).

The above process is diagrammatized in Figure 3.19. It is similar to a power flow algorithm based on the Newton-Raphson iterative technique. The differences are the formation of Y_{bus} and the update with the capacitor C_f, and then, changes in diagonal elements of the Jacobian matrix. Using iterative technique is a major adaptation compared to the conventional fault calculation which employs the Thevenin's theorem and the superposition method. At the IBDG bus, the reference current $I_{inv,ref}$ is computed at every iteration using (3.5). Once it reaches the threshold, the PQ source at Bus p is switched to the constant current source with the injected current $I_{inv,sat}$. In that case, a new branch occurs (the filter capacitor C_f) in the model of the IBDG as seen in Figure 3.18 causing a change in the system configuration. Thus, the

algorithm must restart. The bus admittance matrix Y_{bus} is updated with the occurrence of C_f. The maximum restarting number is equal to the number of IBDGs occupied in the system.
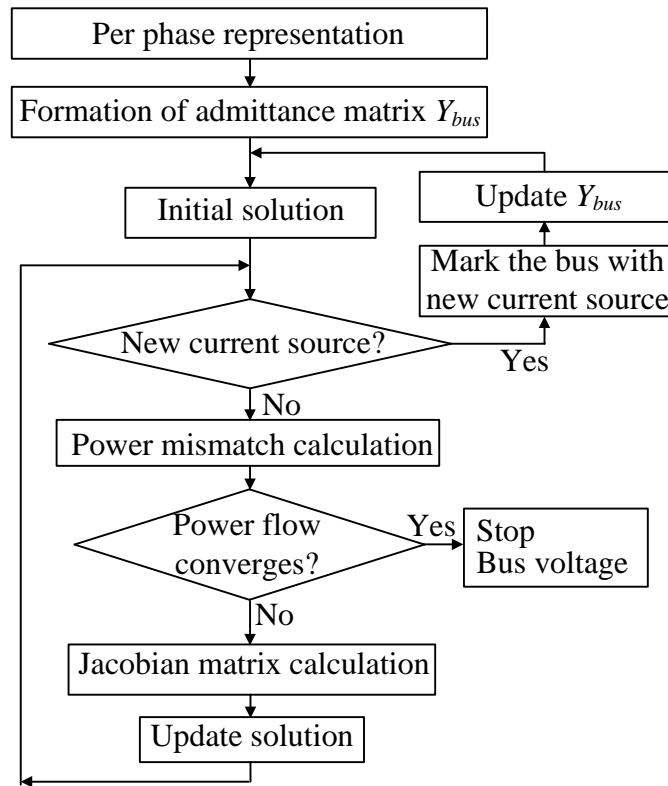
Figure 3.19 Algorithm for the adaptive balanced fault calculation

Results of the program comprise voltages at all buses. Line current vectors can be computed by using (3.20) that is the same as the equation in the conventional method.

$$I_{ij}(F) = \frac{V_i(F) - V_j(F)}{z_{ij}} \tag{3.20}$$

where z_{ij} is the impedance of line ij.

3.2.2 Algorithm for Unbalanced Fault Calculation

A sequence network connection circuited from positive, negative, and zero-sequence networks is performed similarly to the conventional fault calculation with some modifications. This network is treated in the same way as the system in Figure 3.18. However, the added branch is the equivalent impedance Z_{eq} of the circuit including the negative and zero-sequence networks instead of only Z_f; the network per-phase representation is replaced by the positive-sequence network.

The value of equivalent impedance Z_{eq} is determined according to the fault type as depicted in Figure 3.20 and detailed in Table 3.1. In case of a 3F, it is equal to Z_f; whereas, in case of an unbalanced fault, it is the equivalent impedance of the circuit comprising the negative and zero-sequence impedances occupying in the sequence network connection. For instance, Z_{eq} for a single line-to-ground is a sum of negative, zero-sequence Thevenin impedances, and three times of the fault impedance.

In order to calculate the unbalanced fault, the algorithm for balanced fault calculation is adjusted for determining positive-sequence voltages at all buses as depicted in Figure 3.21. The sequence currents at the faulted bus are obtained from the positive-sequence voltage V^1_k as summarized in Table 3.2.

Because the IBDG does not support the negative and zero-sequence currents as mentioned in Section 3.1.2, it will not appear in these sequence networks. Therefore, the negative and zero-sequence voltages are computed from the corresponding sequence current at the faulted bus using (3.21) where $Z^{0,2}_{ik}$ come from the zero and negative-sequence impedance matrices; $I^{0,2}_k$ come from Table 3.2. The sequence components of line currents are then obtained from the corresponding voltage using (3.22) where $z^{0,1,2}_{ij}$ are the zero, positive, and negative impedance of line ij.

$$V_i^{0,2} = 0 - Z_{ik}^{0,2} I_k^{0,2} \qquad (3.21)$$

$$I_{ij}^{0,1,2} = \frac{V_i^{0,1,2}(F) - V_j^{0,1,2}(F)}{z_{ij}^{0,1,2}} \qquad (3.22)$$
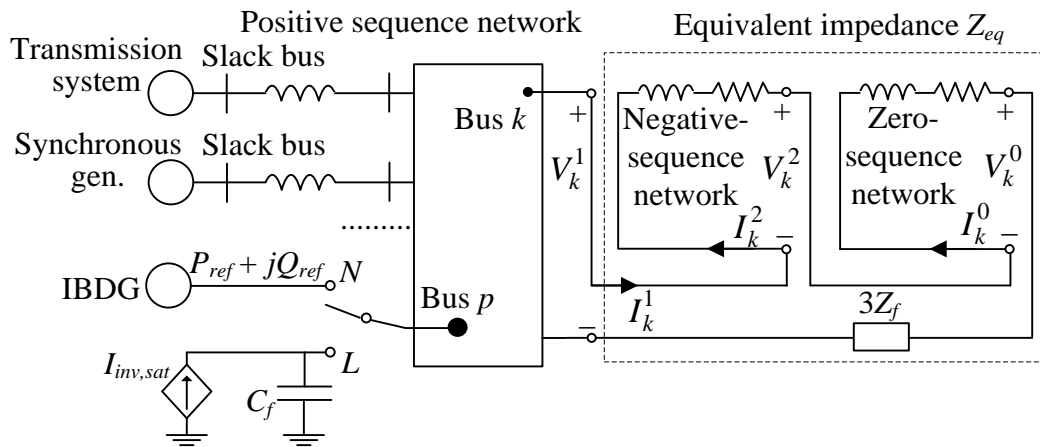
(a) SLGF
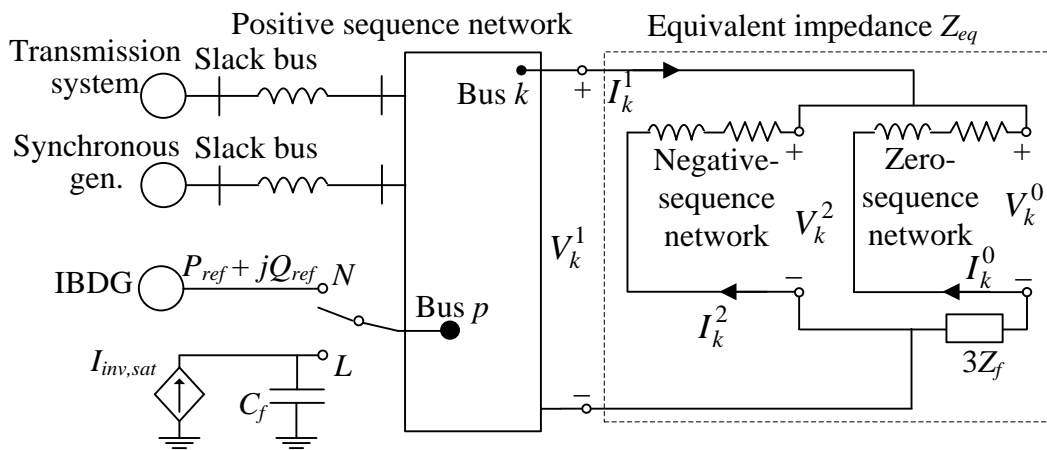
(b) DLGF
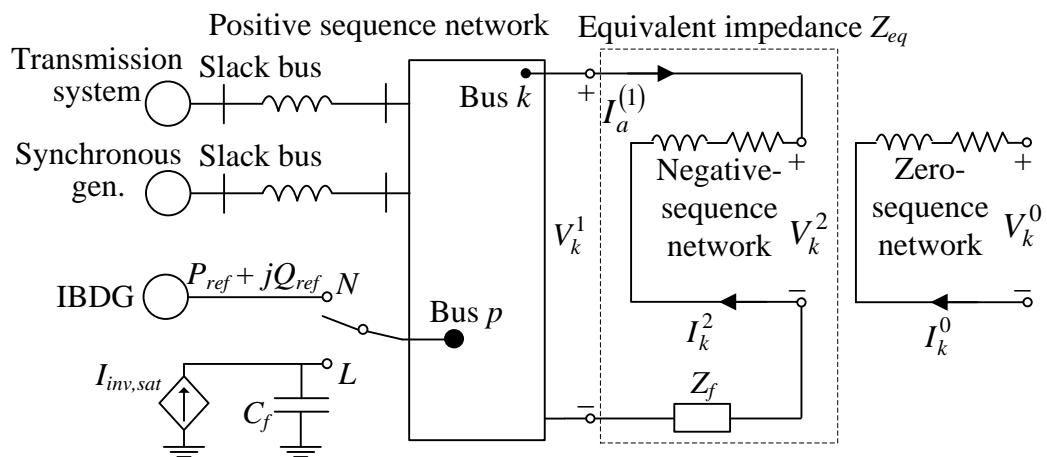
(c) LLF

Figure 3.20 Sequence network connections for an unbalanced fault

Table 3.1 Determination of equivalent impedance at the faulted bus

Fault types	Equivalent impedance, Z_{eq}
SLGF	$Z_{kk}^2 + Z_{kk}^0 + 3Z_f$
DLGF	$Z_{kk}^2\left(Z_{kk}^0 + 3Z_f\right)\Big/\left(Z_{kk}^2 + Z_{kk}^0 + 3Z_f\right)$
LLF	$Z_{kk}^2 + Z_f$
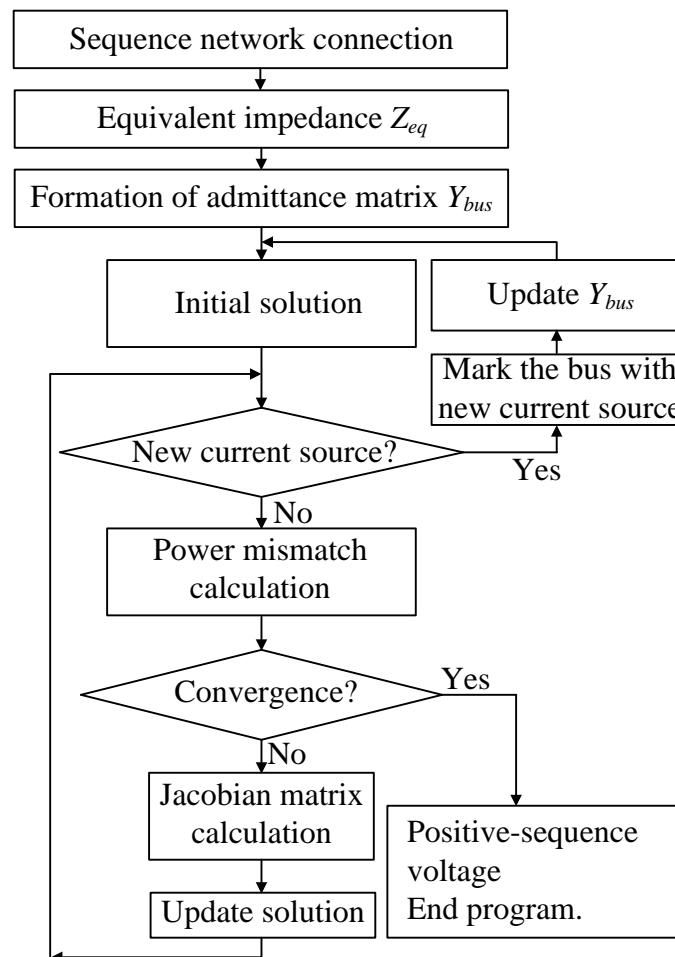
Figure 3.21 Algorithm for the adaptive unbalanced fault calculation

Table 3.2 Determination of sequence currents at the faulted bus

Fault types	Negative-sequence current, I^2	Zero-sequence current, I^0
SLGF	$I^2 = I^1 = V_k^1/Z_{eq}$	$I^0 = I^1 = V_k^1/Z_{eq}$
DLGF	$I^2 = -V_k^1/Z_{kk}^2$	$I^0 = -V_k^1/(Z_{kk}^0 + 3Z_F)$
LLF	$I^2 = -I^1 = -V_k^1/Z_{eq}$	$I^0 = 0$

3. 3 Summary of Chapter 3

This chapter explores the fault response of a selected IBDG with consideration of the FRT requirement including the capability of remaining connected and reactive current support during a fault. A simple model is proposed based on the analysis of the response. The model is then utilized by an adaptive fault calculation algorithm using Newton-Raphson iterative technique. This algorithm is executed in a modified sequence-network connection. Some adaptations compared to the conventional fault calculation are the employment of power flow-based algorithm, the formation of Y_{bus}, the update in Y_{bus} with the capacitor C_f, and changes in diagonal elements of the Jacobian matrix. The validation of the proposed algorithm will be illustrated in Chapter 5.

CHAPTER IV

MAXIMUM ALLOWABLE DISTRIBUTED GENERATION WITH CONSIDERATON OF FAULT RIDE THROUGH REQUIREMENT AND UTILITY PROTECTION SYSTEM

This chapter proposes algorithms to determine the maximum allowable distributed generation. The reach reduction of utility relay is emphasized so that it becomes a constraint in combination with system operating limits to maximize the DG as mentioned in Chapter 2. In order to analyze the effects of DG on the protection reach reduction, both the "phase" and "ground" faults are included. This involves the consideration of DG transformer connection. Section 2.3.2 has already analyzed this issue and proposed the grounded wye-delta transformer for connecting DG to the utility system. This chapter firstly analyzes the utility relay reach reduction in Section 4.1 in more details than the discussion in Section 2.3.1.1. Then, the temporary overvoltage problem, which may occur if a part of the system is unintentionally islanded, is captured in Section 4.2. Lastly, Section 4.3 develops a practical and robust algorithm for maximizing DG by employing a sensitivity-based method. This method gradually increases the size of DG until the constraints of system operating limits and protection reach reduction are violated. In order to extend the method for several DGs, a multi-variable optimization problem is formulated and resolved by employing Tabu search algorithm as presented at the end of this chapter.

4.1 Analysis of DG Impacts on Utility Relay Reach

The protection reach reduction problem, as introduced in Chapter 2, occurs at any DG size. It increases the tripping time of relays. In the worst case, overcurrent-based protective devices are blind, meaning that they cannot detect a fault in the protected area and take its responsibility.

4.1.1 SBDG Impact on Utility Relay Reach

4.1.1.1 Reach Reduction of Phase Overcurrent Function (POF) (3F and LLF)

Figure 4.1 (a) illustrates a network representation of a simple system with one source represented by impedance Z_1. When a three phase fault occurs at Bus 3, the condition can be simulated with a Thevenin voltage or a prefault voltage, $V_3(0)$, connected in series with a fault impedance, Z_f, at Bus 3. The fault current flowing through the source (system substation) is calculated by (4.1).
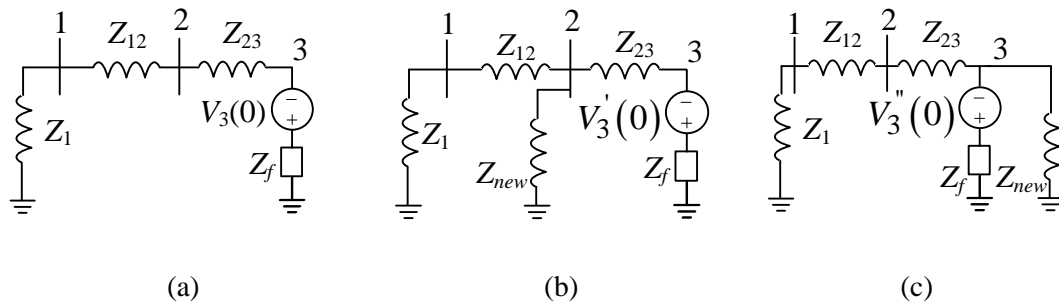
Figure 4.1 Equivalent networks of simple system

$$I_{12} = \frac{V_3(0)}{Z_1 + Z_{12} + Z_{23} + Z_f} \tag{4.1}$$

where $V_3(0)$ indicates the prefault voltage at Bus 3, and Z_f indicates the fault impedance.

Figure 4.1 (b) and (c) represent the equivalent networks after installing a new source (SBDG) represented by impedance Z_{new} at Buses 2 and 3, respectively. The fault currents flowing through the substation are given by (4.2) and (4.3), respectively.

$$I'_{12} = \frac{V'_3(0)}{Z_1 + Z_{12} + Z_{23} + Z_f + \left(Z_f + Z_{23}\right)\left(Z_1 + Z_{12}\right)/Z_{new}} \tag{4.2}$$

$$I''_{12} = \frac{V''_3(0)}{Z_1 + Z_{12} + Z_{23} + Z_f + Z_f\left(Z_1 + Z_{12} + Z_{23}\right)/Z_{new}} \tag{4.3}$$

where $V'_3(0)$ and $V''_3(0)$ indicate prefault voltages at Bus 3 after the new source is added into Buses 2 and 3, respectively.

It is evident that adding a new source usually results in reduction of fault current flowing through the old source (utility substation). The smaller the new source impedance is, the more the reduction is. However, the current flowing through the substation does not depend on SBDG impedance when a fault occurs at the terminal of the new source with zero fault impedance as in Figure 4.1 (c). In case the SBDG impedance is large enough, the reduction amount will be small so that the utility relay is still able to sense the fault. This means the relay sensitivity, represented by the ratio of fault current through the relay to the corresponding relay pick-up current, is high enough (larger than 1) for the relay to operate. This can be achieved by limiting the

SBDG size because of the inverse relationship between the SBDG size and its transient reactance.

In practice, setting of utility relay, i.e. the POF, is based on the current under the maximum load condition. Before adding the SBDG, this current can be estimated from a load flow program with the maximum system load condition. Settings of the SBDG relay are based on the current generated at the nominal SBDG power. Thus, the pick-up current of the SBDG relay will increase if the generator size increases. Figure 4.2 illustrates the relation between the generator size and the pick-up current of its relay. In order to detect a fault successfully, the sensitivity of utility relay must be higher than one. This is obtained if the SBDG size is smaller than the $SBDG_{max}$ as shown in Figure 4.2.
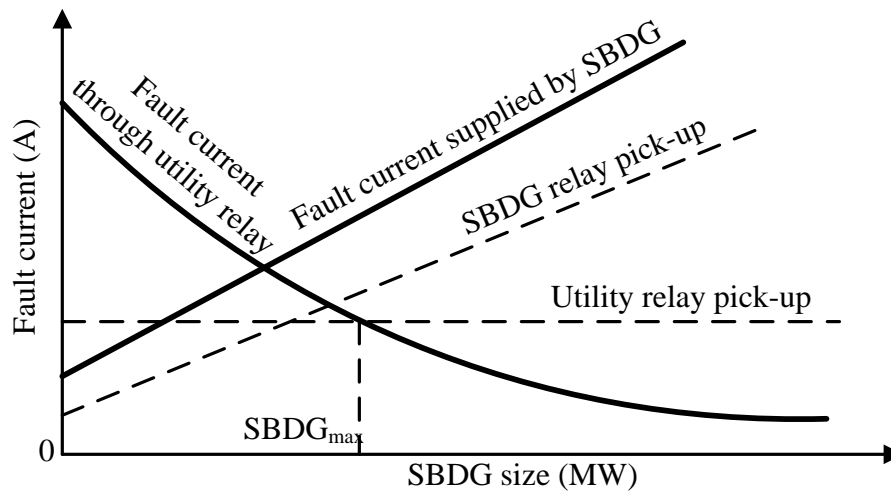
Figure 4.2 Impact of DG size on the POF

4.1.1.2 Reach Reduction of Ground Overcurrent Function (GOF) (SLGF and DLGF)

The analysis of SBDG impacts on GOF is based on the changes of residual current, which is equal to three times of zero-sequence current in each phase. The connection and grounding types of the interconnection transformer should be taken into account. The grounded wye (utility)-delta (SBDG) transformer is assumed to be used as discussed in Chapter 2. Generally, impacts on GOF are the same as the one analyzed in Section 4.1.1.1. However, in the case of ground faults, the zero-sequence impedance at the SBDG side plays an important role and needs clarifying. This impedance can be varied by adjusting the value of grounding reactance (or neutral reactance) at the wye winding's neutral point of the interconnecting transformer. That

is, the residual current through the interconnection transformer's neutral point decreases in proportion to the grounding reactance. Similarly to the POF, as the residual fault current from the SBDG is smaller, the reduction amount of utility residual current is also smaller. Consequently, this can help transformer and other devices avoid encountering a high fault current. However, if the residual current through the SBDG relay is lower than the pick-up current, the fault will not be detected.

4.1.2 IBDG Impact on Utility Relay Reach

Model of an IBDG depends on how it responds to voltage drops at the PCC. Chapter 3 has selected a control system so that the IBDG responds to only the positive-sequence voltage at the PCC to keep the power output constant and the current from the IBDG will be always symmetrical. The IBDG controls its output current so that the expected power based on the positive-sequence component of voltage and current is obtained. If the reference current, which is estimated by the expected power and the positive-sequence voltage at the IBDG terminal during fault, exceeds a threshold value I_{thres}, the IBDG is switched to constant current mode as represented in Chapter 3. The predefined current $I_{inv,sat}$ in this mode is to protect the power electronic components from thermal damage. Providing that the dynamic network support requirement is considered, a modified model depicted in Figure 4.3 can be used. Under fault condition, the IBDG is controlled to inject a fully reactive current $I_{inv,sat}$ into the utility system to satisfy the DSOs' requirement. Consequently, the IBDG is only modeled by the dependant current source in parallel with the filter capacitor C_f.

Impact of IBDG on utility relay reach reduction can be predicted by using the model in Figure 4.3. There is a particular amount of reactive power injected to the system during fault. This injection partly compensates the reactive power demand in the system and causes the voltage higher than that of system without the IBDG. Consequently, the current through the utility breaker of the substation source is lower than that of system without the IBDG. Similarly to the analysis in Section 4.1.1, the reduction shortens the protected area set for the utility relay. However, the reduction may be not large because the injected reactive power is small compared to the demand during fault.

$$I_{inv.sat} = I_{IBDG,rated} \angle \left(\delta_{VG} - \frac{\pi}{2} \right)$$

C_f
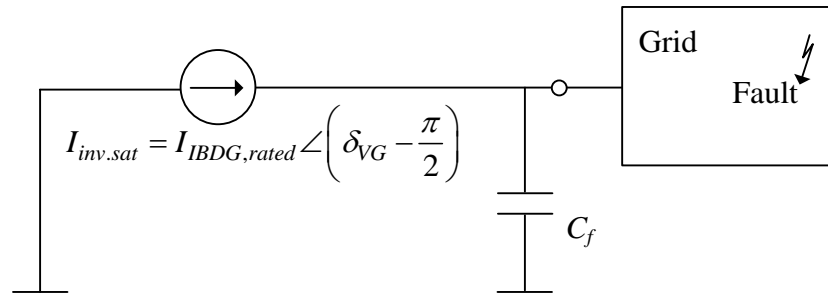
Figure 4.3 Modified model of an IBDG with network support requirement

4.2 Analysis of Temporary Overvoltage Problem

In case of an effectively grounded system, the coefficient of grounding (COG), which is the ratio of line-to-ground power-frequency voltage on a healthy phase at a selected location during a SLGF, to the line-to-line power-frequency voltage at that selected position with the fault removed, is less than or equal to 80% [61], [62]. As a result, the insulation cost is cut down by the phase-to-ground voltage level at the designing stage.

If the ground fault is contributed by only the utility system or both the utility system and the DG, the overvoltage may be insignificant because of the effective grounding mode. However, in some cases, the unintentional islanding occurs when a portion of the distribution system becomes electrically isolated from the remainder of the system. Under this condition, the isolated system is still energized by the DG. With the wye winding grounded through a reactance as shown in Figure 2.8, the overvoltage may be significantly high. Unfortunately, the minimum operating time of the protection system and the circuit breakers is typically longer than the overvoltage withstanding capability of utilized devices such as string insulators which are designed for the effectively grounded system. Although Section 2.3.2 proposes to use a grounding reactance, here, it must be limited in size. However, as long as the fault calculation program has been executed, the line-to-ground overvoltage under fault condition is easily achieved. In most cases, the fault is de-energized and this overvoltage is temporary. Suppose that the line-to-ground voltage with the fault removed is 1 p.u. and the maximum acceptable COG is 80%, then the corresponding temporary overvoltage (TOV) will be 1.39 p.u.

In summary, the DG impacts on the relay reach reduction and the TOV problem must be considered before a DG is installed in a power system. They will be taken into account in building up the DG maximization algorithms later.

4.3 Sensitivity-based Method for Maximizing SBDG

As mentioned earlier, adding SBDG may cause confusion to the relay in operation. In addition, system operating limits and the TOV limit due to ground faults should be considered. The following sections will firstly formulate a maximization problem before constraints of system operating limits, POF, GOF, and TOV are combined to build up an algorithm. The algorithm increases the SBDG size step by step (sensitivity-based) until a maximum value of P_{SBDG} is found.

4.3.1 Formulation of Maximization Problem

Objective function:

$$Max:\ P_{SBDG} \tag{4.4}$$

Subject to:

$$\begin{cases} g\left(P_{SBDG}\right)=0 & \text{(4.5)} \\ h\left(P_{SBDG}, X_N\right)>0 & \text{(4.6)} \end{cases}$$

The equality constraint (4.5) contains power flow equation; whereas the inequality constraint (4.6) contains system operating limits and the reach reduction of relays.

4.3.2 Constraints of System Operating Limits

Adding SBDG will change power flows in the utility system. It may cause some distribution lines and the substation transformer to be overloaded or bus voltages to exceed the limits. Constraints of system operating limits include all equalities and inequalities from (4.7) to (4.11).

SBDG capacity:

$$S_{SBDGmin} \leq S_{SBDG} \leq S_{SBDGmax} \tag{4.7}$$

Power flow equation:

$$\left[\Delta P \quad \dots \quad \Delta Q\right]^T = \begin{bmatrix} J_1 & J_3 \\ J_2 & J_4 \end{bmatrix} \left[\Delta\theta \quad \dots \quad \Delta|V|\right]^T \tag{4.8}$$

Substation capacity:

$$\left|S_{sub}\right| \leq\ S_{sub,\max} \tag{4.9}$$

Line capacity:

$$\left|S_{mn}\right| \leq \; S_{mn,\max} \tag{4.10}$$

Bus voltage:

$$V_{\min} \leq V_{\mathrm{i}} \leq V_{\max} \tag{4.11}$$

4.3.3 POF Constraints

In Figure 4.4, the SBDG is increased in size from the minimum value step by step. In each step, the constraints of system operating limits and POF must be satisfied. If not, the iteration stops then the maximum SBDG size is determined. To identify whether the constraints of POF are satisfied, both three-phase and line-to-line faults are applied sequentially at each bus inside the required protected area. As long as the utility and SBDG relays can detect all faults, these constraints are satisfied.
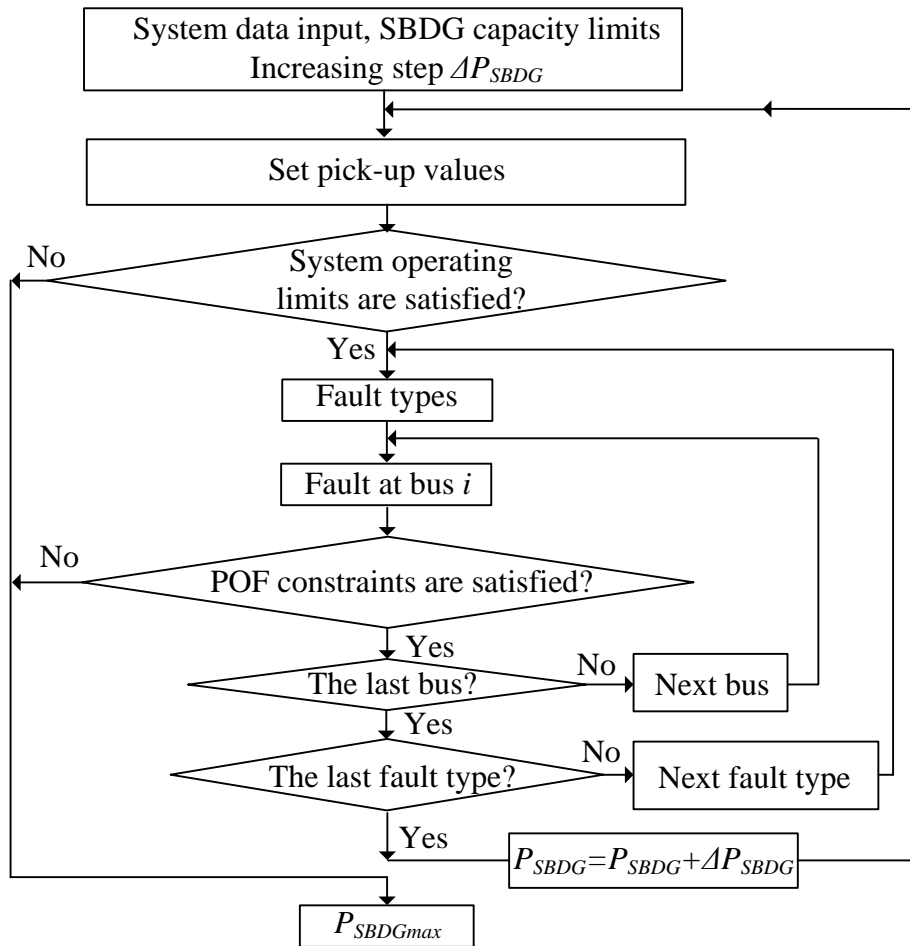
Figure 4.4 Algorithm to maximize DG considering POF

Regarding Section 4.1, POF constraints are to remain the normal operations of both utility and SBDG relays in POF:

Utility relay: $$I_{fault}^{utility\,relay} > I_{pick-up}^{utility\,relay}$$ (4.12)

SBDG relay: $$I_{fault}^{SBDG\,relay} > I_{pick-up}^{SBDG\,relay}$$ (4.13)

4.3.4 GOF Constraints

The maximum DG obtained from Figure 4.4 ensures to remain the operation of the POF. However, the GOF of utility relay may not sense the ground faults inside the required protected area. As mentioned in Chapter 2, a grounding reactance should be installed at the SBDG transformer's neutral point. This impedance plays the part of parallel impedance with the existing zero-sequence impedance at the SBDG side. Consequently, the relay at the SBDG side will sense the smaller fault current while the fault current through the utility relay will be less reduced as well. Generally, this reactance is expected to be as low as possible for cutting down the investment and operation cost.

By increasing step by step the grounding reactance, X_N, and applying ground faults at all buses sequentially inside the required protected area, the first X_N, at which both the utility and the SBDG relays can sense the fault, is the minimum reactance. Figure 4.5 illustrates the algorithm to determine the minimum grounding reactance. If X_N is stepped forward from X_{Nmin}, the ground fault current through SBDG relay decreases and may become lower than the pick-up current for the SBDG relay to detect the fault. Therefore, the reactance is limited by the constraints of the GOF of SBDG relay. The algorithm for determining X_{Nmax} is shown in Figure 4.6.

4.3.5 TOV Constraints

Regarding Section 4.3.4 if X_N is too large, TOV may exceed the limitation of 1.39 p.u. Therefore, the maximum acceptable grounding reactance, X_{Nmax}, must be specified. The algorithm for determining X_{Nmax} under the islanding condition is similar to the algorithm in Figure 4.6 but the GOF constraints checking block is replaced by the TOV checking block given by (4.14) and the number of faulted buses depends on the section where the islanding occurs. Moreover, X_N in this algorithm starts from zero instead of X_{Nmin} in Figure 4.6.

$$TOV_i \le 1.39\,p.u.$$ (4.14)
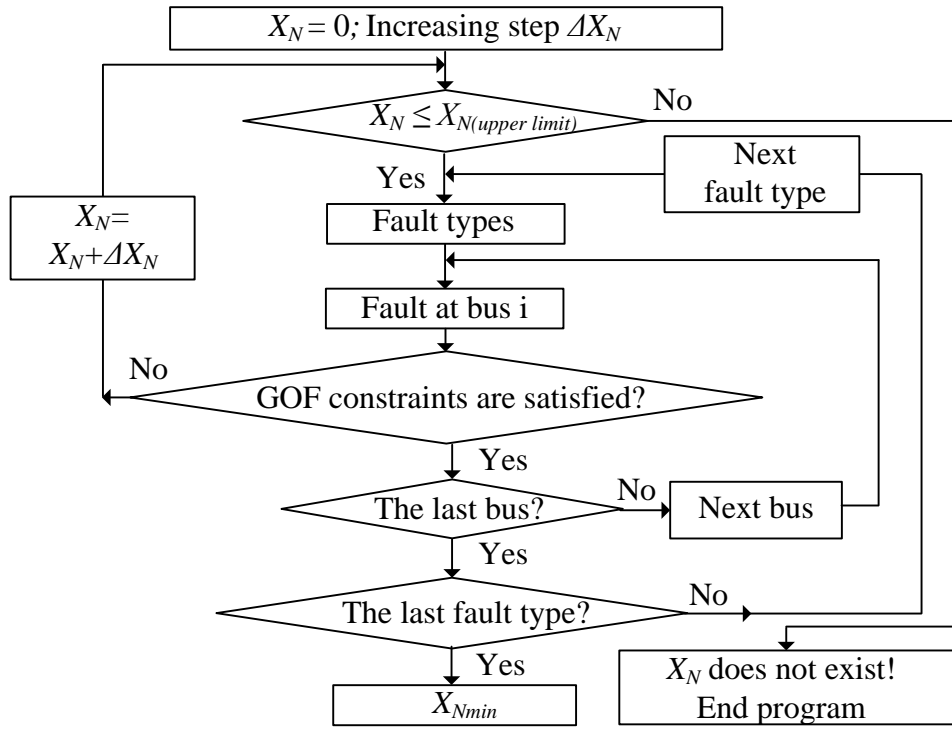
Figure 4.5 Determination of X_{Nmin} under ground fault conditions
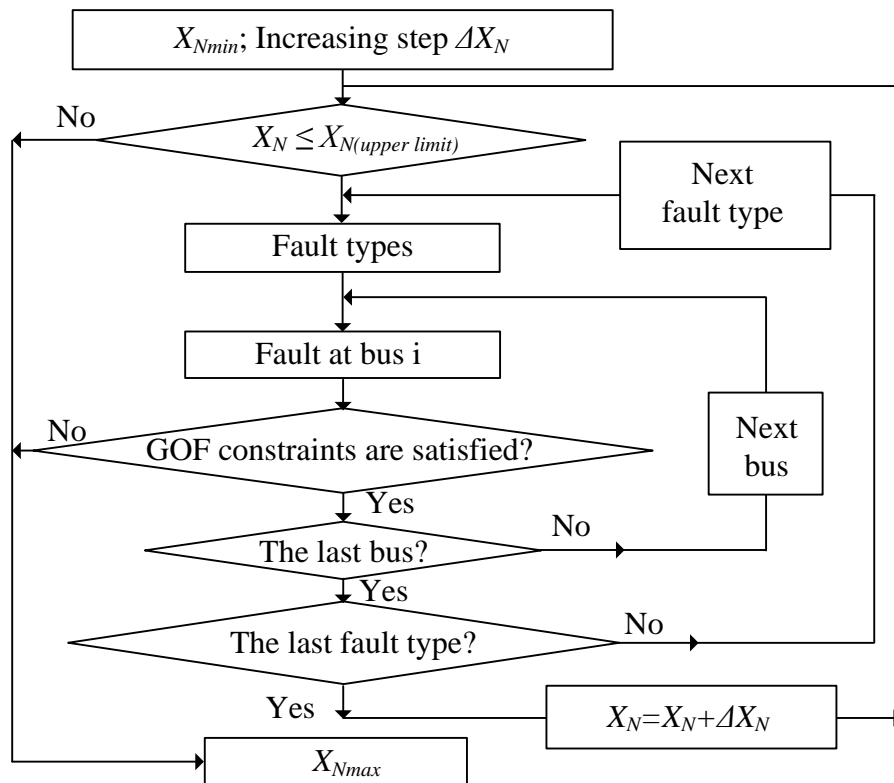
Figure 4.6 Determination of X_{Nmax} under ground fault conditions

4.3.6 Summary of Sensitivity-based Algorithm

The algorithm for determining $P_{SBDGmax}$ along with an acceptable range of X_N can be summarized in Figure 4.7. At each value of P_{SBDG}, constraints of system operating limits are checked first. If these constraints are satisfied, the POF and GOF constraints are analyzed to determine $P_{SBDGmax}$ and an acceptable range of X_N. Lastly, X_{Nmax} is adjusted lower after the TOV constraint check.
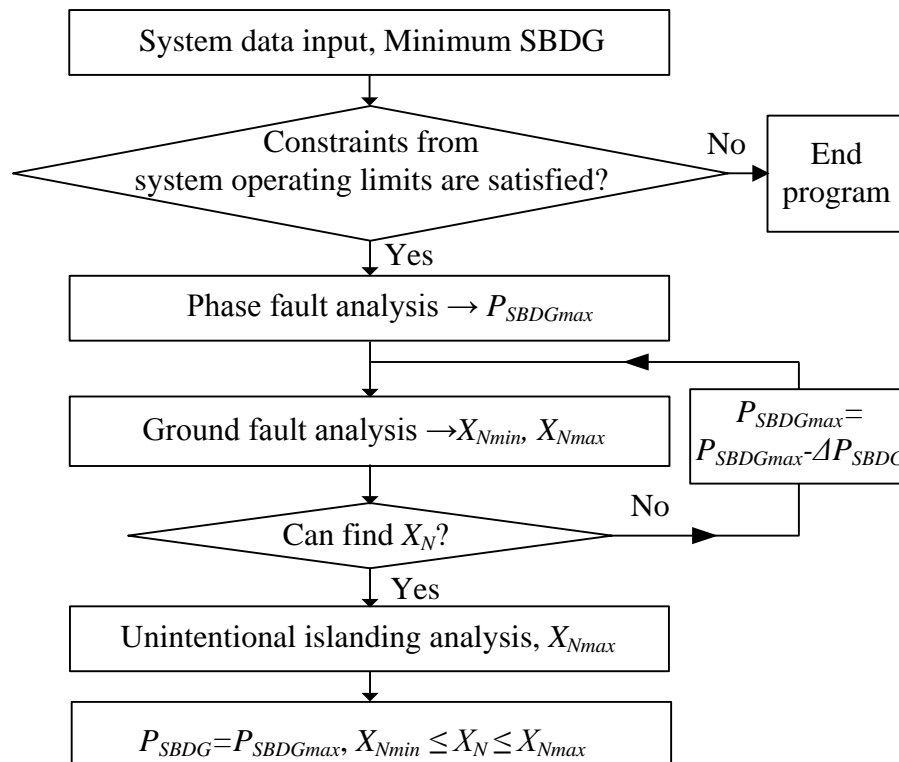
Figure 4.7 Algorithm to determine the optimal SBDG size

4.4 Tabu Search for Maximizing DG

The sensitivity-based method is suitable for one variable, i.e., one DG unit. In more practical situations, this method consumes much time for solving multi-variable optimization problems, i.e., several DG units. To reduce the running time, the number of checking points should be cut down. This problem can be resolved by Tabu search method [63]-[65]. The problem in Section 4.3 is reformed in another objective function formulation where all DG units are variables and the total size is expected to be maximized.

4.4.1 Maximization of SBDG Using Tabu Search

The problem in Section 4.3 is reformed as follows.

4.4.1.1 Optimization Problem Reformulation

Objective function

$$Max : P_{SBDG} = \sum_{i=1}^{n} P_{SBDG,i} \qquad (4.15)$$

In (4.15), *n* is the total number of SBDG units installed in the system. The objective function in Section 4.3 is the case of $n = 1$.

Constraints

All constraints can be summarized from Section 4.3 as shown in (4.7)-(4.11) and (4.16)-(4.18):

- Constraints of system operating limits: (4.7)-(4.11).
- Constraints under fault condition:

Utility relay: $\Delta I_{utility} = I_{fault,utility} - I_{pick\text{-}up,utility} > 0$ $\qquad (4.16)$

$$I_{fault,utility} = f(P_{SBDG}, X_N)$$

SBDG relay: $\Delta I_{SBDG} = I_{fault\,(SBDG)} - I_{pick\text{-}up\,(SBDG)} > 0$ $\qquad (4.17)$

$$I_{fault,\,SBDG} = g_1(P_{SBDG}, X_N), I_{pick\text{-}up,\,SBDG} = g_2(P_{SBDG})$$

Overvoltage due to ground faults: $TOV = h(P_{SBDG}, X_N) \leq 1.39\,p.u.$ $\qquad (4.18)$

4.4.1.2 Tabu search algorithm

Important aspects including neighborhood generation, moving attributes, diversification, and stopping criteria of the Tabu search algorithm proposed in [63]-[65] are analyzed in this section.

a. Neighborhoods definition

It is assumed that each DG is operated at the constant power factor mode. The S_{DG} is therefore represented by the active power P_{DG}. From a current point P_{cur}, a neighborhood P_{neigh} can be defined by (4.19).

$$P_{neigh} = P_{cur} + s.*\Delta P \qquad (4.19)$$

where $\Delta P = [\Delta P_i]$ is the incremental amount vector of DG size, $i = 1...n$ and the operator (.*) indicates the product of two elements which have the same position in two matrices. The vector $s = [s_i]$, which has the same size as ΔP, must be non-zero to

adjust P_{cur}. Each element s_i has one of three values: -1, 0, and +1. A random generator is employed to generate all elements of the vector s.

b. Moving attributes

After N_{neigh} neighborhoods are generated, they are sorted in a descending order based on their objective function values. Neighborhoods in the new order are named candidate list. Then, the searching process moves to the top of the list and checks the constraints at that element. If all constraints are not satisfied, the searching process moves downward to the next element until it reaches an element that satisfies all constraints.

In order to prevent the algorithm from going back to the rejected neighborhoods after moving to the best one, a short-term memory is utilized in the form of the Tabu list. The list keeps all rejected neighborhoods for a particular iteration number, which is named Tabu tenure. For instance, if the tenure is set to 10, an element of the Tabu list is released after 10 consecutive iterations. Once being released, the element is ready to be selected as a candidate in the next iteration.

The flexibility to choose a good move may be improved by adding an aspiration criteria function. If a candidate configuration is in the Tabu list but satisfies the aspiration criterion, its Tabu status can be overridden. In this section, the aspiration criterion is defined as the best value of the objective function. That means, when a a vector P_{DG} is likely to be the best neighborhood of the current point but being realized as a Tabu element, the objective function value is evaluated for this point. If the obtained value is less than the current best value, the P_{DG} is chosen to be a new solution.

c. Diversification

The searching process is diagnosed with falling in a trap of local optimum if at least one of the following symptoms occurs.

1. After a specific number of consecutive iterations, e.g. $count_{max}=10$, the current optimum has not been updated by a better one. A variable $count$ is increased by 1 whenever a current optimum is not updated. Otherwise, it is reset to zero.

2. There is no feasible candidate to update the current solution. A case for this symptom to occur is when all generated neighborhoods do not satisfy the constraints or they are Tabu elements and do not satisfy the aspiration criteria at the same time. Whenever a diversification is performed, the variable $count$ is reset to zero.

A diversified moving technique assists the searching process in escaping the trap. The simplest method is to force the searching direction to move to a neighborhood that does not follow the chosen moving attributes. For instance, a new point is generated randomly to become an initial solution. Then, the searching process continues following the moving attributes in Section (b) until it falls into another trap of local optimum.

d. Stopping criteria

The searching algorithm stops when the total number of iterations exceeds a specific value, e.g., it_{max}=100. The last best solution is assumed to be the global optimum, i.e. the final solution of the optimization problem. The it_{max} setting affects noticeably on the number of diversifications, hence, the possibility to arrive at the global optimum. Although a huge iteration number brings higher possibility of reaching the global optimum, it requires higher computational cost as well. Therefore, the limit of the iteration number depends on each optimization problem and is usually selected empirically.

e. Flow chart of the algorithm

Figure 4.8 illustrates a flow chart of the Tabu search algorithm for SBDG maximization. The algorithm starts with an initial solution that satisfies all constraints (4.7)-(4.11) and (4.16)-(4.18). The current solution is now set to the initial one and so is the current best optimum. A set of *s* is then generated randomly to create N_{neigh} neighborhoods of the current solution. The candidate list is formed based on the objective function values (4.15) of those neighborhoods: These values are sorted in a descending order. The corresponding index is used to order of the neighborhoods to form the candidate list. Starting from the top element of the candidate list, all constraints are checked. The first element at which all constraints are satisfied is selected as the best neighborhood to update the current solution.

The Tabu status and the aspiration criterion are checked before updating the current solution, which is the best neighborhood. Rejected neighborhoods are then added into the Tabu list. The objective function value of the current solution $f(x_{cur})$ is compared to the one of the current best optimum $f(x_{best})$ as the following logic.

{ if $f(x_{cur}) > f(x_{best})$ then

    Update the current best solution: $x_{best} = x_{cur}$;

    Reset the consecutive not updating times: count = 0;

  else Increase the consecutive not updating times: count = count + 1

end }

The diversification is then checked as the following logic.

{ *if count > count$_{max}$ then*

    Diversification: x$_{cur}$ = random(P$_{DG}$);

    Reset the consecutive not updating times: count = 0;

else Increase the iteration index: it = it + 1

end }

The above process is repeated until *it > it$_{max}$*. The last "current best solution" is assumed to be the global optimum: *x$_{opt}$ = x$_{best}$*.

It can be seen that for each value of vector *P$_{DG}$ = P$_{DGmax}$* in Figure 4.8, there may be a grounding reactance vector *X$_N$* that can assist the vector *P$_{DG}$* in satisfying constraints. This is because fault currents and *TOV* are affected by *X$_N$* as shown in (4.16)-(4.18). The question is how much the *X$_N$* should be to assist the *P$_{DG}$*. If we assumed that the small grounding reactance is better for savings such as the investment and maintenance cost, *X$_N$* should be minimized. The Tabu search algorithm continues to be applied to determine the minimum *X$_N$* that can aid the expected *P$_{DG}$* in satisfying constraints. This algorithm is illustrated in Figure 4.9. There are two situations as follows.

1. *X$_N$* does not exist: This means the expected *P$_{DG}$* is too high. The output of the block "Satisfy constraints" in Figure 4.8 is "No". The next point of the candidate list is thus selected to repeat looking for another *X$_N$*.

2. A vector *X$_N$ = [X$_{Ni}$]* is found: *X$_{Ni}$* is the grounding reactance at the transformer neutral point of *DG$_i$*. The output of the block "Satisfy constraints" in Figure 4.8 is "Yes".

The block "Does [*P$_{DG}$, X$_N$*] satisfy constraints?" is explored in Figure 4.10 where all constraints of system operating limits, POF, GOF, and TOV are checked. This process comprises two steps: (1) running load flow for the system operating limits constraints and (2) calculating fault current for the reach reduction constraint. A conventional fault calculation program is employed at this step to estimate phase and residual currents flowing through the utility relay and the SBDG relays, and then, bus voltages in unintentional islanding. The currents are compared to the respective overcurrent pick-up values for testing operation of relays; the bus voltages are compared to 1.39 p.u. to check the TOV limit given by (4.18).
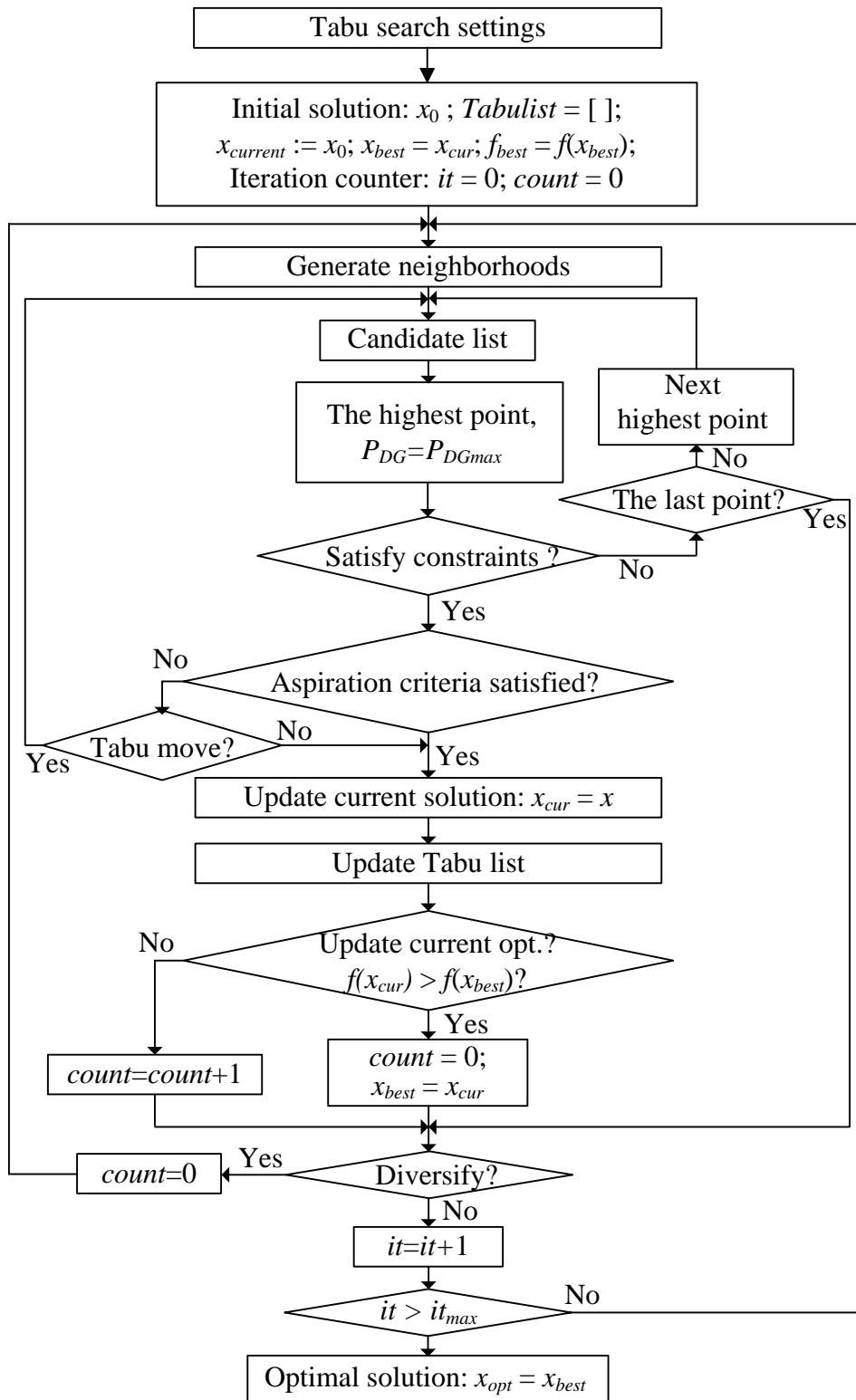
Figure 4.8 General algorithm for SBDG maximization using Tabu search
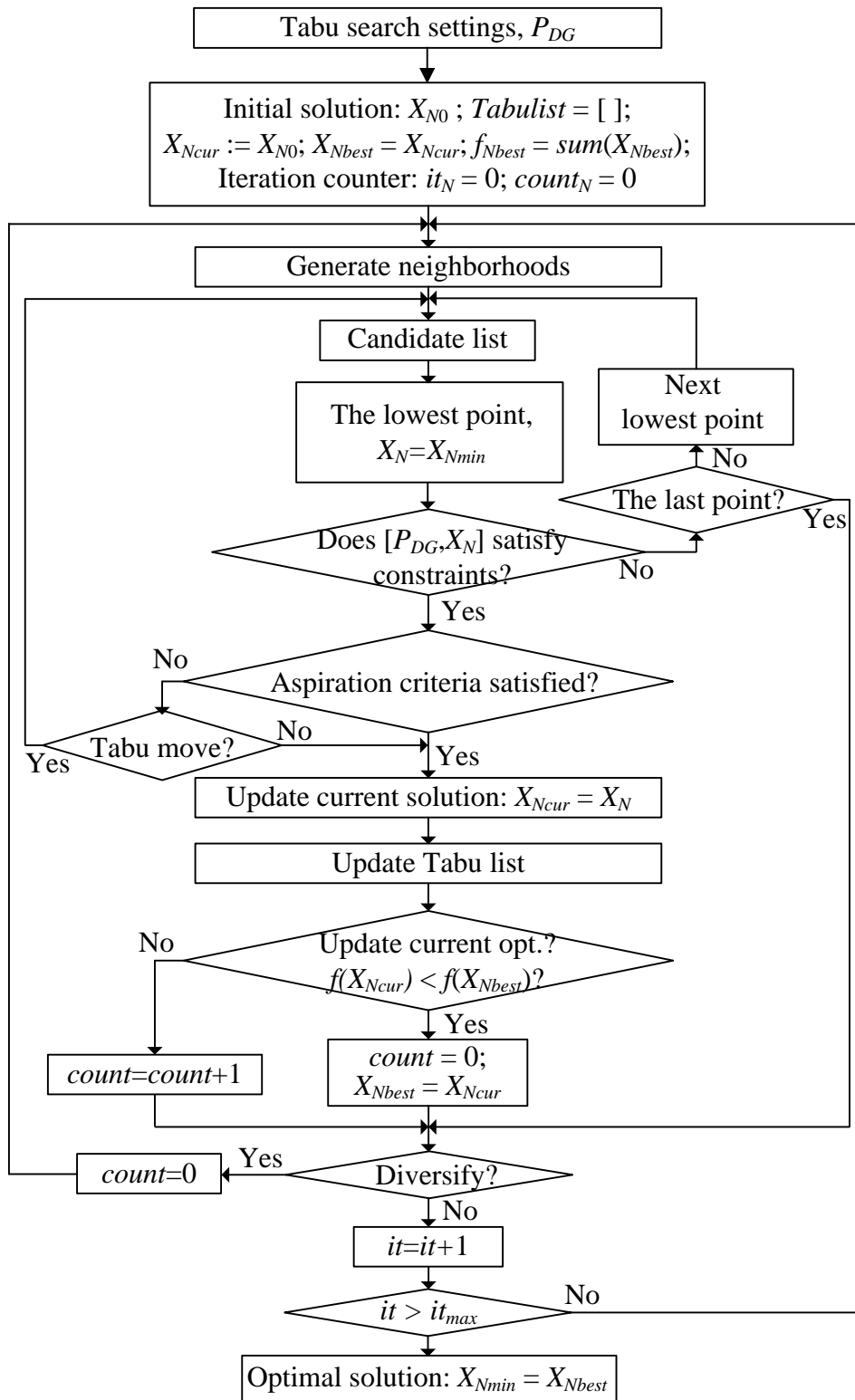
Figure 4.9 Algorithm for minimization of X_N using Tabu seach
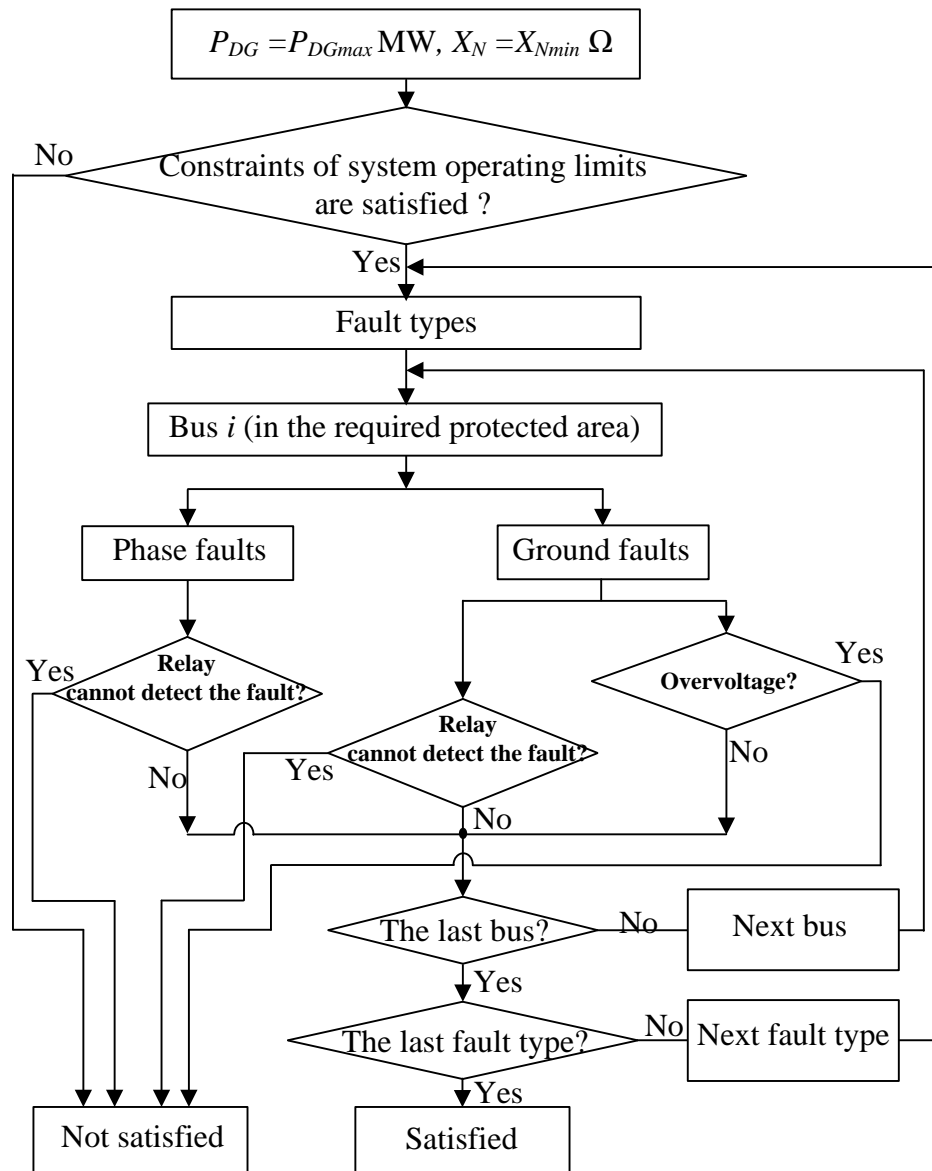
Figure 4.10 Algorithm inside the block "Does [P_{SBDG}, X_N] satisfy constraints?"

4.4.1.3 Application to the case of one SBDG

This section is to validate the proposed Tabu search algorithm. It can be seen that the sensitivity-based algorithm in Section 4.3 is reliable because the searching process visits all feasible point from the $S_{SBDGmin}$ to the $S_{SBDGmax}$. The point having the maximum SBDG is selected as the optimum point so that all constraints are satisfied. The result obtained by using the sensitivity-based algorithm is the reference to validate the Tabu search algorithm as follows.

The maximum SBDG achieved from the Tabu search is expected to be the same as the one from the sensitivity-based algorithm in Section 4.3 in the case of $n = 1$ (one

SBDG unit). The expected result here is ($P_{SBDGmax}$, X_{Nmin}) from Section 4. 3. In this case, s, P_{SBDG}, and X_N are scalar.

The Tabu search algorithm have not shown its advantage in one variable optimization compared to the sensitivity-based one as explained as follows. Assuming that both algorithm start searching at the same initial solution and the Tabu search algorithm generate one neighborhood at each iteration, the needed number of searched points to reach the maximum SBDG is the same for both algorithm. However, whilst the sensitivity one can stop immediately after reaching the maximum point, the Tabu search must continue until the it_{max} iterations finishes.

4.4.1.4 Maximization of multiple SBDGs

The effectiveness of the algorithm in Figure 4.8 manifested in this section is about multiple SBDGs. For instance, in case a system has 2 SBDGs and each DG has N possible discreted values. The total number of combinations is $2N^2$. Obviously, the sensitivity-based algorithm consumes much time to visit all combinations and select the best one. The Tabu search algorithm does not go though all combinations of DG, hence reduces the computational cost. This advantage is presented clearer if the number of variables, i.e. DGs, is higher. However, the case study in Chapter 6 evaluates 2 SBDGs case in order to easier observe and illustrate the searching process.

4.4.2 Maximization of SBDG and IBDG Using Tabu Search

This Section considers the case that the FRT capability is required by the distribution system operator. As discussed in Chapter 3, Section 3.2, a voltage-based function is supplemented to the interconnection protection system of the SBDG. The IBDG in this case remains connected to the utility system during fault calculation and it operates in a current control mode to meet the requirement of reactive current support from the distribution system operator as discussed in Chapter 2.

Objective function

$$Max : P_{DG} = \sum_{i=1}^{n} P_{DG,i} \tag{4.20}$$

In (4.20), n is the total number of DG units installed in the system. In case one SBDG and one IBDG are planned to be installed in the system, $n = 2$ and (4.20) is detailed by (4.21).

$$Max : P_{DG} = P_{SBDG} + P_{IBDG} \tag{4.21}$$

Constraints

Limits of IBDG size are added into the system operating limits constraints and given by (4.22).

$$S_{IBDG\min} \leq S_{IBDG} \leq S_{IBDG\max} \tag{4.22}$$

Due to the FRT requirement, constraints of fault condition are adjusted as in (4.23).

Utility relay:

$$\begin{cases} \Delta I_{utility} = I_{fault,utility} - I_{pick-up,uility} > 0 \\ I_{fault,utility} = f\left(P_{SBDG}, P_{IBDG}, X_N\right) \end{cases} \tag{4.23}$$

SBDG relay:

Overcurrent function*:*

$$\begin{cases} \Delta I_{SBDG} = I_{fault,SBDG} - I_{pick-up,SBDG} > 0 \\ I_{fault,SBDG} = g_1\left(P_{SBDG}, P_{IBDG}, X_N\right) \\ I_{pick-up,SBDG} = g_2\left(P_{SBDG}\right) \end{cases} \tag{4.24}$$

Overvoltage due to ground faults:

$$TOV_i = h\left(P_{SBDG}, P_{IBDG}, X_N\right) \leq 1.39 \; p.u. \tag{4.25}$$

where *i* is the bus index in the islanding system.

Algorithm

The algorithms in Section 4.4.1 are still applicable here with some adjustments. Firstly, the constraint of IBDG relay overcurrent function is removed. Secondly, the TOV constraint is necessary for an islanding system with SBDG and/or IBDG. For an islanding system with IBDG only, there is no TOV problem because the IBDG is not a voltage source under fault condition as mentioned in Chapter 3. In addition, the proposed fault calculation program in Chapter 3 must be used because the IBDG participates in the faulted utility system.

Generally, the algorithm in Figure 4.8 is applicable to an unbalanced system. The unbalance requires new power flow and fault calculation algorithms inside the block "Satisfy constraints". If an unbalanced system is concerned, for instance, including one-phase DG, the obtained maximum allowable DG may decrease compared to the

case of balanced system. One reason is the overburdened line connecting the DG to the remainder of system. Obviously, auxiliary methodologies are needed for power flow and fault calculation algorithms to make the algorithm in Figure 4.13 applicable. Nevertheless, unbalance issue is out of scope of this thesis.

4.5 Summary of Chapter 4

This chapter proposed algorithms to maximize DG installed in a utility system. There are two techniques including sensitivity-based and Tabu search-based algorithms. These algorithms took the DG impacts on a utility system into account in three cases: one SBDG, two SBDGs, and one SBDG one IBDG. These impacts were accounted as constraints of system operating limits and relay reach. The sensitivity-based algorithm was proposed to provide a reliable result in case a system with one SBDG. This result is the reference to confirm the accuracy of the Tabu search-based algorithm. After validating, the Tabu search-based algorithm was applied to determine the maximum allowable SBDG and IBDG in case the system with more than one DG. Chapter 6 will show a case study of the proposed algorithms on the IEEE 34 Node test Feeder.

CHAPTER V
VALIDATION OF THE ADAPTIVE FAULT CALCULATION

The adaptive fault calculation in Chapter 3 is validated here. Firstly, the proposed algorithm is applied to a system without IBDG in Section 5.1. Results are then compared to those obtained from the conventional fault calculation algorithm. Secondly, a time-variant simulation is performed in Section 5.2 to validate the algorithm for another system with IBDG. In this section, Matlab/Simulink tools are utilized for simulating the tested system.

5.1 Validation by Conventional Fault Calculation

A three-bus system in Chapter 10 of [44] is used to compare the proposed fault calculation algorithm with the conventional one. Diagram of this system is depicted in Figure 5.1 where each generator is represented by an *emf* behind a transient reactance. The neutral of each generator is grounded through a current-limiting reactor of 0.25/3 per unit on 100 MVA base. The system data expressed in per unit is tabulated in Table 5.1. The generators are running on no-load at their rated voltage and rated frequency with their *emfs* in phase. The fault currents are required to be calculated in four cases of fault at Bus 3 with the fault impedance $Z_f = j0.1$ p.u.: a three-phase fault, a SLGF, a line-to-line fault, and a DLGF. However, if voltages obtained from both methods are identical, line currents will be the same because they are computed by the same equations from the corresponding voltages. Therefore, the results are shown in voltages instead of currents. The sequence impedance networks of this system are illustrated in Figure 5.2.
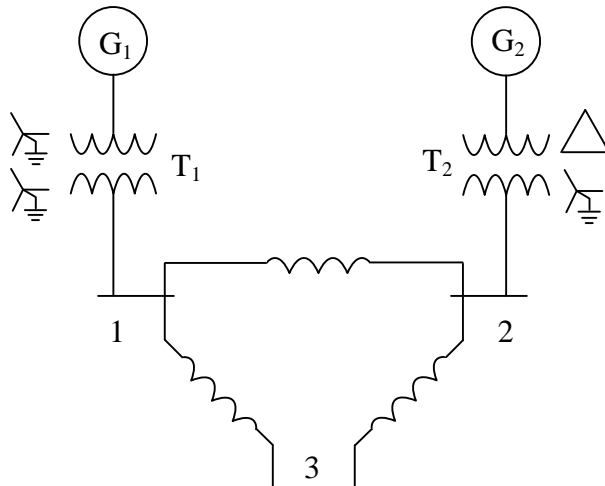
Figure 5.1 Diagram of the simple system in [44]

Table 5.1 System data of the simple system for the validation by the conventional fault calculation [44]

Item	Base MVA	Voltage rating	X^1, p.u.	X^2, p.u.	X^0, p.u.
G_1	100	20 kV	0.15	0.15	0.05
G_2	100	20 kV	0.15	0.15	0.05
T_1	100	20/220 kV	0.10	0.10	0.10
T_2	100	20/220 kV	0.10	0.10	0.10
L_{12}	100	220 kV	0.125	0.125	0.30
L_{13}	100	220 kV	0.15	0.15	0.35
L_{23}	100	220 kV	0.25	0.25	0.7125
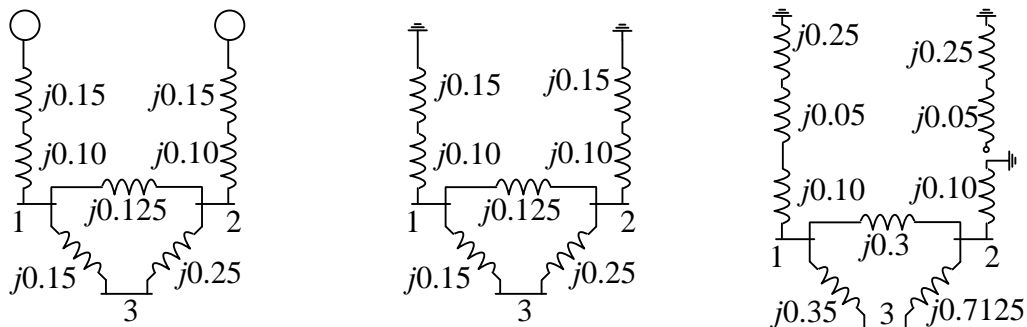
(a) Positive-sequence network   (b) Negative-sequence network   (c) Zero-sequence network

Figure 5.2 Sequence networks of the system in [44]

The conventional algorithm uses the symmetrical components method such that a faulted system is split into three sequence networks: positive, negative, and zero. Each network is reduced into a Thevenin's equivalent circuit as viewed from the faulted bus. Changes in bus voltages are obtained by applying Thevenin's theorem. Bus voltages during the fault are obtained by superposition of the prefault bus voltages and changes in the bus voltages. The prefault bus voltages may be obtained from the results of the power flow solution. Here, load and resistance are neglected, thus, the prefault voltages at all buses are 1 p.u. The calculated bus voltage magnitudes obtained by using the conventional fault calculation are summarized in Table 5.2.

In order to make the system in Figure 5.1 compatible with the proposed fault calculation method, the respective positive-sequence impedance diagram under fault condition is represented as a fashion in Figure 5.3. In this diagram, two terminals of the voltage sources that represent the two generators are treated as slack buses in a power flow program. The negative and zero-sequence impedance diagrams are the same as the representations in the conventional method (Figure 5.2 (b) and (c)). The value of the equivalent impedance Z_{eq} is determined in corresponding to the fault type as explained in Table 3.1. In the case of a three-phase fault, Z_{eq} is the same as the fault impedance; whereas, In the case of an unbalanced fault, Z_{eq} is the equivalent impedance of the circuit comprising the Thevenin negative and zero-sequence

following the sequence network connection at the faulted bus (Bus 3). The sequence network connection is represented in Figure 5.3.
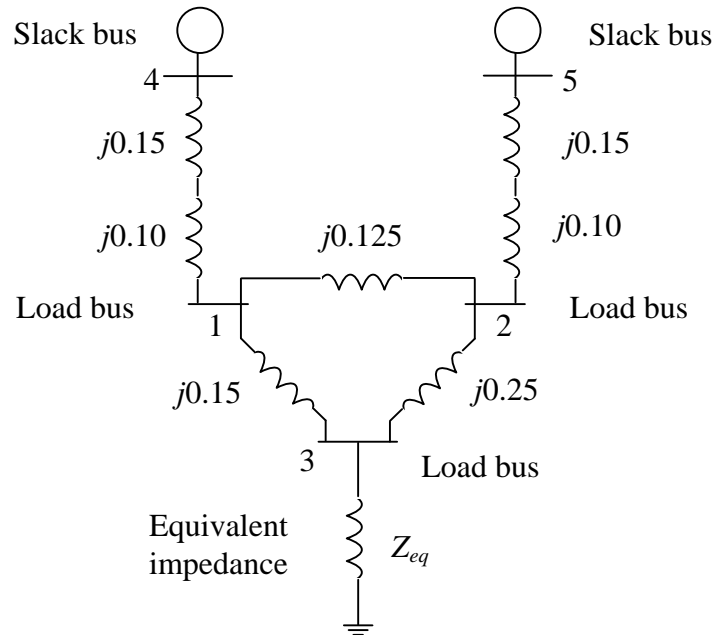
Figure 5.3 Sequence network connection of the system in [44] for applying the adaptive fault calculation

In the case of a three-phase fault, the bus voltages are obtained directly from running the proposed algorithm in Figure 3.14. For an unbalanced fault, the positive-sequence voltages at all buses instead of phase voltages are obtained by the algorithm in Figure 3.16. Then, the sequence components of current at the faulted bus are determined as explained in Table 3.2. From the negative and zero-sequence currents at the faulted bus, the corresponding sequence voltages at all buses are determined by using (3.17). Lastly, phase voltages are obtained from superposing three sequence components. Results of the proposed fault calculation program are listed in Table 5.3.

Phase voltages obtained from the proposed fault calculation algorithm in Table 5.3 are very close to voltages obtained from the conventional method [44] in Table 5.2. Consequently, the currents obtained from both of them are close to each other. As a result, the proposed fault calculation algorithm is validated by the conventional method for a system without IBDG. It is also concluded here that the proposed fault calculation algorithm can replace the conventional one for fault calculation in all cases.

Table 5.2 Bus voltages obtained from the conventional fault calculation method [44]

Fault types	Bus	1	2	3
	Load	0	0	0
	Prefault voltage	1	1	1
3F	Phase A	0.5938	0.6250	0.3125
SLGF	Phase A	$0.6330\angle 0^0$	$0.7207\angle 0^0$	$0.2752\angle 0^0$
	Phase B	$1.0046\angle -120.45^0$	$0.9757\angle -117.43^0$	$1.0647\angle -125.56^0$
	Phase C	$1.0046\angle +120.45^0$	$0.9757\angle +117.43^0$	$1.0647\angle +125.56^0$
LLF	Phase A	$1\angle 0^0$	$1\angle 0^0$	$1\angle 0^0$
	Phase B	$0.6720\angle -138.07^0$	$0.6939\angle -136.10^0$	$0.5251\angle -162.21^0$
	Phase C	$0.6720\angle +138.07^0$	$0.6939\angle +136.10^0$	$0.5251\angle +162.21^0$
DLGF	Phase A	$1.0066\angle 0^0$	$0.9638\angle 0^0$	$1.0855\angle 0^0$
	Phase B	$0.5088\angle -135.86^0$	$0.5470\angle -136.70^0$	$0.1974\angle +180^0$
	Phase C	$0.5088\angle +135.86^0$	$0.5470\angle +136.70^0$	$0.1974\angle +180^0$

Table 5.3 Bus voltages obtained from the proposed fault calculation algorithm

Fault types	Z_{eq}	Bus	1	2	3
		Load	0	0	0
3F	j0.1000	Phase A	0.5938	0.6250	0.3125
SLGF	j0.8634	V^1	0.8800	0.8892	0.7969
		I^1_f	0	0	$-j0.9230$
		V^2	-0.1200	-0.1108	-0.2031
		V^0	-0.1213	-0.0576	-0.3170
		Phase A	$0.6387\angle 0^0$	$0.7208\angle 0^0$	$0.2768\angle 0^0$
		Phase B	$1\angle -120.06^0$	$0.9745\angle -117.29^0$	$1.0615\angle -123.11^0$
		Phase C	$1\angle +120.06^0$	$0.9745\angle +117.29^0$	$1.0615\angle +123.11^0$
LLF	j0.3200	V^1	0.7593	0.7778	0.5926
		I^1_f	0	0	$-j1.8519$
		V^2	0.2407	0.2222	0.4074
		V^0	0	0	0
		Phase A	$1\angle 0^0$	$1\angle 0^0$	$1\angle 0^0$
		Phase B	$0.6721\angle -138.07^0$	$0.6939\angle -136.10^0$	$0.5251\angle -162.22^0$
		Phase C	$0.6721\angle +138.07^0$	$0.6939\angle +136.10^0$	$0.5251\angle +162.22^0$
DLGF	j0.1639	V^1	0.6614	0.6874	0.4269
		I^1_f	0	0	$-j2.6046$
		V^2	0.2523	0.2329	0.4269
		V^0	0.0872	0.0414	0.2279
		Phase A	$1\angle 0^0$	$0.9617\angle 0^0$	$1.0817\angle 0^0$
		Phase B	$0.5120\angle -136.22^0$	$0.5747\angle -136.77^0$	$0.1990\angle +180^0$
		Phase C	$0.5120\angle +136.22^0$	$0.5747\angle +136.77^0$	$0.1990\angle +180^0$

5.2 Validation by Matlab/Simulink Simulation

In this section, a simulation in Matlab/Simulink environment is applied to show the changes of fault currents due to the interconnection of IBDG with a simple system depicted in Figure 5.4. Then, the algorithm proposed in Chapter 3 is utilized to determine the fault current. Results from this application will be compared with the time-variant results from the Simulink simulation in two cases: the inverter current does not reach the limit (I_{thres}) and reaches the limit causing the IBDG to be switched to the current source mode. The simple system has one IBDG connected to Bus 4, which is a low voltage bus of a step up transformer. The details of this system are as follows.

System parameters:

- Grid: V_1 = 6 kV, $Z_{sc,grid}$ = 0 Ω, Z_{line1}= 0.72 + j2.7 Ω, Z_{line2} = 0.5×Z_{line1}, P_{load} + jQ_{load} = 1 + j0.5 MVA
- Transformer: 0.80 MVA, 6kV/380V, Yn/D11, R = 0.002 p.u, X = 0.08 p.u (in transformer rating).
- IBDG: S_{nom}=0.55 MVA, P_{ref} = 0.5 MW, Q_{ref} = 0 MVAr, I_{thres} = 1.5 p.u., $I_{inv,sat}$ = 1 p.u., (in IBDG rating), C_f = 900 μF, L_f = 0.85 mH, f_c = 5 Hz, K_i=2000, K_p = 6000.
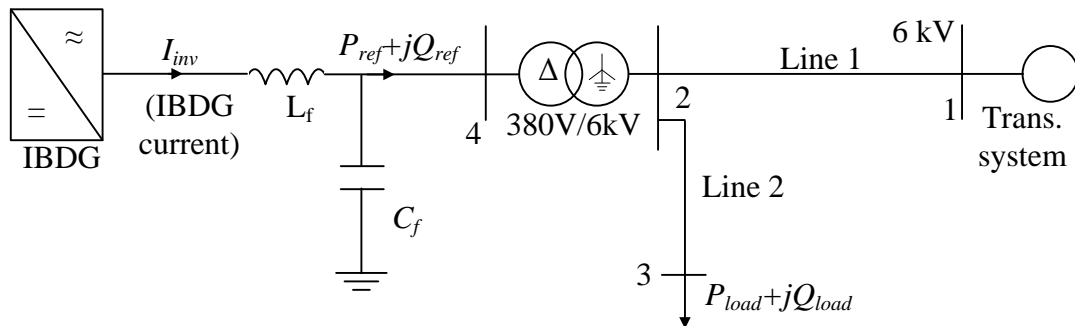
Figure 5.4 Simple system with an IBDG

5.2.1 Results from Matlab/Simulink Simulation

The Simulink is employed to simulate the system in Figure 5.4. The simulated model contains three blocks: power system, control system, and measurement blocks. Details of the model are in Appendix B.

5.2.1.1 Power system model in Simulink

The IBDG has a control system in a similar structure to the selected one in Chapter 3. Four main elements inside the Simulink model are line, transformer, transmission system, and load. They are represented as follows.

A line is simply represented by an impedance. This impedance is simulated by a resistor in series with a reactor. Their parameters are in Ohm and Henry, respectively. In order to convert the reactance X of the reactor into the corresponding inductance L, the power frequency f=50 Hz should be used. Therefore, lines 1 and 2 are simulated by (R_{line1} = 0.72 Ω; L_{line1} = 8.6e−3 H) and (R_{line2} = 0.36 Ω; L_{line2} = 4.3e−3 H).

The transformer in this power system is a two winding transformer. The low voltage winding is connected in delta and the high voltage one is connected in grounded-wye. The YnD11 connection indicates that the voltage at the delta winding leads the respective one at the wye winding by 30 degrees. The parameters in transformer rating of each winding is R=0.001 p.u. and L=0.004 p.u. The selected connection can mitigate the effect of the voltage drop, which is caused by a SLGF on the high voltage side, on the operation of the IBDG as illustrated later on.

The transmission system is assumed to be infinitive. This means, the short-circuit impedance of the system is $Z_{sc,grid}$ = 0 Ω. In another word, voltage at Bus 1 is remained $1\angle0^0$ p.u. during both normal operation and fault condition.

Load is represented by a constant impedance to reflect the change of load power following the change of voltage. The voltage used to convert the constant power

model into constant impedance is generally the nominal voltage. However, the voltage obtained from a power flow program under prefault condition can model the load with higher accuracy than using the nominal voltage.

5.2.1.2 Prefault condition

Voltages at Buses 2, 3, and 4 are obtained from a power flow program for prefault condition. Load under this condition is modeled as a constant power of 1+j0.5 MVA. Results in phase-phase rms value are as follows.

- Bus 2: $V_{2pre} = 5.65\angle\text{-}1.64^0$ kV
- Bus 3: $V_{3pre} = 5.46\angle\text{-}3.82^0$ kV
- Bus 4: $V_{4pre} = 357.96\angle 31.59^0$ V

Voltage at load bus 3 is $5.46\angle\text{-}3.815^0$ kVrms. The respective load impedance is $23.8493+j11.9246$ Ω. Thus, it is represented in Simulink by a circuit comprising a resistor $R_{load} = 23.8493$ Ω in series with an inductor $L_{load} = 0.038$ H.

5.2.1.3 SLGF-under limit case

At time $t = 2$ s, a SLGF occurs at Bus 3 through a ground impedance $Z_f = 0.2$ Ω.

Figure 5.5 illustrates faults current at the fault point before and after installing the IBDG at Bus 4. It can be seen that the fault currents at the faulted bus (Bus 3) are higher after installing IBDG, i.e. 1,266 A compared to 1,145 A. The increase is 121 A or 10.57%. The peak values of fault currents after installing IBDG are 1,755 A occurring in the first cycle from the fault instant. Currents become stable very fast after that moment.
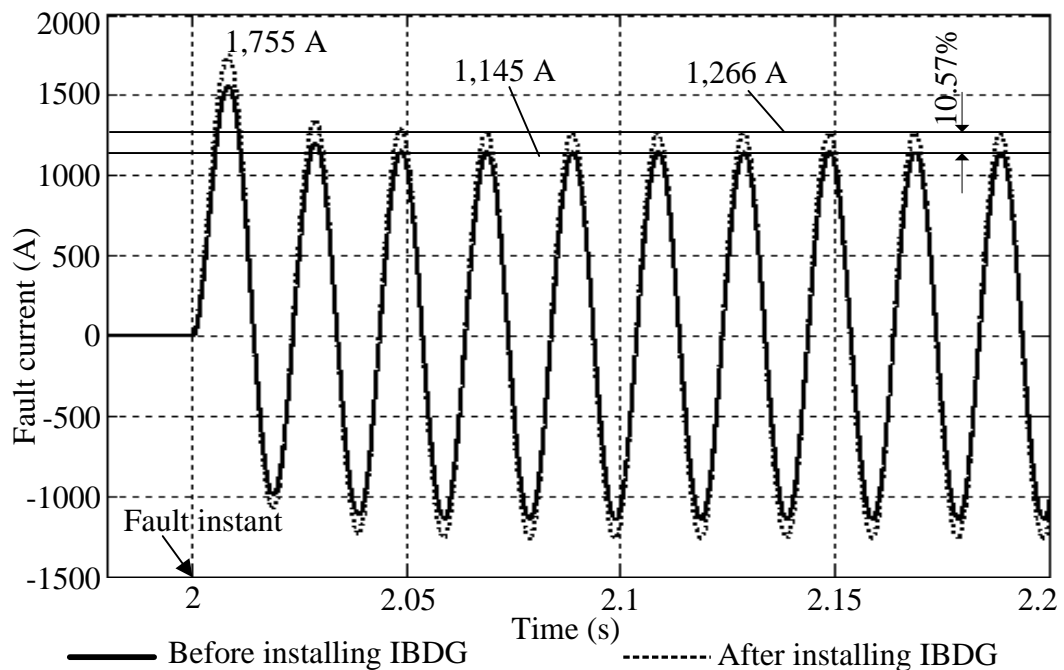
Figure 5.5 Fault current changes due to IBDG's installation - SLGF with $Z_f = 0.2$ Ω

During this unbalanced fault period, currents contributed by the IBDG are still almost symmetrical. The the peak phase value after the fault is 1,480 A rising from

1,140 A at the prefault instant (29.82% increase) as shown in Figure 5.6. This is because the IBDG responds only the positive-sequence component and generates the respective symmetrical current.

In Figure 5.7, voltage at phase A on the high voltage side is 2 kV, meaning that the drop is 59.16 % of the nominal voltage. Due to the effect of the YnD11, voltages at phases A and C drop instead of phase A. The drop is 35.54%, i.e lower than that on the high voltage side. Therefore, the reference current has not reached the limit I_{thres} = 1,772.66 A (peak value). Consequently, the power output is still maintained at 0.5 MW during the fault as shown in Figure 5.8.
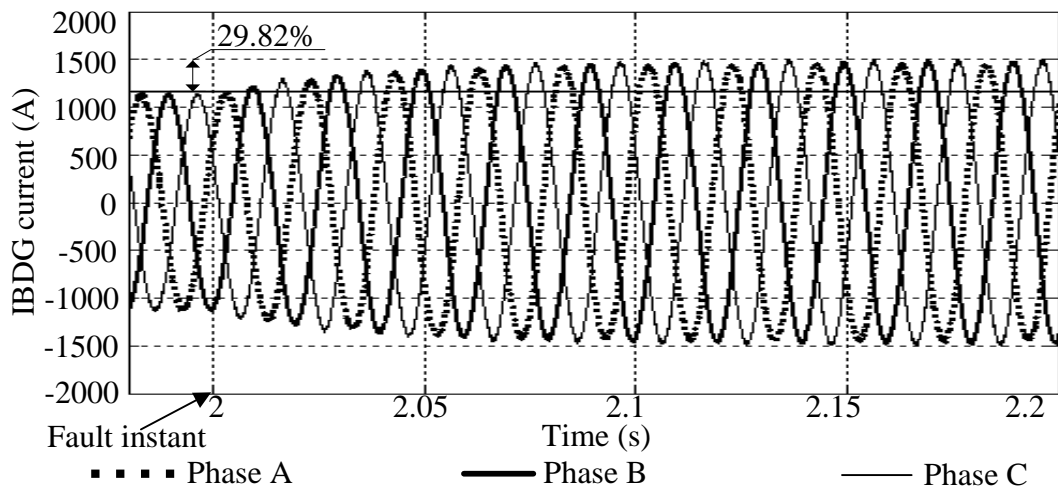
Figure 5.6 Currents from IBDG during a SLGF with Z_f = 0.2 Ω
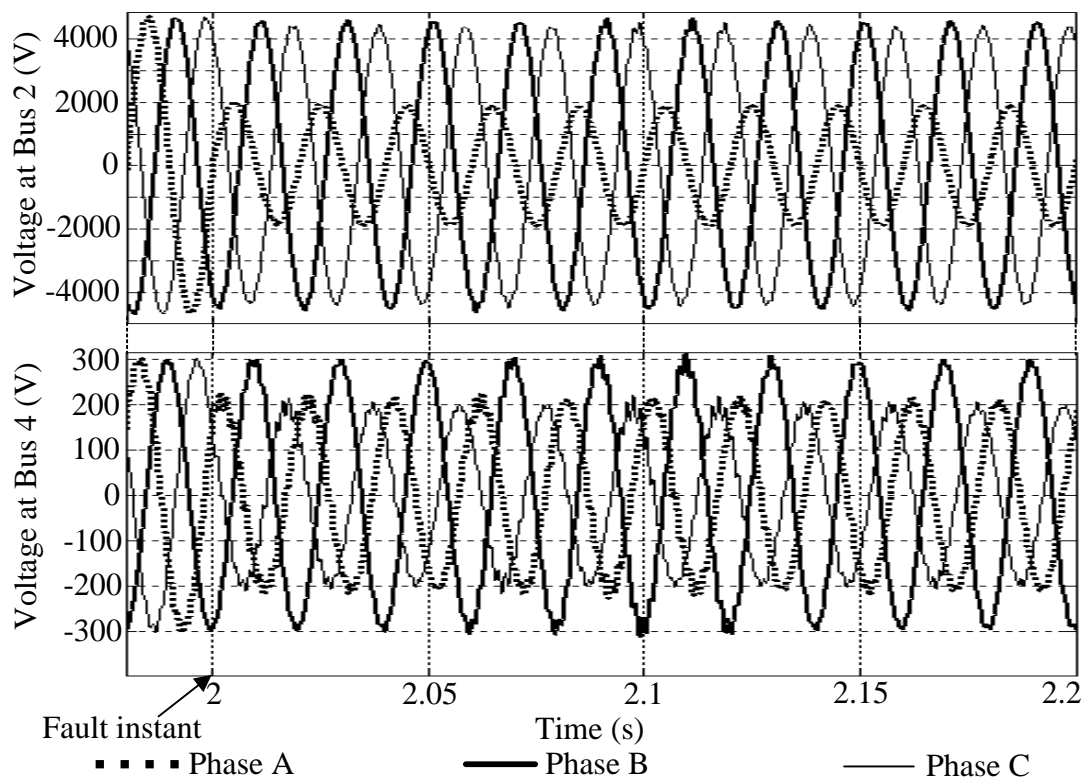
Figure 5.7 Voltages on two sides of the transformer during a SLGF with Z_f = 0.2 Ω
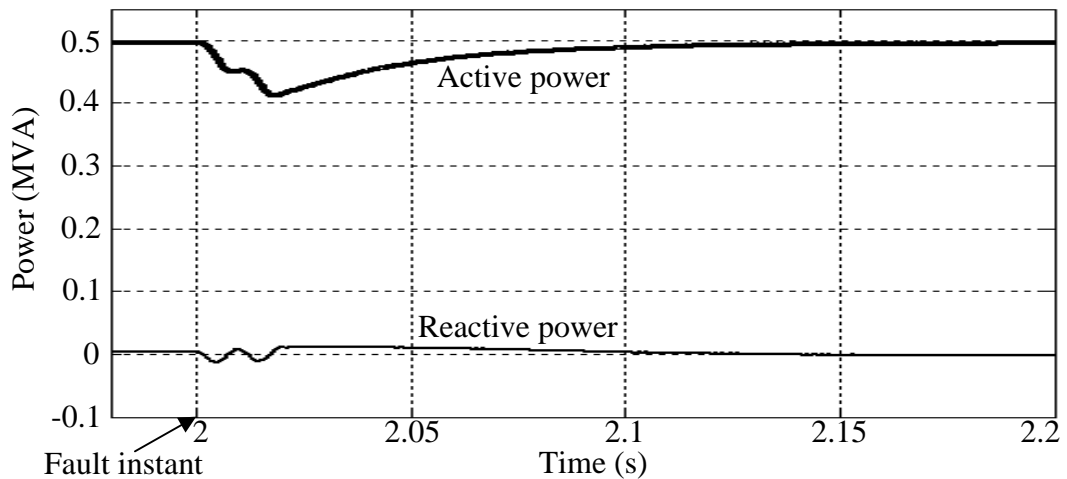
Figure 5.8 IBDG power output based on positive-sequence components during a
SLGF with $Z_f = 0.2\ \Omega$

Table 5.4 summarizes results of voltages and currents obtained from Simulink simulation of the SLGF case so as to easily compare with those from the proposed fault calculation algorithm which will be used later.

Table 5.4 Peak voltages and currents obtained from Simulink-SLGF case

	Bus 2	Bus 3	Bus 4
Pos.-seq. voltages	$3,555\angle{-0.85}^0$	$2,865\angle{-4.18}^0$	$225\angle34.50^0$
Phase A	$1,869\angle{-3}^0$	$254\angle{-70}^0$	$206\angle52^0$
	IBDG current	Fault current	
Pos.-seq. currents	$1,474.6\angle36.52^0$	-	
Phase A	$1,474.6\angle36.52^0$	$1,266\angle{-70}^0$	

5.2.1.4 Double line-to-ground fault-over limit case

In the case of a DLGF (phases B and C) through $Z_f = 0.2\ \Omega$, a big dip at phases B and C of the IBDG terminal voltage (Bus 4) occurs. The drop of voltage causes the reference current to increase until it reaches the limit $I_{thres} = 1,772.66$ A (peak value) and passes the limit at time $t = 2.06$ s. The IBDG is switched to the current source mode causing the IBDG current becomes constant immediately after that with the value of $I_{inv,sat} = 1,181.77$ A (peak value) as shown in Figure 5.9. The phase of the IBDG current lags the phase of the positive-sequence component of the IBDG terminal voltage by 90^0. This lagging phase satisfies the FRT requirement as discussed in Chapters 2 and 3.

Similarly to the SLGF case, the voltage characteristics at Buses 4 and 2 are not in the same waveform as illustrated in Figure 5.10 because of the transformer connection

of YnD11. Both voltages at phases B and C at Bus 2 that is on the high voltage side of the transformer decrease due to the fault. At Bus 4, which is on the low voltage side of the transformer, the voltage dip at Phase B is bigger than that at phases A and C whose voltages are almost the same as 225 V. Thus, the phase shift caused by the transformer connection should be taken into consideration at the stage of forming the bus admittance matrix for running the proposed algorithm.

The fault currents at the faulted bus in this case are shown in Figure 5.10 where the peak value of the current at Phase B and C are 1,311.25 and 1,228.25 A, respectively. Because the IBDG is controlled in current mode, the power output is no longer maintained the predefined value of 0.5 MW as shown in Figure 5.11. In addition, the 90^0 phase lagging of the IBDG current causes the active power output to become zero and the reactive one to increase to 0.34 MVAr.
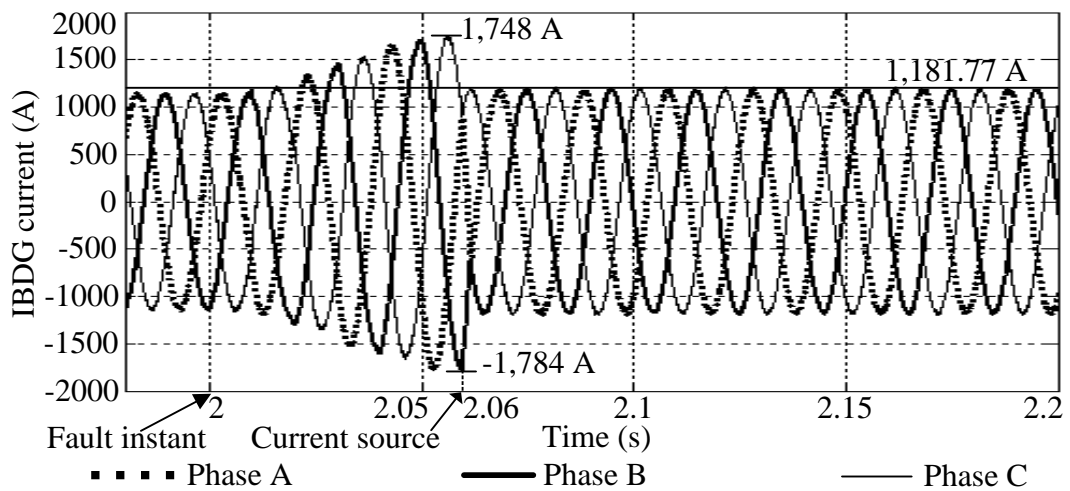
Figure 5.9 Currents from IBDG during a DLGF $Z_f = 0.2\ \Omega$
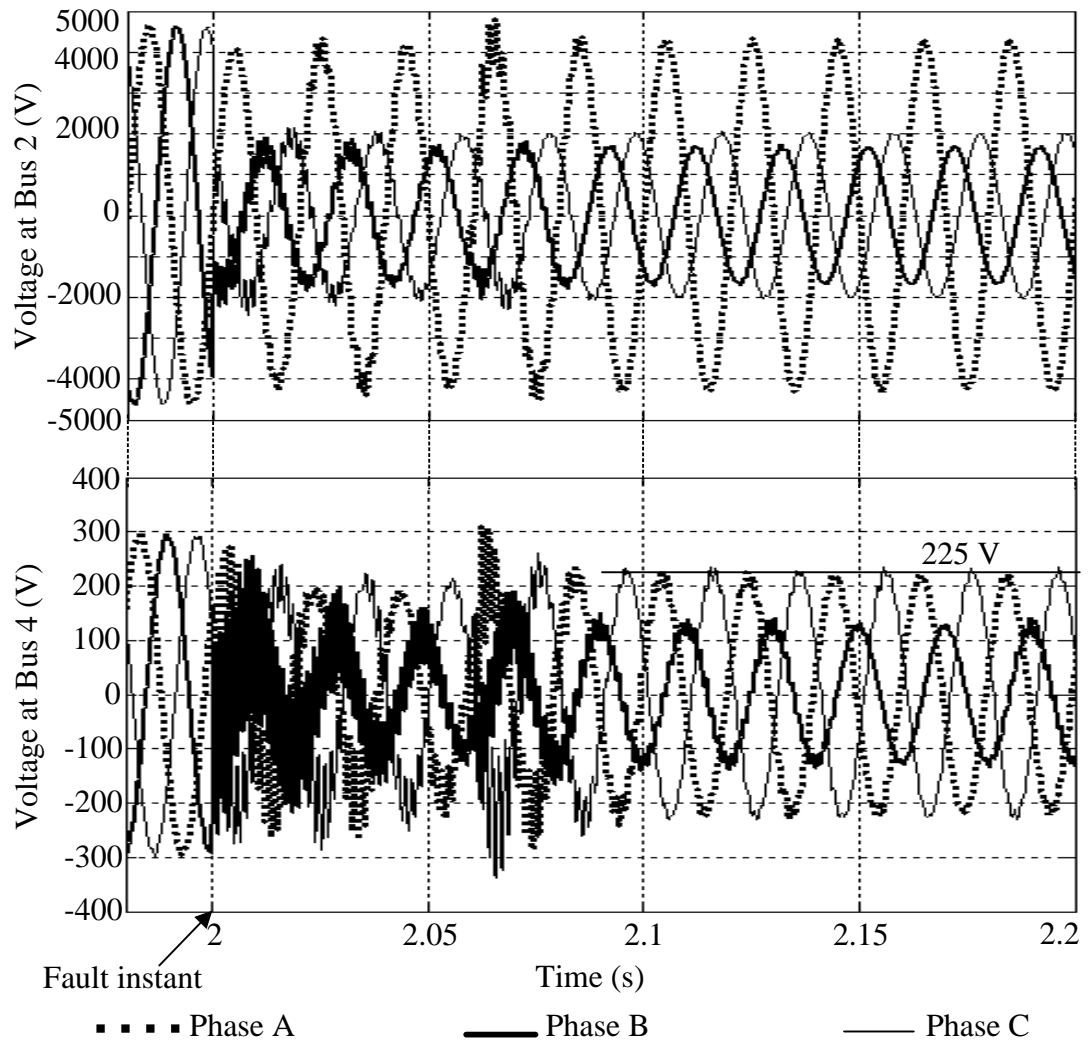
Figure 5.10 Voltages at Buses 2 and 4 during a DLGF $Z_f = 0.2\ \Omega$
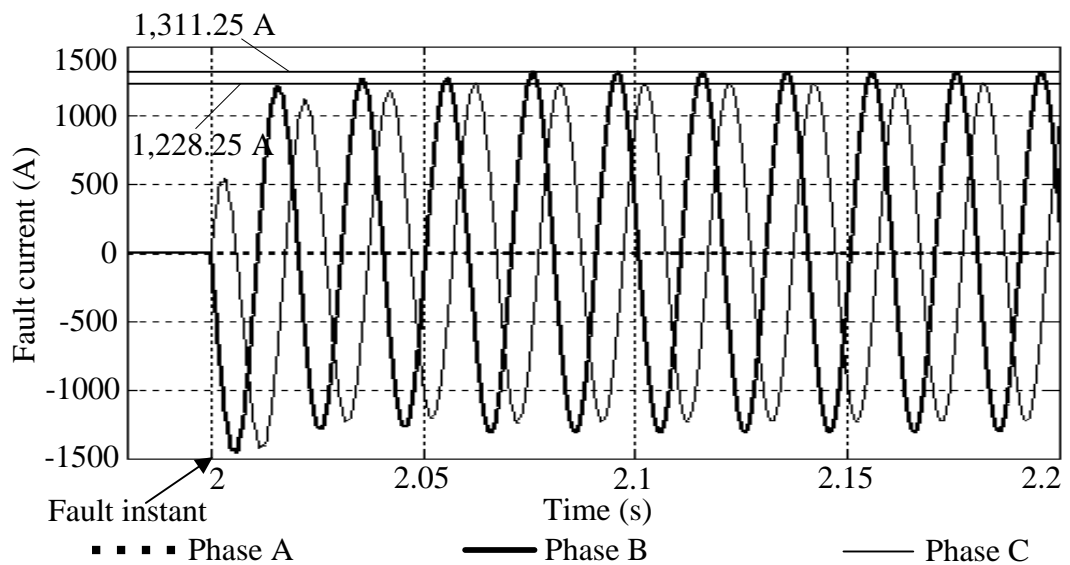
Figure 5.11 Fault current during a DLGF $Z_f = 0.2\ \Omega$
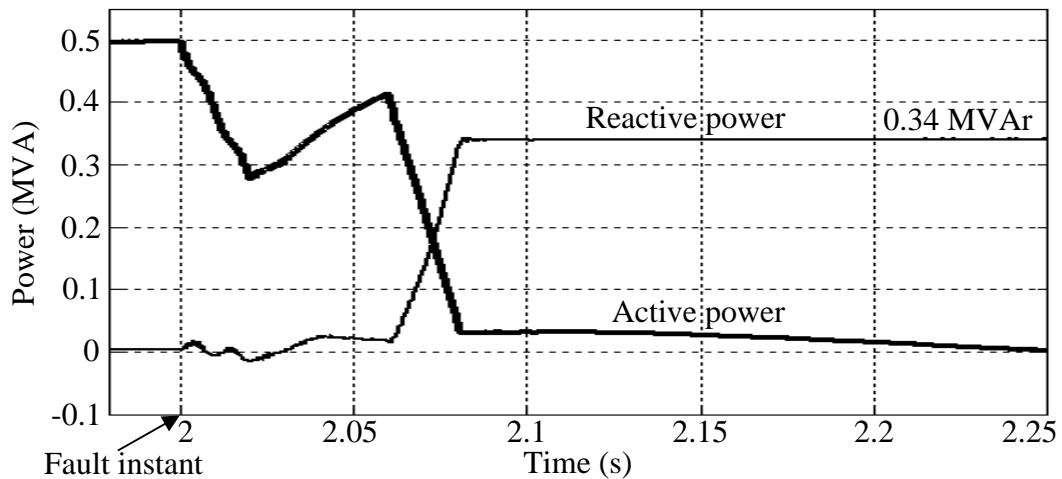
Figure 5.12 IBDG power output based on positive-sequence components during a DLGF with $Z_f = 0.2\ \Omega$

Table 5.5 summarizes results of voltages and currents obtained from the Simulink simulation of the DLGF case so as to easily compare with those from the proposed fault calculation algorithm which will be used later.

Table 5.5 Peak voltages and currents obtained from Simulink-DLGF case

	Bus 2	Bus 3	Bus 4
Pos.-seq. voltages	$2{,}638\angle{-3.88}^0$	$1{,}414\angle{-9.4}^0$	$185\angle25.93^0$
Phase A	$4{,}266\angle{-3.88}^0$	$4{,}119.3\angle{-5.93}^0$	$216.9\angle11.4^0$
Phase B	$1{,}672\angle{-131.6}^0$	$282.57\angle108.1^0$	$125.19\angle{-91.5}^0$
	IBDG current	Fault current	
Pos.-seq. currents	$1{,}777.6\angle{-64.24}^0$	-	
Phase A	$1{,}777.6\angle{-64.24}^0$	0	
Phase B	$1{,}777.6\angle{-64.24}^0$	$1{,}308\angle162^0$	

5.2.2 Results from the Proposed Fault Calculation Algorithm

In order to determine the equivalent impedance Z_{eq} for running the proposed algorithm, the system in Figure 5.4 is represented in the fashions of negative and zero-sequence networks as in Figure 5.13. For easily comparing with the results from the simulation in Section 5.2.1, the load is also modeled as a constant impedance with respect to the prefault voltage obtained from a power flow program.
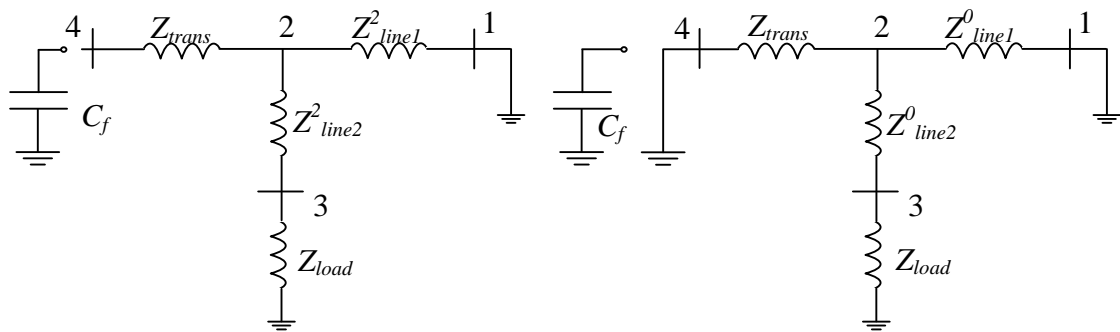
(a) Negative-sequence network   (b) Zero-sequence network

Figure 5.13 Sequence networks of the simple system with the installation of an IBDG

It is assumed that all sequence impedances are identical for each system component as the following calculation. All values are expressed in per unit with: $baseMVA = 1$ MVA; base voltage on the high voltage side: $basekV = 6$ kV; base voltage on the low voltage side: $baseV = 380$ V.

$Z_{basekV} = basekV^2/baseMVA = 6^2/1 = 36\ \Omega$

$Z_{baseV} = baseV^2/baseMVA = 0.380^2/1 = 0.1444\ \Omega$

$I_{basekV} = baseMVA \times 10^3/(\sqrt{3} \times basekV) = 1 \times 10^3/(\sqrt{3} \times 6) = 96.225$ A

$Z^0_{line1} = Z^1_{line1} = Z^2_{line1} = (0.7200 + 2.7000i)/36 = 0.0200 + j0.0750$ p.u.

$Z^0_{line2} = Z^1_{line2} = Z^2_{line2} = (0.3600 + 1.3500i) = 0.0100 + j0.0375$ p.u.

$Z^0_{trans} = Z^1_{trans} = Z^2_{trans} = (0.002 + j0.08) \times 1/0.8 = 0.0025 + j0.1$ p.u.

Run power flow with $S_3 = 1 + j0.5 \rightarrow V_3 = 0.910\angle\ -3.815^0$ p.u.

$Z^0_{load} = Z^1_{load} = Z^2_{load} = |V_3|^2/S^*_{load} = 0.6625 + j0.3312$ p.u.

$Z_{Cf} = [-j1/(\omega C_f)]/Z_{baseV} = [-j1/(2\pi \times 50 \times 900 \times 10^{-6})]/0.1444 = -j24.4929$ p.u.

$I_{invsat} = S^*_{nom}/(\sqrt{3} \times V^*_{IBDG}) = 0.55 \times 10^6/(\sqrt{3} \times 380) = 835.64$ A (rms value).

$I_{thres} = 1.5 I_{invsat} = 1,253.49$ A (rms value).

The equivalent negative and zero-sequence impedances of the system viewed from Bus 3 are $(0.0376 + j0.0979)$ p.u. and $(0.0219 + j0.0739)$ p.u., respectively. According to the sequence network connection in Figure 3.20, these two impedances and three times of the fault impedance $(3Z_f)$ can be replaced by an equivalent impedance $Z_{eq} = 0.0761 + j0.1718$ p.u for the SLGF case and $Z_{eq} = 0.0194 + j0.0423$ p.u for the DLGF case. The equivalent impedance is connected to the faulted bus (Bus 3) in the positive-sequence network as illustrated in Figure 5.14 for applying the proposed fault calculation algorithm.
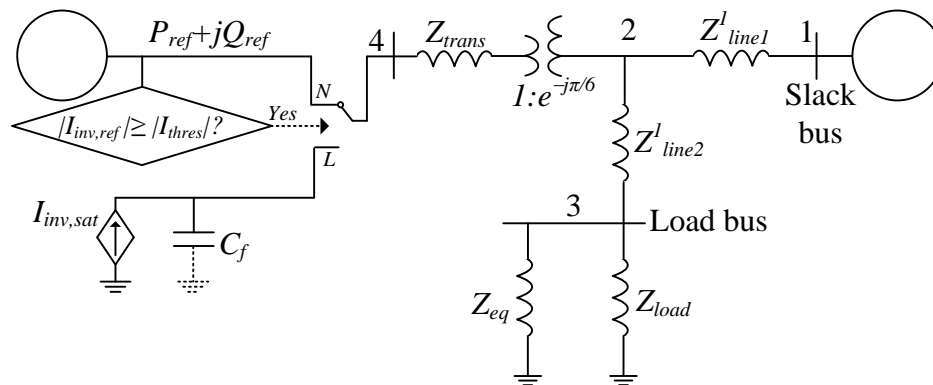
Figure 5.14 Modified sequence network connection during fault of the test system with IBDG

In both cases of fault, the connection of YnD11 is taken into account by a complex tap setting value $a = e^{-j\pi/6}$ for the positive-sequence component and $a = e^{j\pi/6}$ for the negative-sequence component. The tap setting indicates that the positive-sequence component of delta voltage leads the positive-sequence component of Y voltage by 30 degrees; whereas, the negative-sequence component of delta voltage lags the one of Y voltage by 30 degrees. These tap setting values are inputted in the data to formulate the bus admittance matrix Y_{bus} of the modified sequence network connection in Figure 5.14.

In the case of the SLGF, the reference current from IBDG (through the filter inductance) does not reach the limit I_{thres}. The power output is maintained at the reference value of 0.5 MW. Thus, the IBDG current can be estimated from the positive-sequence voltage at Bus 4 by using (3.5).

During the DLGF, the IBDG is switched to the current source mode with $I_{inv,sat} = 835.64$ A rms (or 1,181.77 A peak value) at the second iteration. The algorithm restarts and updates C_f to the bus admittance matrix Y_{bus}. The solution is reached after new 7 iterations. After the algorithm converges, the phase of $I_{inv,sat}$ automatically lags the positive-sequence voltage at Bus 4 by 90 degrees. The power output during this fault case is no longer maintained at 0.5 MW.

Currents at the faulted bus (Bus 3) are computed from the positive-sequence voltage at Bus 3 according to Table 3.2. Peak values of fault current I_F in Ampere are obtained by multiplying the corresponding per unit value by the base value of $96.225\sqrt{2}$ A.

Summary of results from fault calculation for SLGF and DLGF are in Tables 5.6 and 5.7, respectively. Comparing the results from the simulation in Section 5.2.1 and the proposed fault calculation algorithm in Section 5.2.2, fault currents, bus voltages, and currents contributed from IBDG obtained by using the proposed algorithm listed in Tables 5.6-5.7 and the respective results from the Simulink simulation listed in Tables 5.4-5.5 are in close proximity. The proposed fault calculation algorithm is therefore used for all calculations hereinafter.

In Table 5.6:

$$I_{inv} = \frac{S^*_{ref}}{V^*_{4pos}} + \frac{V_{4pos}}{-jX_C} = \frac{0.5}{0.7237\angle -0.6046^{rad}} + \frac{0.7237\angle 0.6046^{rad}}{-j24.4929} = 0.5516 + j0.4171 \text{ p.u.}$$

$$\rightarrow I_{inv} = (0.5516 + j0.4171) \times \frac{1\sqrt{2}}{380\sqrt{3}} = 1,485.9\angle 37.1^0 \, A$$

$$I^0_F = I^1_F = I^2_F = \frac{V_{3pos}}{Z_{eq}} = \frac{0.5845\angle -0.0721}{0.0761 + j0.1718} = 1.0523 - j2.9271 \text{ p.u.}$$

$$\rightarrow I^0_F = I^1_F = I^2_F = 423\angle -70.2264^0 \, A$$

The negative-sequence impedance between Buses 3 and 4 is:

$$Z^2_{34} = 0.0543 + j0.0440, \text{ p.u.}$$

Negative-sequence voltage at Bus 4: $V^2_4 = 0 - I^2_F Z^2_{34} = -0.1859 + j0.1128$ p.u.

Other sequence voltages at Bus 4: $V^0_4 = 0$ p.u., $V^1_4 = 0.7237\angle 0.6046^{rad}$ p.u.

Therefore, phase A of the voltage at Bus 4 is $V_{4A} = 0.6652\angle 0.9076^{rad}$ p.u.

In Table 5.7:

The IBDG is switched to the current source I_{invsat} with the phase specified by the phase of the positive-sequence voltage at Bus 4.

$$I_{inv} = I_{invsat} \angle (\delta_{V4pos} - \pi/2) = 835.64\sqrt{2}\angle (25.9894^0 - 90^0) = 1,181.77\angle -64.0106^0 \, A$$

Sequence components of the fault current are determined according to Table 3.2.

$$I^0_F = \frac{-V_{3pos}}{Z^0_{33} + 3Z_f} = \frac{-0.2886\angle -0.1640}{0.0219 + j0.0739 + 3 \times \dfrac{0.2}{36}} = -1.0792 + j3.2893 = 3.4618\angle 1.8878^{rad} \text{ p.u.}$$

$$I^1_F = \frac{V_{3pos}}{Z_{eq}} = \frac{0.2886\angle -0.1640}{0.0194 + j0.0423} = 1.6322 - j5.9852 = 6.2038\angle -1.3046^{rad} \text{ p.u.}$$

$$I^2_F = \frac{-V_{3pos}}{Z^2_{33}} = \frac{-0.2886\angle -0.1640}{0.0376 + j0.0979} = -0.5541 + 2.6953i = 2.7516\angle 1.7735^{rad} \text{ p.u.}$$

Negative-sequence voltage at Bus 4: $V^2_4 = 0 - I^2_F Z^2_{34} = 0.1486 - j0.1221$ p.u.

Table 5.6 Results from the program using the proposed algorithm –SLGF case

Voltages		Bus 2	Bus 3	Bus 4	
Pos.-seq. component,	p.u.	$0.7253\angle-0.0144^{\text{rad}}$	$0.5845\angle-0.0721^{\text{rad}}$	$0.7237\angle0.6046^{\text{rad}}$	
	V peak	$3,553.2\angle-0.8251^0$	$2,863.5\angle-4.1310^0$	$224.5415\angle34.6410^0$	Current source at Bus 4: No
Phase A	p.u.	$0.3814\angle-0.0506^{\text{rad}}$	$0.0518\angle-1.2265^{\text{rad}}$	$0.6652\angle0.9076^{\text{rad}}$	
	V peak	$1,868.5\angle-2.8992^0$	$253.7671\angle-70.2733^0$	$206.379\angle52.0003^0$	

Current		IBDG current	Fault current		
			I^0_F	I^1_F	I^2_F
Seq. comp.	A peak	$1,485.9\angle37.1^0$	$423\angle-70.2264^0$	$423\angle-70.2264^0$	$423\angle-70.2264^0$
Phase current	A peak	$1,485.9\angle37.1^0$		$1,269\angle-70.2^0$	

Table 5.7 Results from the program using the proposed algorithm –DLGF case

Voltages		Bus 2	Bus 3	Bus 4	
Pos.-seq. component,	p.u.	$0.5384\angle\text{-}0.0673^{\text{rad}}$	$0.2886\angle\text{-}0.1640^{\text{rad}}$	$0.5958\angle0.4536^{\text{rad}}$	
	V peak	$2{,}637.6\angle\text{-}3.856^0$	$1{,}413.8\angle\text{-}9.3965^0$	$184.8581\angle25.9894^0$	
Phase A	p.u.	$0.8704\angle\text{-}0.0652^{\text{rad}}$	$0.8406\angle\text{-}0.1031^{\text{rad}}$	$0.6982\angle0.2004^{\text{rad}}$	Current source at Bus 4: Yes
	V peak	$4{,}264.3\angle\text{-}3.7^0$	$4{,}117.9\angle\text{-}5.9^0$	$216.6162\angle11.4831^0$	
Phase B	p.u.	$0.3416\angle\text{-}2.2939^{\text{rad}}$	$0.0577\angle1.8882^{\text{rad}}$	$0.4047\angle\text{-}1.5961^{\text{rad}}$	
	V peak	$1{,}673.7\angle\text{-}131.4^0$	$282.6\angle108.2^0$	$125.5671\angle\text{-}91.4514^0$	

Current		IBDG current	Fault current		
			I^0_F	I^1_F	I^2_F
Seq. comp.	p.u.	-	$3.4618\angle1.8878^{\text{rad}}$	$6.2038\angle\text{-}1.3046^{\text{rad}}$	$2.7516\angle1.7735^{\text{rad}}$
	A peak	$1{,}181.77\angle\text{-}64.0106^0$	$471.0911\angle108.1834^0$	$844.2299\angle\text{-}74.7622^0$	$2.7516\angle1.7735^{\text{rad}}$
Phase A	p.u.	-		0	
	A peak	$1{,}181.77\angle\text{-}64.0106^0$		0	
Phase B	p.u.	-		$9.6286\angle2.8203^{\text{rad}}$	
	A peak	$1{,}181.77\angle\text{-}64.0106^0$		$1{,}310.3\angle161.6^0$	

5.3 Summary of Chapter 5

This chapter has validated the proposed fault calculation algorithm successfully by the comparisons with the conventional algorithm for a system without IBDG and the time-variant simulation for a simple system with IBDG. Results obtained from the proposed algorithm and those from the reference are close in proximity. The algorithm is convenient for calculating fault currents with all fault types. Calculated fault currents can be used to set parameters of protective devices and to check their protection capability. Chapter 6 utilizes this fault calculation algorithm under an optimization algorithm umbrella.

CHAPTER VI

APPLICATIONS OF THE DG MAXIMIZATION ALGORITHM

This chapter applies algorithms in Chapter 4 on a real distribution system to show their effectiveness. A power distribution circuit, or feeder, is typically supplied through a single circuit breaker or recloser located at the supplying substation. It is divided into some zones by other line reclosers, automatic sectionalizing devices, and fuses that operate after counting current interruptions within a predefined time period. Along the main feeder, there are some load taps off the main distribution line, called laterals. These laterals are usually protected by line reclosers or fuses at the point where they tap off the main feeder. The IEEE 34 Node Test feeder, which is an actual feeder located in Arizona, USA, is employed in this chapter. This system is characterized originally by a long feeder with unbalanced loads including both spot and distributed loads. Besides, there are two in-line regulators required to maintain good voltage profile as well as some shunt capacitors [50]. However, for simply applying the proposed algorithm, the test feeder is simplified as explained in Appendix C. In this chapter, a balance system with spot loads is considered.

6.1 Impacts of SBDG and IBDG on the Utility Relay Reach Reduction

As discussed in Chapter 2, adding DG causes fault currents to be changed. Hence, the operation of protection system may be affected. This section uses the IEEE 34 Node Test Feeder to illustrate how the fault currents are changed and the protection system is affected. An SBDG is assumed to be connected to Bus 15 and an IBDG is connected to Bus 32 via grounded wye-delta transformers as shown in Figure 6.1. Parameters of these DGs are listed as follows.

SBDG parameters

The transient reactance and the zero-sequence reactance are assumed in machine rating:

- Nominal voltage: 480 V
- Transient reactance: $X_{transSBDG} = 0.2$ p.u.
- Zero-sequence reactance: $X_{0SBDG} = 0.05$ p.u.
- Power factor: $pf = 0.9$.

IBDG parameters

- The reference power output is $P_{ref} = 0.75$ MW, $Q_{ref} = 0$ MVAr.
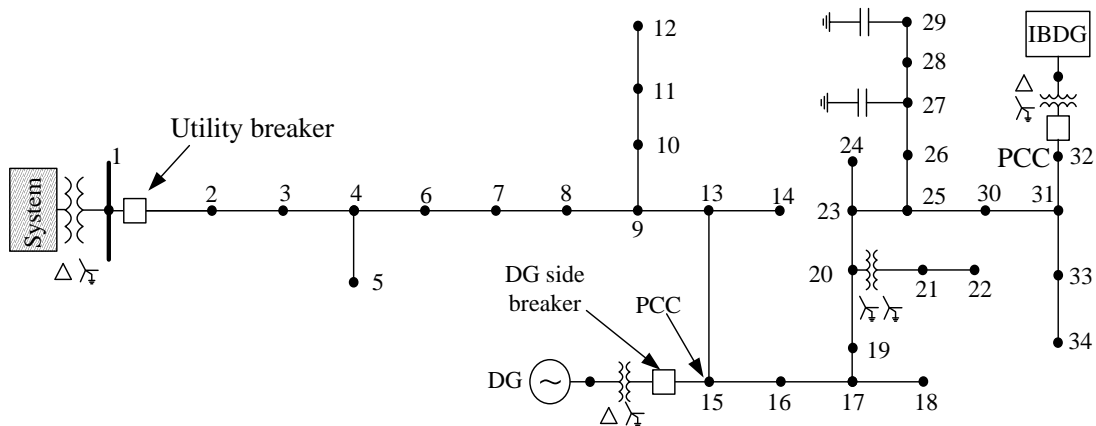
Figure 6.1 IEEE 34 Node Test Feeder with one SBDG and one IBDG

- Current contributed by the IBDG is limited at I_{thres} = 1.5 p.u. (in IBDG rating).
- The the overcurrent is estimated, the IBDG contributed a saturated current at $I_{inv,sat}$ = 1.5 p.u. (in IBDG rating).
- Parameters of the output filter are C_f = 900 μF and L_f = 0.85mH. The filter cut-off frequency is f_c = 5 Hz.

6.1.1 Protection System Settings

A utility relay is placed at the starting point of the feeder (Bus 1). The relay includes the overcurrent function whose inverse time phase/ground overcurrent functions (51/51N) are set to be the main protection. The required protected area for utility relay covers Buses 2, 5, 12, 14, 15, 18, 24, 29, 32, and 34, which are the outermost buses. In order to protect the interconnection transformer and the SBDG, another overcurrent relay is located at the PCC. It is assumed that the IBDG and its related facilities are protected by electronic-based devices. Thus, the protection is not concerned here.

Phase overcurrent function settings

The pick-up current for the POF is set so that the relay can distinguish the difference between fault current and maximum load current to operate correctly. The simplest method is to set the pick-up current to be larger than the maximum load current by an acceptable factor. The setting here used the factor K = 2.3 as recommended by IEEE standard [67].

- For utility relay: the maximum load current is 0.81 p.u. (from the load flow program before adding the SBDG). Therefore, the utility relay pick-up current is 2.3×0.81=1.86 p.u.

- For the SBDG relay: the maximum load current is based on the maximum power generated by the SBDG (P_{SBDG}) and its power factor (*p.f.*) with the terminal voltage is 1 p.u. Thus, the relay pick-up current can be set by (6.1).

$$I_{phase\_pick-up}(\text{SBDG})=2.3\times P_{SBDG}/pf \tag{6.1}$$

Ground overcurrent function settings

The pick-up current for the GOF is set to be 0.35 times of the POF pick-up current [67].

- For the utility relay: $I_{ground\_pick-up}(\text{utility}) = 0.35\times1.86 = 0.65$ p.u.
- For the SBDG relay:

$$I_{ground\_pick-up}(\text{SBDG})=0.35\times2.3\times P_{SBDG}/pf \tag{6.2}$$

6.1.2 Fault Currents and the Operation of Protection System

Assuming the size of SBDG connected to Bus 15 is $P_{max} = 1.2$ MW. Table 6.1 records the fault currents including both phase current (I_{phase}) and residual current (I_{res}) flowing through the utility relay when a SLGF occurs with a fault impedance Z_f = 20 Ω in the required protected area. The operation of the utility relay is easily performed using the ratio of fault current to the pick-up current (or the relay sensitivity). In this calculation, the wye winding neutral point of the interconnection transformer is grounded solidly to the earth (grounding reactance is zero).

Before adding the SBDG, the utility relay can detect the fault occurring inside the required protected area defined by the set of Buses {2, 5, 12, 14, 15, 18, 24, 29, 32, 34}. When the single line to ground fault occurs at one of the buses {24, 29, 32, 34}, neither POF nor GOF of utility relay can sense the fault. This is because the installation of the SBDG and the interconnection transformer created new flowing paths for fault currents. As a result, sensitivities of utility relay reduce to be less than 1, causing the fault to be undetected.

During the transient period, which usually lasts from 0.5 to 2 seconds after the fault instant, an SBDG can be modeled as a voltage source connected in series with an impedance. This impedance represents the transient reactance of the SBDG. At a larger size of the SBDG, the respective transient reactance is smaller and vice versa. Therefore, the fault current from the SBDG is higher if its size is larger, causing current flowing through the utility relay to be smaller. Installation of a large SBDG causes significant reduction in the reach of the utility relay as illustrated in Figure. 6.2.

Table 6.1 Fault current changes and the operation of the protection system

Case	Function	Faulted bus									
		2	5	12	14	15	18	24	29	32	34
Without SBDG, Pick-up values: I_{pPOF}=1.86 p.u. I_{pGOF}=0.65 p.u.	I_{phase}, p.u.	8.75	5.84	2.76	3.61	3.67	2.82	2.60	2.47	2.48	2.42
	I_{res}, p.u.	8.11	5.01	1.80	2.56	2.61	1.79	1.46	1.35	1.35	1.31
	I_{phase}/I_{pPOF}	4.71	3.14	1.48	1.94	1.97	1.52	1.40	1.33	1.33	1.30
	I_{res}/I_{pGOF}	12.48	7.71	2.77	3.93	4.01	2.75	2.25	2.08	2.08	2.01
	Detection	Yes	Yes	Yes	Yes	Yes	Yes	Yes	Yes	Yes	Yes
With SBDG, Pick-up values: I_{pPOF}=1.86 p.u. I_{pGOF}=0.65 p.u.	I_{phase}, p.u.	7.56	4.85	1.69	2.76	2.87	1.72	1.46	1.35	1.35	1.31
	I_{res}, p.u.	7.73	4.55	0.94	1.36	1.39	0.76	0.57	0.52	0.52	0.50
	I_{phase}/I_{pPOF}	4.07	2.61	0.91	1.49	1.54	0.93	0.78	0.73	0.73	0.71
	I_{res}/I_{pGOF}	11.89	7.00	1.45	2.09	2.13	1.16	0.88	0.80	0.80	0.77
	Detection	Yes	Yes	Yes	Yes	Yes	Yes	No	No	No	No

In Figure 6.2, the reductions of both phase and residual currents from Bus 1 to Bus 2, which are also the fault currents through the utility relay, increase when the SBDG increases from 0 MW (system without SBDG) to 2 MW in size. It can be seen that when the SBDG exceeds 0.6 MW, the POF cannot detect the fault but the utility relay still senses the fault with the GOF. When the SBDG exceeds 1.5 MW, both of the two functions cannot sense the fault and the feeder is no longer protected successfully.
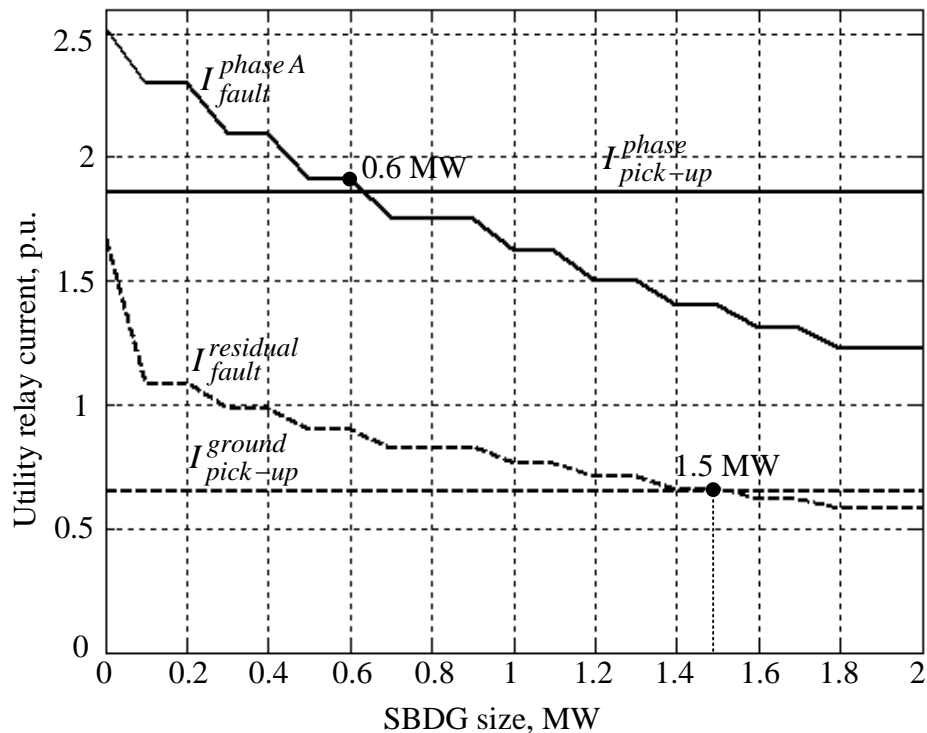
Figure 6.2 Utility relay current changes due to a SLGF at Bus 29

The utility relay reach reduction is manifested through consequently testing a SLGF from Bus 1 to Bus 34 as shown in Figure 6.3. The utility relay can protect the whole feeder before installing the SBDG except Buses 21 and 22. These two buses are covered by the protective devices at the XFM-1 substation. After installing a 2 MW SBDG, the protection zone is reduced from Bus 34 to Bus 20 as in Figure 6.4. At Bus 34, both phase and residual currents through the utility relay are lower than the respective overcurrent pick-up values, causing the relay to be blind to the fault. This illustration is the evidence for the necessity of the consideration of the utility reach reduction as a constraint in maximizing the SBDG size later on.
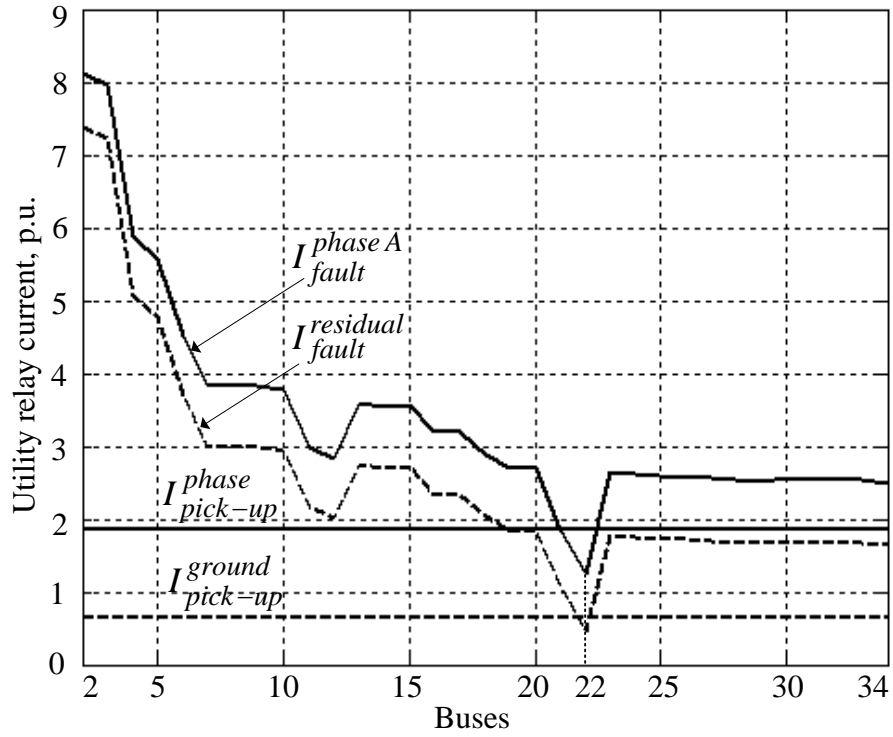
Figure 6.3 Utility relay reach before installing SBDG (SLGF case)
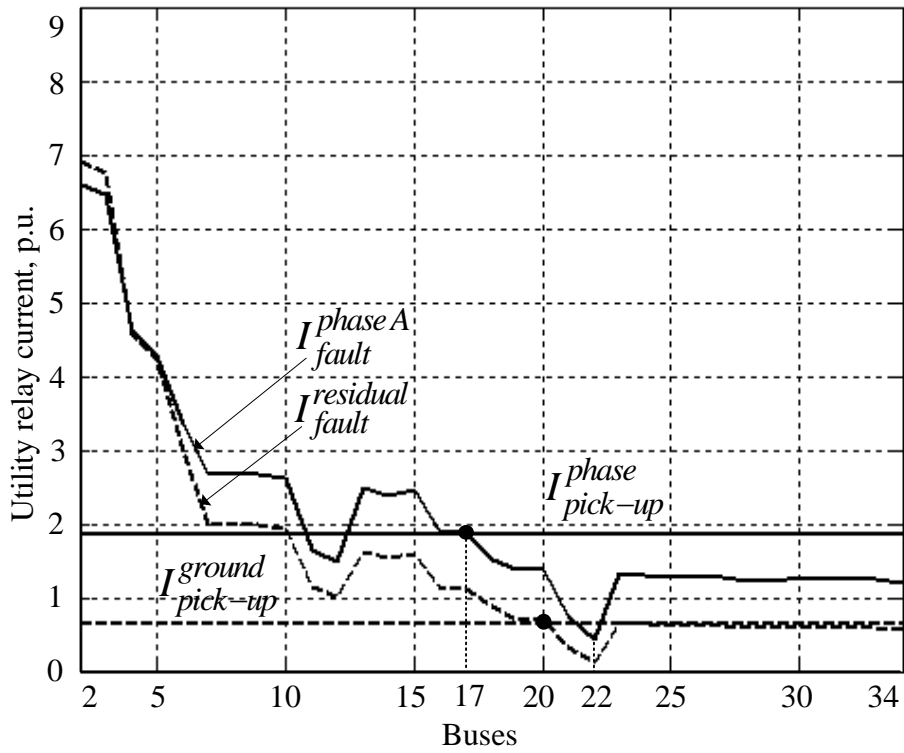
Figure 6.4 Utility relay reach after installing SBDG = 2MW (SLGF case)

As discussed in Chapter 2, the IBDG installation also presents impact on the reduction of utility relay reach even that the change is small. For instance, when a three-phase fault is assumed to occur at Bus 29 through the impedance of 20 Ω, Table 6.2 shows the reduction of the fault current through the utility relay in percent of that fault current before installing IBDG. The IBDG is assumed to operate at the maximum active power output and unity power factor mode before the fault. It can be seen that the larger the IBDG is, the higher the reduction becomes in this case. Although the highest reduction in this fault case is quite small, it still has an effect on the total maximum DG which is determined by the reach reduction constraint.

Impacts of IBDG installation on the reach of the utility relay is prominent if the GOF is considered. This is because the IBDG installation requires an interconnection transformer. In the case of the delta-grounded-wye winding transformer, a new path for the zero-sequence current to flow is created. The larger IBDG size means a smaller impedance in per unit of the system base. Thus, the zero-sequence current flowing through the utility relay tend to decrease if a larger IBDG is installed. Although the reduction in case of three-phase fault is small, a SLGF case can illustrate larger reduction in the residual current flowing through the utility relay as shown in Table 6.2.

Table 6.2 Reduction of fault current through the utility relay due to the IBDG's installation

Fault case	Items	Without IBDG	With IBDG			
	IBDG size, MW	-	0.5	1.0	1.5	2.0
3F at Bus 29	Utility relay current, p.u.	2.91	2.90	2.89	2.88	2.88
	Reduction, %	-	0.34	0.69	1.03	1.03
SLGF at Bus 29	Utility relay current, p.u.	1.67	1.14	0.85	0.68	0.57
	Reduction, %	-	31.74	49.10	59.28	65.87

6.2 SBDG Maximization

This section proposes a method to determine the maximum DG added to Bus 15 along with a grounding reactance at the wye winding's neutral point of the interconnection transformer subject to maintaining the relay sensitivity greater than 1. The sensitivity-based algorithm is firstly applied to show the validity of the concept.

Then, the Tabu search algorithm is used to illustrate its advantages in the multi-variable optimization.

6.2.1 SBDG Maximization Using the Sensitivity-based Algorithm

The method presented in Chapter 4 is applied here. Constraints from the system operating limits are added into the POF constraints. The analysis here follows the order of appearance discussed in Chapter 4.

6.2.1.1 Phase Overcurrent Function (POF) Analysis

Constraints of system operating limits

The SBDG capacity is limited to the range of 0 to 2.5 MVA and the SBDG is modeled as a constant PQ source in load flow program with a constant power factor of 0.9. The substation transformer capacity is 2.5 MVA and the line capacity is 2 MVA throughout the test system. Bus voltages are limited from 0.95 p.u. to 1.05 p.u.

POF constraints

The fault impedance is 20 Ω. Pick-up currents for the utility and SBDG relays are the same as those computed in Section 6.1. For illustration, a three-phase fault at Bus 29 is used.

Figure 6.5 illustrates the changes of phase currents through the utility breaker (Line 1-2 in Figure 6.1) and the SBDG breaker at the PCC (Bus 15). It can be seen that the fault current through the utility relay decreases while the fault current through the SBDG relay increases. From this figure, when the SBDG size reaches 1.2 MW, the fault current flowing through the utility breaker is lower than the pick-up value, or the protection is lost. Thus, to remain the reach of utility relay for three-phase fault at Bus 29, the SBDG size must be less than 1.2 MW, i.e. $P_{SBDGmax}$=1.1 MW if ΔP_{SBDG}=0.1 MW.

Phase currents vs. DG size
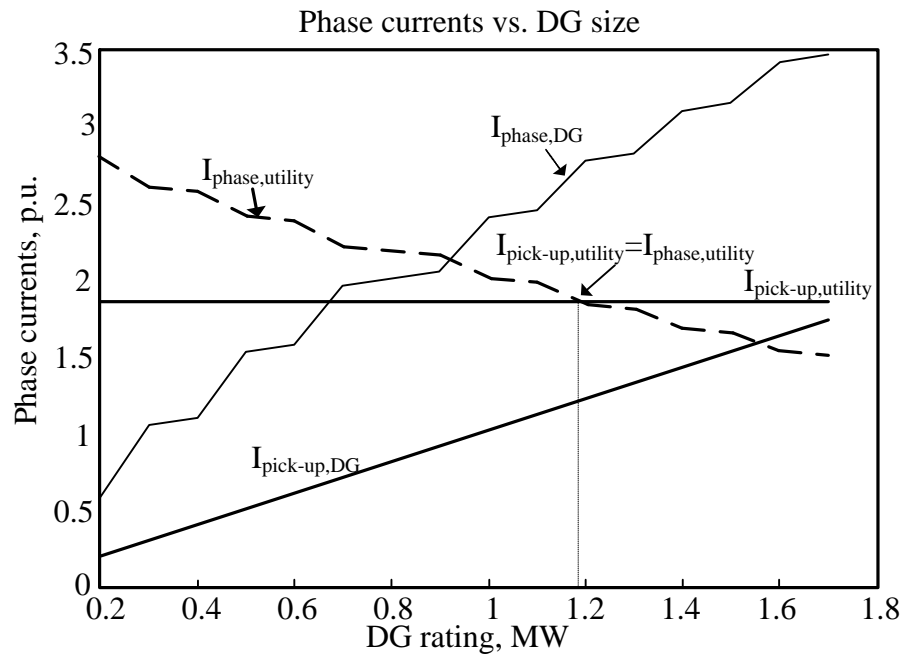
Figure 6.5 Phase current changes

After both the three-phase and line-to-line faults are applied to all buses sequentially inside the required protection area, the SBDG size of 1.1 MW is the maximum value that can be installed at Bus 15 subject to maintaining the POF function of the utility relay.

6.2.1.2 Ground Overcurrent Function (GOF) Analysis

The maximum SBDG from the POF analysis is used to obtain X_N as the flow chart depicted in Figure 4.6. Firstly, the value of X_N is increased with the incremental amount $\Delta X_N = 0.1$ Ω. The first value of X_N at which the residual current through the utility breaker is greater than the ground overcurrent pick-up value of utility relay (0.65 p.u. as computed in Section 6.1) is accepted as X_{Nmin}. Secondly, Figure 4.7 is applied to obtain X_{Nmax}.

Figure 6.6 illustrates the changes of residual currents, which are used to compare with the GOF pick-up values, through the utility and SBDG relays versus the reactance grounding when a single line to ground fault occurs at Bus 29. According to this figure, the residual current at the utility breaker is less than the pick-up current until X_N reaches a value of 1.5 Ω; whereas, the residual current at the SBDG side decreases following the increase of X_N. After X_N reaches the value of 105 Ω, the residual current becomes lower than the GOF pick-up value of the SBDG relay.
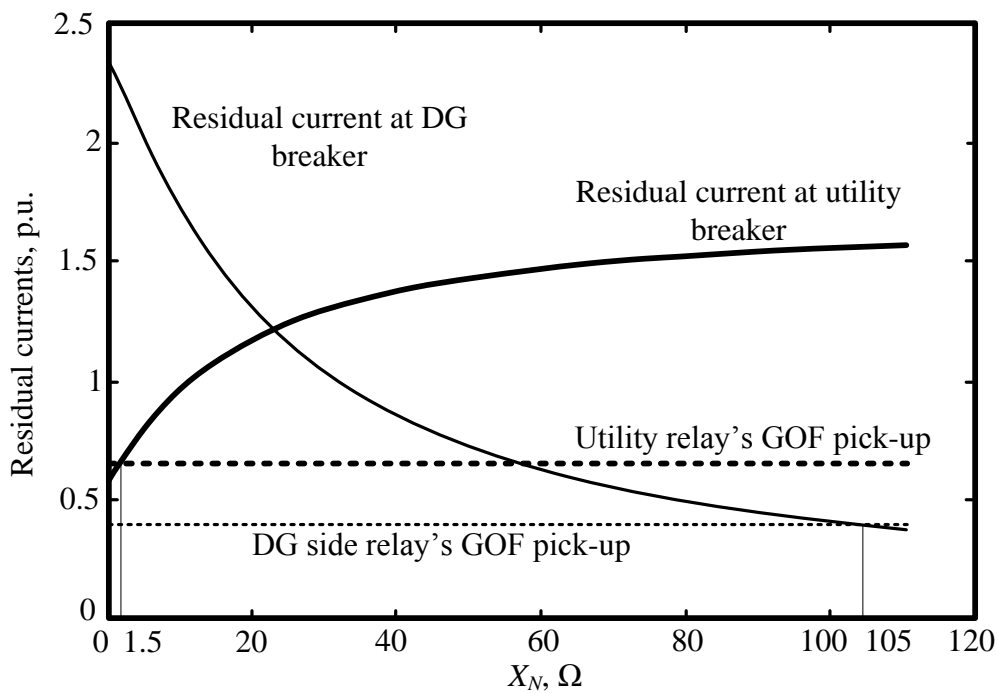
Figure 6.6 Residual current changes
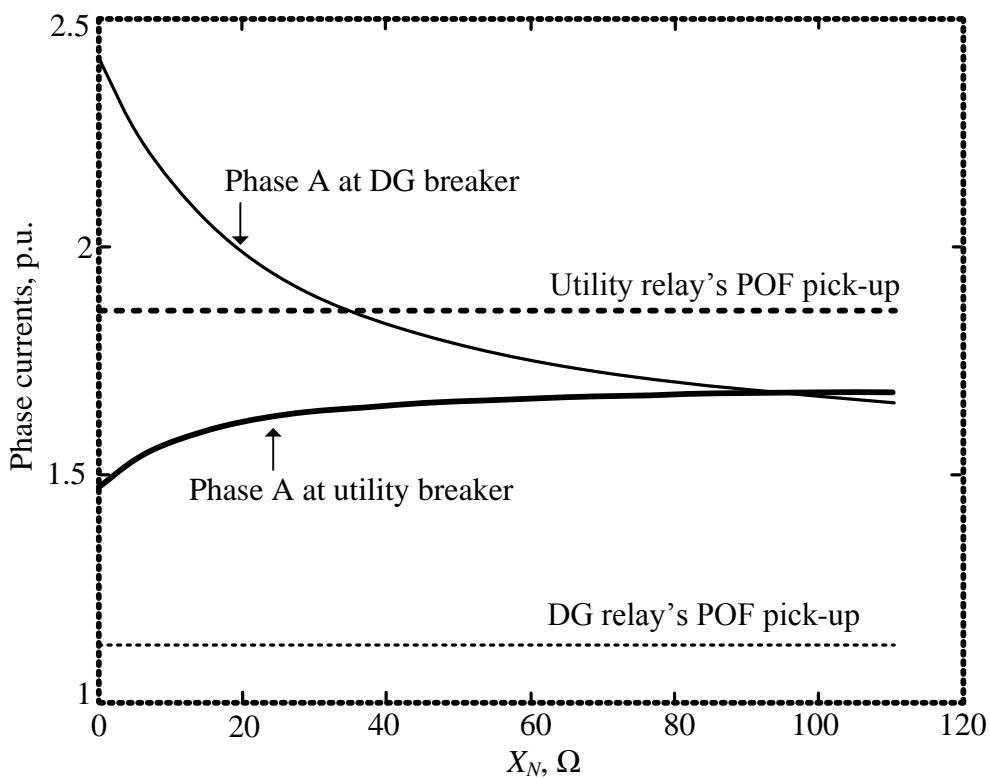
Figure 6.7 Phase currents under ground fault condition

Figure 6.7 illustrates the changes of phase currents in this case and shows that when a single line to ground fault occurs at Bus 29, the POF of utility relay cannot detect the fault because $I_{phase}/I_{pPOF} < 1$. For the SBDG relay, although the GOF cannot detect the fault when X_N is greater than 105 Ω (Figure 6.6), it still senses the fault with the POF as in Figure 6.7. Thus, for a SLGF at Bus 29, the grounding reactance must be greater than 1.5 Ω and smaller than the designed limit of the reactor that is 150 Ω.

When both the single and DLGFs are applied to all buses sequentially inside the required protection area, in correspondence to the 1.1 MW SBDG, X_N must be in a range of 2 to 150 Ω.

6.2.1.3 Temporary Overvoltage (TOV) Analysis Under Islanding Condition

As discussed in Chapter 4, the inequality (4.16) is checked with the ground faults under the unintentional islanding condition. Simulation results show that the TOV depends much on the zero-sequence impedance viewed from the faulted bus (Thevenin impedance). As a result, not only X_N but also the equivalent load impedance can affect the TOV. Under the light load condition, the islanding system has a higher TOV than the one in system under the full load condition as shown in Figure 6.8, which illustrates the unfaulted phase voltage at Bus 15 when a single line to ground fault occurs at this bus.
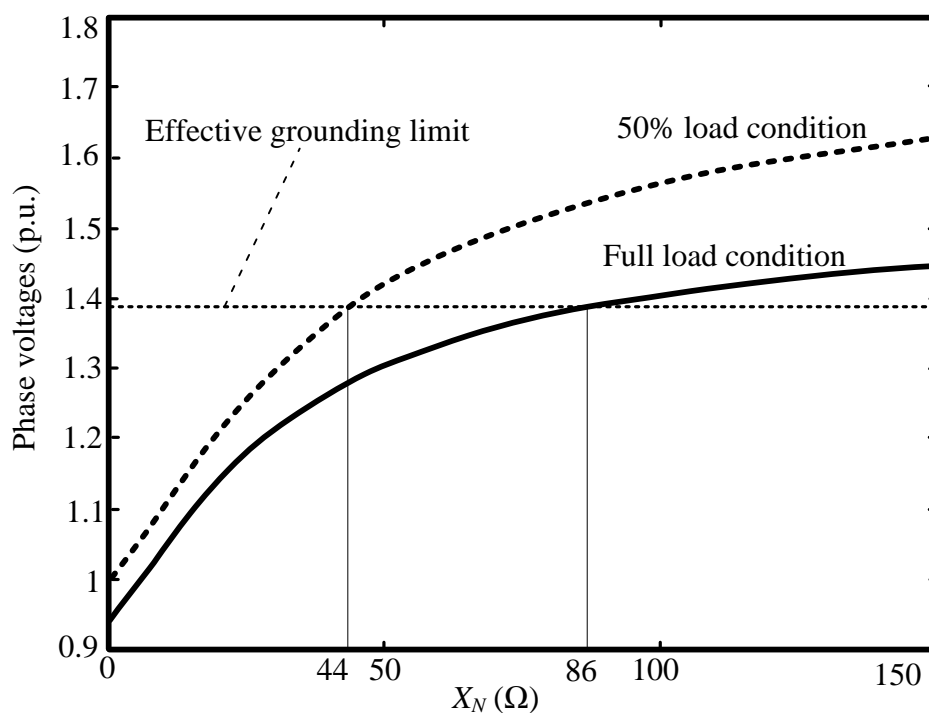
Figure 6.8 TOV under different load conditions

Due to the effective grounding limit, voltage of the unfaulted phase should not be greater than 1.39 p.u. If the full load condition is taken for limiting X_N, 86 Ω is the maximum reactance that ensures the effectively grounded condition for the system under the unintentional islanding condition.

As a summary after using the sensitivity-based algorithm, the maximum SBDG size that can be installed in the system at Bus 15 is 1.1 MW. A grounding reactance having the value ranging from 2 to 86 Ω should be used to mitigate the operation of the protective devices.

6.2.2 SBDG Maximization Using the Tabu Search Algorithm

6.2.2.1 Verification of the Tabu Search Algorithm

The initial point (starting point) is assumed to be the minimum value of SBDG active power (0.1 MW). From the starting point, the Tabu search algorithm generates its neighborhoods and selects the best one based on the objective function value. The selected neighborhood then turns to be a new starting point in the next iteration. The searching process stops when there are no better neighborhoods. That is, one local optimum point may be found. In order to reinforce the possibility of reaching the global optimum, a diversification technique is applied. For instance, the iteration goes back to the initial point to form a new searching path. It may go to another local optimum point. The program stops after a certain number of iterations. For the discussing problem, after the first five iterations, the maximum point of 1.1 MW is achieved as illustrated in Figure 6.9. Then, the searching process is diversified. After another process of five iterations, the point of 1.1 MW is still found and the algorithm stops. The best maximum point is accepted as 1.1 MW. With this value, another Tabu search as mentioned in Section 4.4 is applied to minimize X_N. The result is 2 Ω and this value is the same as X_{Nmin} obtained from the sensitivity-based algorithm introduced in Section 6.2.1.

On the other hand, the sensitivity-based method moved from the initial point (0.1 MW) to the final result (1.1 MW) discretely with an increasing step of 0.1 MW. At each SBDG level, the grounding reactance was changed from zero to X_{Nmax} (Figures 4.6 and 4.7) for checking. If X_{Nmax} and the upper design limit of the grounding reactance are identical, the calculation time may be longer.
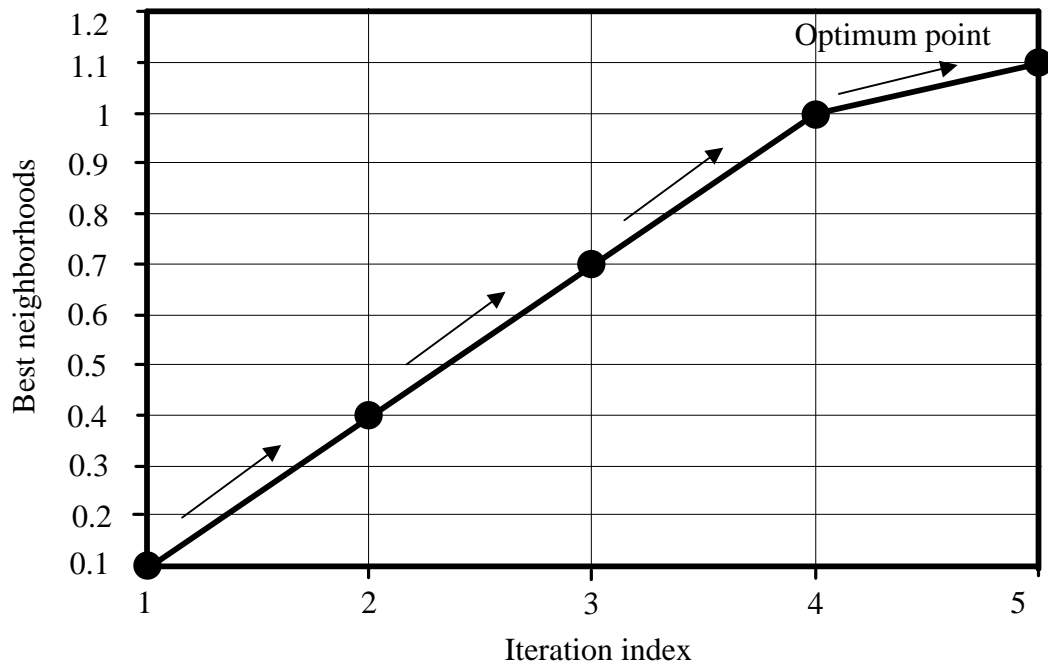
Figure 6.9 Moving process in the 1st five iterations of Tabu search

It can be summarized that although the sensitivity-based method and the Tabu search method give the same result from the same initial point, the latter reaches the optimum point faster than the former does. This summary is more significant in the case of the optimization problem with multi variable, i.e. several SBDG units.

6.2.2.2 Tabu Search Application in a Multi-variable Optimization Problem

In this section, the Tabu search algorithm is employed to solve a multi-variable optimization problem, e.g. 2 variables. Assuming another SBDG is installed at Bus 32, the objective function (4.17) has $n = 2$. In this application, $P_{DG,1}$ and $P_{DG,2}$ are searched at the same time. The grounding reactance is also minimized by using the Tabu search algorithm. The result from the program shows that the total maximum installed power is 1.5 MW. Figure 6.10 represents the relation between power from the SBDG units, [$P_{SBDG,1}$; $P_{SBDG,2}$], and the grounding reactance [$X_{Nmin,1}$; $X_{Nmin,2}$]. If X_{Nmin} is set as a priority to maximize SBDG, from Figure 6.10, the maximum size for SBDGs is [0.4, 1.1] MW which is corresponding to the minimum grounding reactance of [0, 2.1] Ω.
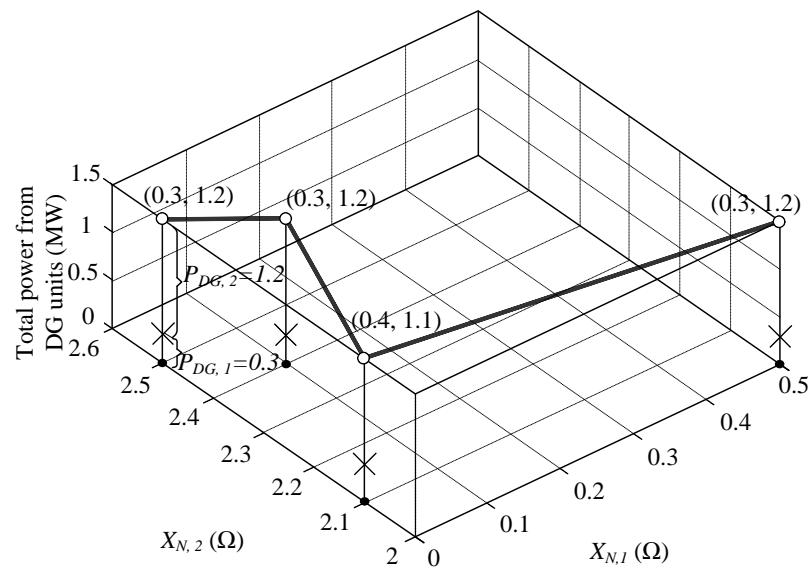
Figure 6.10 Minimization of X_N with respect to $P_{SBDGmax}$

6.3 SBDG and IBDG Maximization

The SBDG at Bus 32 in Section 6.2.2 is replaced by an IBDG. The fault current supported from the IBDG is not far from its rated current so that the protection system of the IBDG employs other methods to detect abnormal conditions. One of them uses voltage at the PCC (Bus 32). As a result, the grounding reactance is not concerned for installing at the neutral point of the IBDG interconnection transformer. The protection system of the SBDG still uses the overcurrent scheme as the main function. In a fault event, both SBDG and IBDG are required the FRT capability mentioned in Chapter 2. Additionally, the dynamic network support is also required for the IBDG as discussed in Chapters 2 and 3. The optimization algorithm utilized in Section 6.2 is possible to be used here with an integration of the fault calculation algorithm in Chapter 3.

There is a maximum IBDG in corresponding to a specific SBDG for installing in the test system in order to satisfy the system operating limits constraints. Table 6.3 lists such 11 pairs of (SBDG, IBDG) without the consideration of the utility relay reach constraint. The total maximum size ranges from 1.8 to 2.3 MW. If the IBDG is large, e.g., 2 MW, the corresponding maximum SBDG will be small, i.e., 0.3 MW, and vice versa.

The maximization algorithm starts with a random selection of DG capacity (P_{SBDG} = 0.1 MW, P_{IBDG} = 0.2 MW) as an initial point. From this point, a neighborhood is created by varying the discrete capacity of each DG. In this case study, DG capacity is varied discretely with the step 0.1 MW. Therfore, if the radius is chosen as $R_1 = 3$, the

furthest neighborhood is (3×0.1 = 0.3 MW) far from the standing point. For instance, in Figure 6.11, there are 12 neighborhoods being generated from the standing point. Whenever a move is selected, the point at the opposite direction (the previous point) is added into the Tabu list.

In order to determine the maximum allowable DG, all types of fault (3F, SLGF, DLGF, and LLF) are sequentially applied to each bus in the system (from Bus 1 to Bus 34) for each checking point (P_{SBDG}, P_{IBDG}) as the algorithm illustrated in Chapter 4. The adaptive fault current calculation is applied to calculate the fault currents for checking the operation of the utility relay. In each iteration, a point becomes the local optimum if there are no any better neighborhoods around it. Figure 6.12 illustrates a trace through local optimums. The optimum (P_{SBDG} = 0.3 MW, P_{IBDG} = 2 MW) is reached from the initial point (P_{SBDG} = 0.1 MW, P_{IBDG} = 0.2 MW) after going through eight local optimums.

Table 6.3 Maximum DGs installed in the system for system operating limits constraints (without utility relay reach constraint)

DG	Generation, MW										
P_{SBDG}	0.3	0.5	0.6	0.7	0.8	1.0	1.2	1.4	1.5	1.6	1.7
P_{IBDG}	2	1.8	1.5	1.4	1.2	1.0	0.7	0.5	0.3	0.2	0.1
Sum	2.3	2.3	2.1	2.1	2.0	2.0	1.9	1.9	1.8	1.8	1.8
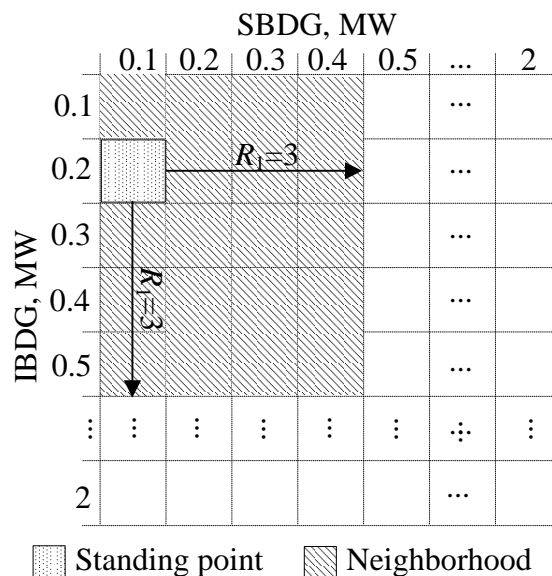
Figure 6.11 An example of neighborhoods generation
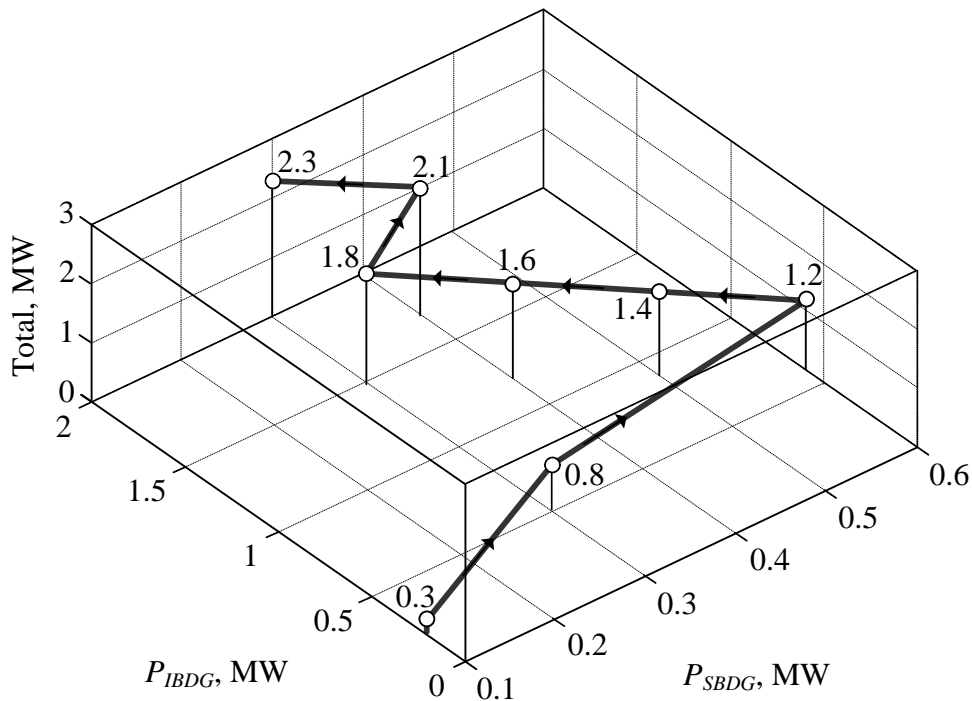
Figure 6.12 A path from the initial point to the optimum point

The final result shows that the maximum allowable DG is 2.3 MW at which ($P_{SBDGmax}$ = 0.3 MW, $P_{IBDGmax}$ = 2 MW). According to Table 6.3, although the pair (P_{SBDG} = 0.5 MW, P_{IBDG} = 1.8 MW) has the sum of 2.3 MW, it is not the maximum allowable DG. The reason is that the reach reduction constraint is not satisfied at this point. That is, the utility relay cannot sense a SLGF at Bus 34 with both phase and ground overcurrent functions. It should be noted that the maximum allowable DG is found as a sum of all DG capacities. However, the proposed algorithm in this paper can identify exactly the allowable capacity for each DG.

6.4 Summary of Chapter 6

This chapter used the algorithms in Chapter 4 and tested them with IEEE test system. Impacts of DGs on the utility system were illustrated: SBDG caused the reach reduction for the utility overcurrent relay, causing a part of the feeder to become unprotected; whereas, IBDG had remarkable effects on utility relay reach reduction. By comparing with the sensitivity-based algorithm, which is more reliable, the Tabu search algorithm was verified successfully in case of one variable optimization. The Tabu search algorithm was then extended to multi-variable optimization for a system with SBDG and IBDG. The maximum installation capacities of DGs obtained from the proposed algorithms assure the capability of detecting faults for the utility relay

under the impacts DGs on fault current considering the fault ride through requirement. The system operating parameters are set in optimization constraints so that these parameters can be maintained within the limited ranges during the normal operation of the system with the maximum installed DGs.

CHAPTER VII

CONCLUSION AND RECOMMENDATIONS

7.1 General Conclusion

This thesis proposes an algorithm for DG maximization in distribution networks. The maximum installation capacity of DG obtained from the proposed algorithm assures the capability of detecting faults for the utility relay under the impacts DGs on fault current considering the fault ride through requirement. The system operating parameters including substation transformer capacity, bus voltages, and line currents are maintained inside the allowable bounds during the normal operation of the system with the identified maximum installed DG. The algorithm considers a set of DGs, which are expected to be installed in the system, at the same time. After installing these DGs, if another DG is expected to integrate to the system, it has to follow the condition of the system including the installed DGs.

This thesis also proposes an adaptive fault calculation algorithm for a distribution network with SBDG and IBDG in order to assist the DG maximization algorithm in estimating fault currents in the system. Time-variant response of an IBDG to a fault occurring in the network to which it is connected is analyzed. With the proposed control system for the inverter of the IBDG, the current output of the inverter purely symmetrical in corresponding to the positive-sequence voltage at the connection point of the IBDG. The transient duration in the fault response lasts a few cycles and can be neglected in fault analysis. If the power output is controlled to be constant, the IBDG can be represented by a constant PQ or current source in a balanced and symmetrical system for fault calculation. Bus voltages and line currents are solved by employing Newton Raphson algorithm. The fault calculation algorithm proposed in this thesis is practical and fast applicable. This algorithm can replace the conventional fault calculation for a system without IBDG. But more importantly, it can be applicable in a system with IBDG.

Impacts of SBDG and IBDG on utility relay reach have been analyzed in the thesis: SBDG causes the prominent reach reduction for the utility overcurrent relay, causing a part of the feeder to become unprotected; whereas, IBDG has remarkable effects on utility relay reach reduction. These impacts are necessarily to be taken into account in practice to prevent unexpected effects of DG on the operation of the utility protection system. This thesis shows that the utility relay is aided in reaching the

required bus in the system if a proper DG size is used. Besides, other auxiliary assistance can be used such as suitable grounding reactance and interconnection transformer. If saving cost is preferred, the grounding reactance can be minimized by the proposed DG maximization algorithm in this thesis.

The algorithm for DG maximization can be applicable in a smart grid. Providing that the settings of protective devices can be adjusted following the changes of load and system configuration, the maximum allowable DG obtained from the algorithm is a reference for the distribution system operators to accept/refuse the connection of DG. In this case, the decision can be generated from adjusting the input of the DG maximization algorithm to take the changes of system configuration, load condition, and DG location.

7.2 Recommendations

1. Maximization of DG should consider more impacts of DG installation such as protection coordination and false tripping problem. The Tabu search algorithm is still suitable but other methods may be more efficient.

2. In practice, not only the IBDG control system in this thesis but also other method is employed to control the IBDG. Thus, the fault response of the IBDG may be different causing the different model for fault calculation. It is a challenge to propose a general model suitable for all control systems.

3. In case of other control mode of the IBDG such as voltage control mode, the fault response of the IBDG may be different from what presented in this thesis. In that case, a new model should be created.

REFERENCES

[1]   Willis, H.L. and Scott, W.G. *Distributed Power Generation: Planning and Evaluation*. First Edition. New York: CRC Press, 2000.

[2]   Dugan, R.C., McGranaghan, M.F., Santoso, S., and Beaty, H.W. *Electrical Power Systems Quality*. Second Edition. New York: McGraw-Hill, 2004.

[3]   Freris, L. and Infield, D. *Renewable Energy in Power Systems*. First Edition. Great Britain: John Wiley and Sons, 2008.

[4]   Coster, E.J., Myrzik, J.M.A., Kruimer, B., and Kling, W.L. Integration Issues of Distributed Generation in Distribution Grids. Proceedings of the IEEE Volume 99 Issue 1 (2011): 28-39.

[5]   Dao Van Tu and Chaitusaney, S. Relay sensitivity approach for maximizing Distributed Generation. in IEEE Xplore Digital Library, Proceedings of the IEEE Region 10 Conference, 1010-1014. Bali-Indonesia: Institute of Electrical and Electronics Engineers (IEEE), 2011.

[6]   Dao Van Tu, Chaitusaney, S., and Yokoyama, A. Maximization of Distributed Generation by Considering System Operating Limits and Protection Reach Reduction as Constraints. *IEEJ Transactions on Electrical and Electronic Engineering* 7 (December 2012): S37-S45.

[7]   The MathWorks Inc. MATLAB. [Software R2009a]. 2009.

[8]   Power Systems Engineering Research Center (PSERC). MATPOWER. [Software Version 4.1]. 2011.

[9]   International Energy Agency. Photovoltaic power systems programme. Trends in Photovoltaic Applications—Survey Report of Selected IEA Countries Between 1992 and 2008 [Online]. 2009, Available from: http://www.iea-pvps.org/fileadmin/dam/public/report/statistics/tr_2008.pdf [October 10, 2011]

[10]   Government of Japan. Energy in Japan 2010. Agency for Natural Resources and Energy. [Online] Available from: http://www.enecho.meti.go.jp/topics/energy-in-japan/english2010.pdf [October 10, 2011].

[11]   Institute of Electrical and Electronics Engineers (IEEE). IEEE Standard for Interconnecting Distributed Resources with Electric Power Systems. IEEE Standard 1547-2003, July 2003.

[12]   Buso, S. and Mattavelli, P. *Digital Control in Power Electronics*. Morgan & Claypool Publishers, 2006.

[13]   Ko, S.H., Lee S.R., Dehbonei H., and Nayar C.V. Application of Voltage- and Current-Controlled Voltage Source Inverters for Distributed Generation Systems. *IEEE Transactions on Energy Conversion* 21 (September 2006): 782-792.

[14]   Strzelecki, R., Benyzek, G. *Power Electronics in Smart Electrical Energy Networks*. London: Springer-Verlag London Limited, 2008.

[15]   Keyhani, A., Marwali, M.N., Dai, M. *Integration of Green and Renewable Energy in Electric Power Systems*. New Jersey: John Wiley & Sons Inc, 2010.

[16]   Barker, P.P. and De Mello, R.W. Determining the impact of distributed generation on power systems-I-Radial distribution systems. in Proceedings of IEEE Power Engineering Society Summer Meeting, Volume 3, 1645-1656. Seattle WA: Institute of Electrical and Electronics Engineers (IEEE), 2000.

[17]   Dugan, R.C. and McDermott, T.E. Operating Conflicts for Distributed Generation on Distribution Systems. in IEEE Xplore Digital Library, Proceedings of IEEE Rural Electric Power Conference, A3/1 - A3/6. Little Rock AR: Institute of Electrical and Electronics Engineers (IEEE), 2001.

[18]   Girgis, A. and Brahma, S. Effect of Distributed Generation on Protective Device Coordination in Distribution System. in IEEE Xplore Digital Library, Proceedings of IEEE LESCOPE'01 Large Engineering System Conference,115-119. Halifax NS: Institute of Electrical and Electronics Engineers (IEEE), 2001.

[19]   Walling, R.A., Saint, R., Dugan, R.C., Burke, J., and Kojovic, L.A. Summary of Distributed Resources Impact on Power Delivery *Systems. IEEE Transactions on Power Delivery* 23 (July 2008): 1636–1644.

[20]   Bloomquist and Walter, C. Select the Right Transformer Winding Connection for Industrial Power Systems. *IEEE Transactions on Industry Applications* IA-11 (November 1975): 641-645.

[21]   Mozina, C.J. Interconnect Protection of Dispersed Generators. in IEEE Xplore Digital Library, Proceedings of IEEE/PES Transmission and Distribution Conference and Exposition, Volume 2, 709 – 723. Atlanta GA: Institute of Electrical and Electronics Engineers (IEEE), 2001.

[22]   Arritt, R.F. and Dugan, R.C. Distributed Generation Interconnection Transformer and Grounding Selection. in IEEE Xplore Digital Library, Proceedings of IEEE Power and Energy Society General Meeting - Conversion and Delivery of Electrical Energy in the 21st Century, 1-7. Pittsburgh PA: Institute of Electrical and Electronics Engineers (IEEE), 2008.

[23] Zhang, W. Y., Zhu, S.Z., Zheng, J.H., and Zhang, H. Impacts of Distributed Generation on Electric Grid and Selecting of Isolation Transformer. in IEEE Xplore Digital Library, Proceedings of IEEE/PES Transmission and Distribution Conference and Exhibition: Asia and Pacific, 1-7. Dalian China: Institute of Electrical and Electronics Engineers (IEEE), 2005.

[24] Ministry of Industry and Trade of Vietnam. Vietnamese Distribution Systems Circular, 32/2010/TT-BCT, July 2010 (In Vietnamese).

[25] Wind Turbines Connected to Grids with Voltages Below 100 kV-Technical Regulations for the Properties and the Control of Wind Turbines, Energinet.dk, Technical Regulations TF 3.2.6. Fredericia, Denmark, Nov. 2004. [Online]. Available from: http://www.energinet.dk. [November, 2012].

[26] Distribution System Operators - ESB Networks. Irish distribution code. 2007.

[27] Bundesverband der Energie- und Wasserwirtschaft e. V. – BDEW, Network and System Rules of the German Transmission System Operators, August 2007.

[28] Bundesverband der Energie- und Wasserwirtschaft e. V. – BDEW, Grid code – Extra high voltage, April 2009.

[29] Bundesverband der Energie- und Wasserwirtschaft e. V. – BDEW, Guideline for generating plants' connection to and parallel operation with the medium-voltage network, June 2008.

[30] Nara, K., Hayashi, Y., Ikeda, K., and Ashizawa, T. Application of Tabu Search to Optimal Placement of Distributed Generators. in IEEE Xplore Digital Library, Proceedings of IEEE Power Engineering Society Winter Meeting, Volume 2, 918-923. Columbus OH: Institute of Electrical and Electronics Engineers (IEEE), 2001.

[31] Jabr, Rabih A. and Pal, Bikash C. Ordinal Optimisation Approach for Locating and Sizing of Distributed Generation. IET Generation, Transmission & Distribution Volume 3 Issue 8 (2009): 713-723.

[32] Piccolo, A. and Siano, P. Evaluating the Impact of Network Investment Deferral on Distributed Generation Expansion. *IEEE Transactions on Power Systems* 24 (August 2009): 1559-1567.

[33] Abu-Mouti Fahad S. and El-Hawary Mohamed, E. Optimal Distributed Generation Allocation and Sizing in Distribution Systems via Artificial Bee Colony Algorithm. *IEEE Transactions on Power Delivery* 26 (October 2011): 2090-2101.

[34] Keane, A. and Malley, M. Optimal Distributed Generation Plant Mix with

Novel Loss Adjustment Factors. in IEEE Xplore Digital Library, Proceedings of IEEE Power Engineering Society General Meeting, 1-6. Montreal Canada: Institute of Electrical and Electronics Engineers (IEEE), 2006.

[35] Keane, A., Denny, E., and O''Malley, M. Quantifying the Impact of Connection Policy on Distributed Generation. *IEEE Transactions on Energy Conversion* 22 (March 2007): 189-196.

[36] Harrison, G.P., Piccolo, A., Siano, P., Wallace, R. Exploring the Tradeoffs Between Incentives for Distributed Generation Developers and DNOs. *IEEE Transactions on Power Systems* 22 (May 2007): 821-828.

[37] Ochoa, L.F. and Harrison, G.P. Minimizing Energy Losses Optimal Accommodation and Smart Operation of Renewable Distributed Generation. *IEEE Transactions on Power Systems* 26 (February 2011): 198-205.

[38] Keane, A. and Malley, M.J.O. Optimal Utilization of Distribution Networks for Energy Harvesting. *IEEE Transactions on Power Systems* 22 (February 2007): 467-475.

[39] Bhowmik, A., Maitra, A., Halpin, M.M., and Schatz, J.E. Determination of allowable penetration levels of distributed generation resources based on harmonic limit considerations. *IEEE Transactions on Power Delivery* 18 (April 2003): 619-624.

[40] Pandi, V.R., Zeineldin, H.H., and Xiao, W. Determining Optimal Location and Size of Distributed Generation Resources Considering Harmonic and Protection Coordination Limits. *IEEE Transactions on Power Systems* 28 (May 2013): 1245- 1254.

[41] Chaitusaney, S. and Yokoyama, A. Prevention of Reliability Degradation from Recloser–Fuse Miscoordination Due To Distributed Generation. *IEEE Transactions on Power Delivery* 23 (October 2008): 2545-2554.

[42] Shayani, R.A., De Oliveira, and Gonçalves, M.A. Photovoltaic Generation Penetration Limits in Radial Distribution Systems. *IEEE Transactions on Power Systems* 26 (August 2011): 1625-1631.

[43] Anderson PM. *Power System Analysis-IEEE PRESS Power Systems Engineering Series*. New York: John Wiley & Sons Inc, 1995.

[44] Saadat H. *Power System Analysis*. Second Edition. New York: McGraw-Hill Companies Inc, 2004.

[45] Anderson PM. *Analysis of Faulted Power Systems-IEEE PRESS Power Systems Engineering Series*. New York: John Wiley & Sons Inc, 1995.

[46]   Morren, J. and De Haan, S.W.H. Short-Circuit Current of Wind Turbines With Doubly Fed Induction Generator. *IEEE Transactions on Energy Conversion* 22 (March 2007):174-180.

[47]   Baran, M.E. and El-Markaby I.L. Fault Analysis on Distribution Feeders with Distributed Generators. *IEEE Transactions on Power Systems* 20 (November 2005): 1757-1764.

[48]   Nimpitiwan R.A.N., Heydt, G.T., and Suryanarayanan. Fault Current Contribution from Synchronous Machine and Inverter based Distributed Generators. *IEEE Transactions on Power Delivery* 22 (January 2007): 634-641.

[49]   Turcotte, D. and Katiraei, F. Fault Contribution of Grid-Connected Inverters. in IEEE Xplore Digital Library, Proceedings of IEEE Electrical Power Conference, 1-5. Montreal Canada: Institute of Electrical and Electronics Engineers (IEEE), 2009.

[50]   Nelson, R.J. and Ma, H.T. Short-Circuit Contributions of Full-Converter Wind Turbines. in IEEE Xplore Digital Library, Proceedings of IEEE Power and Energy Society General Meeting, 1-4. San Diego CA: Institute of Electrical and Electronics Engineers (IEEE), 2011.

[51]   Brucoli, M., Green, T.C., and MacDonald J.D.F. Modelling and Analysis of Fault Behaviour of Inverter Microgrids to Aid Future Fault Detection. in IEEE Xplore Digital Library, Proceedings of IEEE International Conference on System of Systems Engineering, 1-6. San Antonio TX: Institute of Electrical and Electronics Engineers (IEEE), 2007.

[52]   Kaźmierkowski, M.P. and Malesani, L. Current Control Techniques for Three-Phase Voltage-Source PWM Converters: A Survey. *IEEE Transactions on Industrial Electronics* 45 (October 1998): 691-703.

[53]   Carrasco, J.M. et al. Power-Electronic Systems for the Grid Integration of Renewable Energy Sources: A Survey. *IEEE Transactions on Industrial Electronics* 53 (June 2006): 1002-1016.

[54]   Brucoli, M. Fault behavior and fault detection in islanded inverter-only microgrids. PhD Dissertation, Department of Electrical and Electronic Engineering, Faculty of Engineering, Imperial College London, 2008.

[55]   Prodanovic, M. and Green, T.C. Control and Filter Design of Three-phase Inverters for High Power Quality Grid Connection. *IEEE Transactions on Power Electronics* 18 (January 2003): 373-380.

[56]   Wall, S.R. Performance of Inverter Interfaced Distributed Generation. in IEEE Xplore Digital Library, Proceedings of IEEE/PES Transmission and Distribution Conference and Exposition, Volume 2, 945-950. Atlanta GA: Institute of Electrical and Electronics Engineers (IEEE), 2001.

[57]   Keller, J. and Kroposki, B. Understanding Fault Characteristics of Inverter-based DER. [Online] Available from:

http://www.nrel.gov/docs/fy10osti/46698.pdf [2011].

[58]   Yazdanpanahi, H., Li, Y.W., and Xu W. A New Control Strategy to Mitigate the Impact of Inverter-Based DGs on Protection System. *IEEE Transactions on Smart Grid* 3 (September 2012): 1427-1436.

[59]   Teodorescu, R., Blaabjerg, F., Liserre, M., and Loh, P.C. Proportional-resonant Controllers and Filters for Grid-connected Voltage-source Converters. *IEE Proceedings-Electric Power Applications* 153 (September 2006): 750-762.

[60]   Brittain J.E. Thevenin's theorem. *IEEE Spectrum* 27 (March 1990): 42.

[61]   Institute of Electrical and Electronics Engineers (IEEE). IEEE Standard 1159-1995 IEEE Recommended Practice for Monitoring Electric Power Quality, 1995.

[62]   Institute of Electrical and Electronics Engineers (IEEE). IEEE Guide for the Application of Neutral Grounding in Electrical Utility Systems - Part 1 - Introduction, IEEE Standard C62.92.1, (2000).

[63]   Glover. F. Tabu search I. *ORSA Journal of Computing* 1 (Summer 1989): 190-206.

[64]   Glover. F. Tabu search II. *ORSA Journal of Computing* 2 (Winter 1990): 4-32.

[65]   Glover, F. and Laguna, M. *Tabu Search*. Kluwer Academic Publishers, 1997.

[66]   IEEE PES Distribution System Analysis Subcommittee. Distribution Test Feeders. [Online]. Available from:

http://www.ewh.ieee.org/soc/pes/dsacom/testfeeders/index.html [2011].

[67]   Institute of Electrical and Electronics Engineers (IEEE). IEEE Guide for Protective Relay Applications to Distribution Lines, IEEE Standard C37. 230, 2007.

APPENDICES

APPENDIX A

VECTOR TRANSFORMATION

In order to reduce the order of the mathematical model of a quantity in a three-phase electrical system simpler without any loss of information, the frame transformation is employed. Two fundamental tools are *αβ* and *dqo* transformations.

A1. The *αβ* Transformation

Voltages and currents in three-phase balanced system are ideal sinusoidal as in (A.1)

$$\begin{cases} \upsilon_a(t) = V\sin(\omega t + \theta) \\ \upsilon_b(t) = V\sin\left(\omega t + \theta - \frac{2\pi}{3}\right) \\ \upsilon_c(t) = V\sin\left(\omega t + \theta + \frac{2\pi}{3}\right) \end{cases} \tag{A.1}$$

Converting to *αβ* representation:

$$\begin{bmatrix} \upsilon_\alpha(t) \\ \upsilon_\beta(t) \\ \upsilon_\gamma(t) \end{bmatrix} = \frac{2}{3}\begin{bmatrix} 0 & -\frac{\sqrt{3}}{2} & \frac{\sqrt{3}}{2} \\ 1 & -\frac{1}{2} & -\frac{1}{2} \\ \frac{1}{\sqrt{2}} & \frac{1}{\sqrt{2}} & \frac{1}{\sqrt{2}} \end{bmatrix}\begin{bmatrix} \upsilon_a(t) \\ \upsilon_b(t) \\ \upsilon_c(t) \end{bmatrix}$$

$$\upsilon_\alpha(t) = \frac{2}{3}\begin{bmatrix} 0 & -\frac{\sqrt{3}}{2} & \frac{\sqrt{3}}{2} \end{bmatrix}\begin{bmatrix} V\sin(\omega t + \theta) \\ V\sin\left(\omega t + \theta - \frac{2\pi}{3}\right) \\ V\sin\left(\omega t + \theta + \frac{2\pi}{3}\right) \end{bmatrix} = \frac{2}{3}\left(-\frac{\sqrt{3}}{2}V\right)2\cos(\omega t + \theta)\underbrace{\sin\left(\frac{-2\pi}{3}\right)}_{=-\frac{\sqrt{3}}{2}}$$

$$= V\cos(\omega t + \theta)$$

$$\upsilon_\beta(t) = \frac{2}{3}\begin{bmatrix} 1 & -\frac{1}{2} & -\frac{1}{2} \end{bmatrix}\begin{bmatrix} V\sin(\omega t + \theta) \\ V\sin\left(\omega t + \theta - \frac{2\pi}{3}\right) \\ V\sin\left(\omega t + \theta + \frac{2\pi}{3}\right) \end{bmatrix} =$$

$$= \frac{2}{3}\left[V\cos\left(\omega t+\theta\right)+\left(-\frac{1}{2}V\right)2\sin\left(\omega t+\theta\right)\cos\left(\frac{-2\pi}{3}\right)_{=-\frac{1}{2}}\right]=V\sin\left(\omega t+\theta\right)$$

$$\upsilon_\gamma\left(t\right)=\frac{2}{3}V\frac{1}{\sqrt{2}}\left[\sin\left(\omega t+\theta\right)+\sin\left(\omega t+\theta-\frac{2\pi}{3}\right)+\sin\left(\omega t+\theta+\frac{2\pi}{3}\right)\right]=0$$
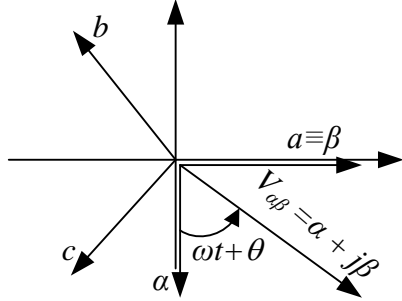
$$\begin{cases}\upsilon_\alpha\left(t\right)=V\cos\left(\omega t+\theta\right)\\\upsilon_\beta\left(t\right)=V\sin\left(\omega t+\theta\right)\\\upsilon_\gamma\left(t\right)=0\end{cases} \tag{A.2}$$

Figure A1. Representation of *abc* and *αβ* coordinates

A2. Park's Transformation

The *dqo* coordinates are obtained from the transformation as in (A.3).

$$\begin{bmatrix}\upsilon_d\\\upsilon_q\\\upsilon_0\end{bmatrix}=\frac{2}{3}\begin{bmatrix}\sin\left(\omega t\right)&\sin\left(\omega t-\frac{2\pi}{3}\right)&\sin\left(\omega t+\frac{2\pi}{3}\right)\\\cos\left(\omega t\right)&\cos\left(\omega t-\frac{2\pi}{3}\right)&\cos\left(\omega t+\frac{2\pi}{3}\right)\\\frac{1}{2}&\frac{1}{2}&\frac{1}{2}\end{bmatrix}\begin{bmatrix}V\sin\left(\omega t+\theta\right)\\V\sin\left(\omega t+\theta-\frac{2\pi}{3}\right)\\V\sin\left(\omega t+\theta+\frac{2\pi}{3}\right)\end{bmatrix}=\begin{bmatrix}V\cos\left(\theta\right)\\V\sin\left(\theta\right)\\0\end{bmatrix}$$

$$\tag{A.3}$$

Three-phase power representation in *dqo* coordinates (for balanced system only):

$$P=3V_{phase}^{rms}I^{rms}\cos\left(\theta_I-\theta_V\right)=\frac{3}{2}VI\cos\left(\theta_I-\theta_V\right)=\frac{3}{2}\left(VI\cos\theta_I\cos\theta_V+VI\sin\theta_I\sin\theta_V\right)$$

$$\rightarrow P=\frac{3}{2}\left(V_dI_d+V_qI_q\right) \tag{A.4}$$

$$Q=\frac{3}{2}VI\sin\left(\theta_I-\theta_V\right)=\frac{3}{2}\left(VI\sin\theta_I\cos\theta_V-VI\cos\theta_I\sin\theta_V\right)\rightarrow Q=\frac{3}{2}\left(V_dI_q-V_qI_d\right)$$

$$\tag{A.5}$$

From (A.4) and (A.5):

$$\begin{bmatrix}I_d\\I_q\end{bmatrix}=\frac{2}{3}\frac{1}{\left(V_d\right)^2+\left(V_q\right)^2}\begin{bmatrix}V_d&V_q\\V_q&-V_d\end{bmatrix}\begin{bmatrix}P\\Q\end{bmatrix} \tag{A.6}$$
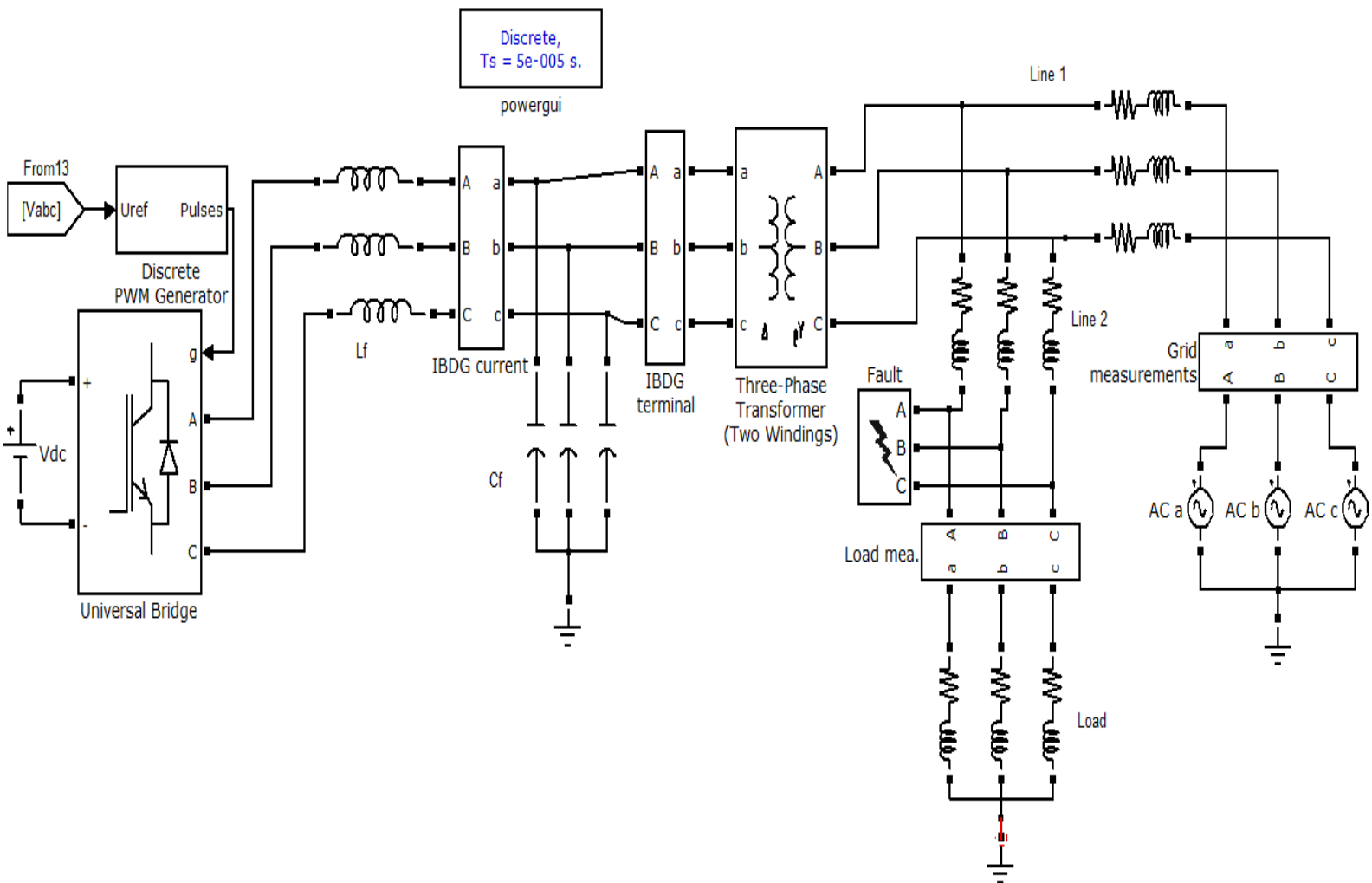
Figure B.1 Power system model in Chapter 5
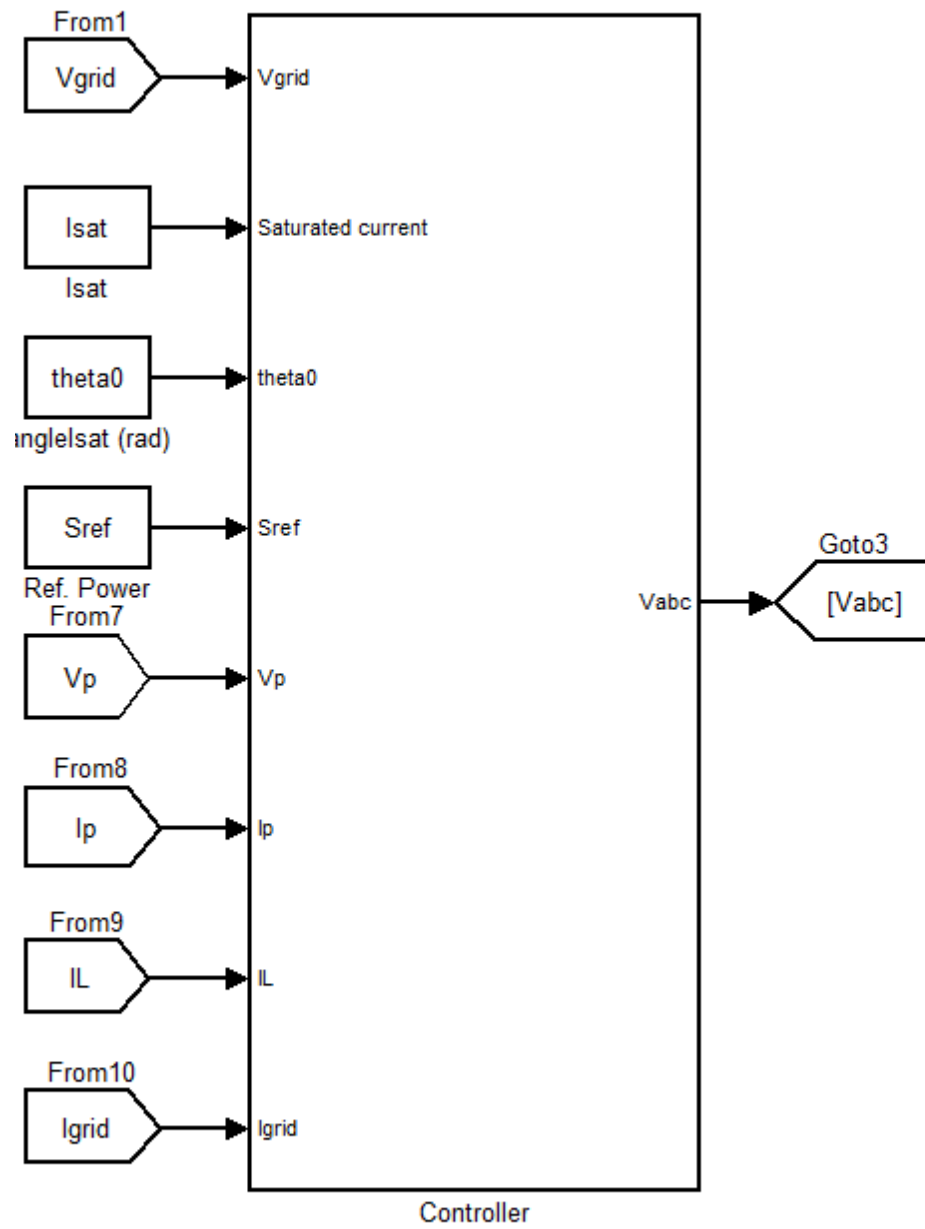
Figure B.2 Controller block
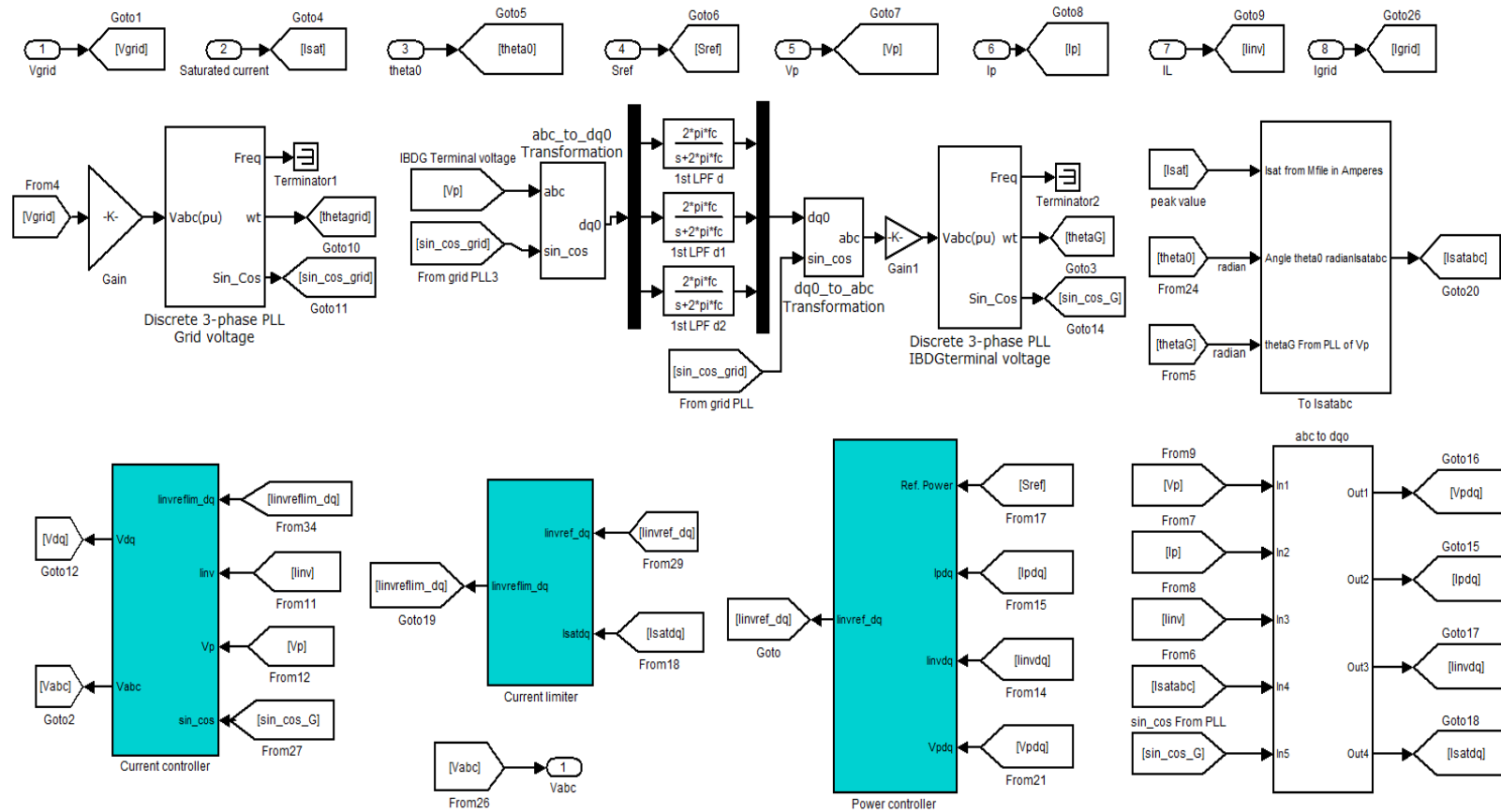
Figure B.3 Inside the Controller block
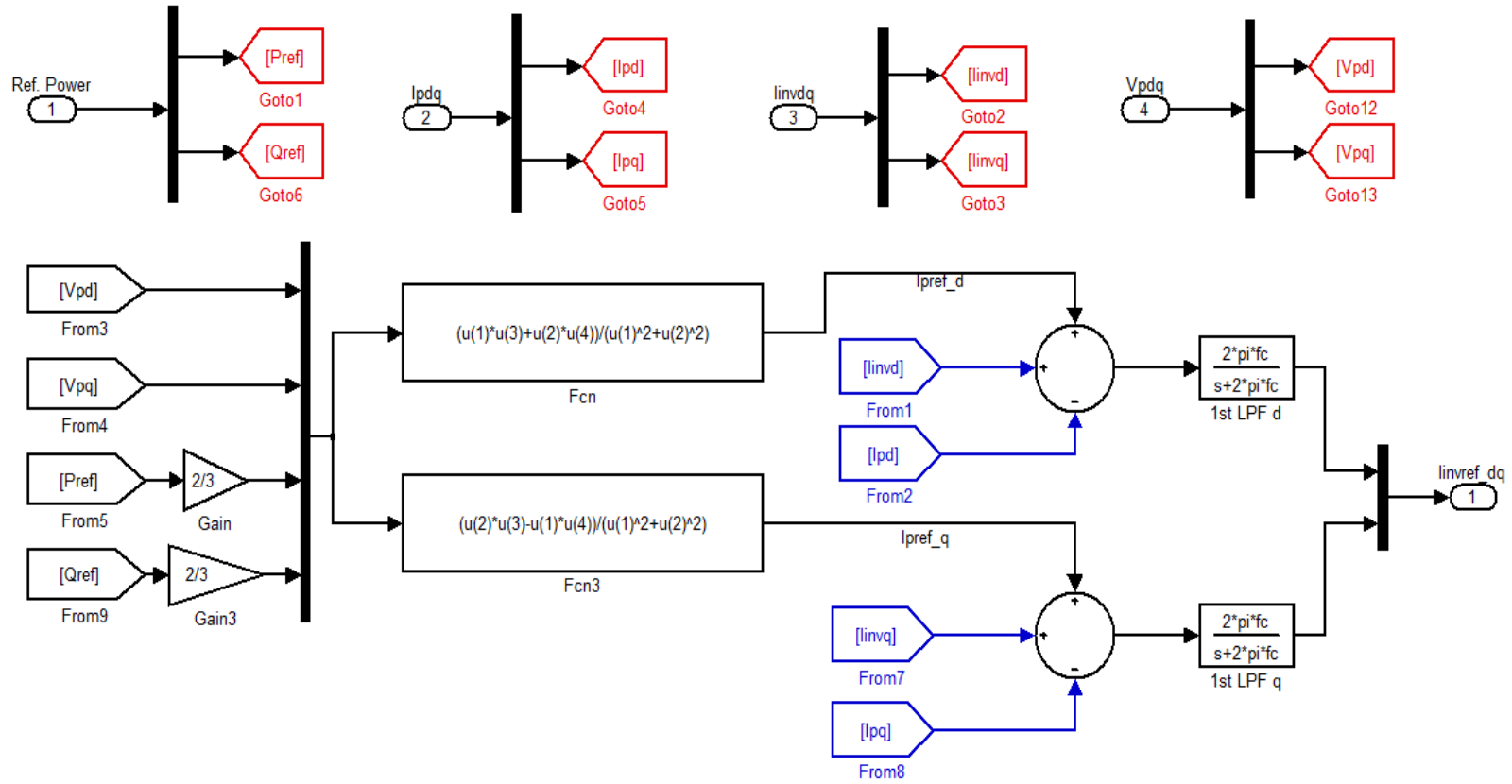
Figure B.4 Inside the Power controller block
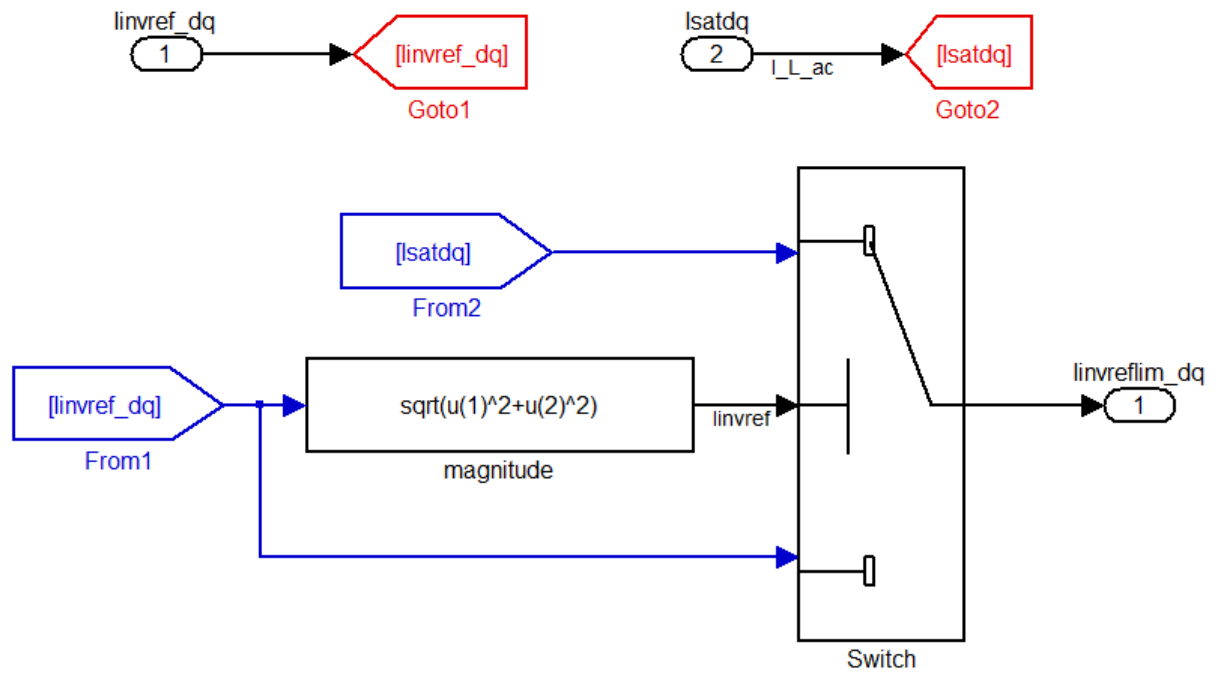
Figure B.5 Inside the Current limiter block
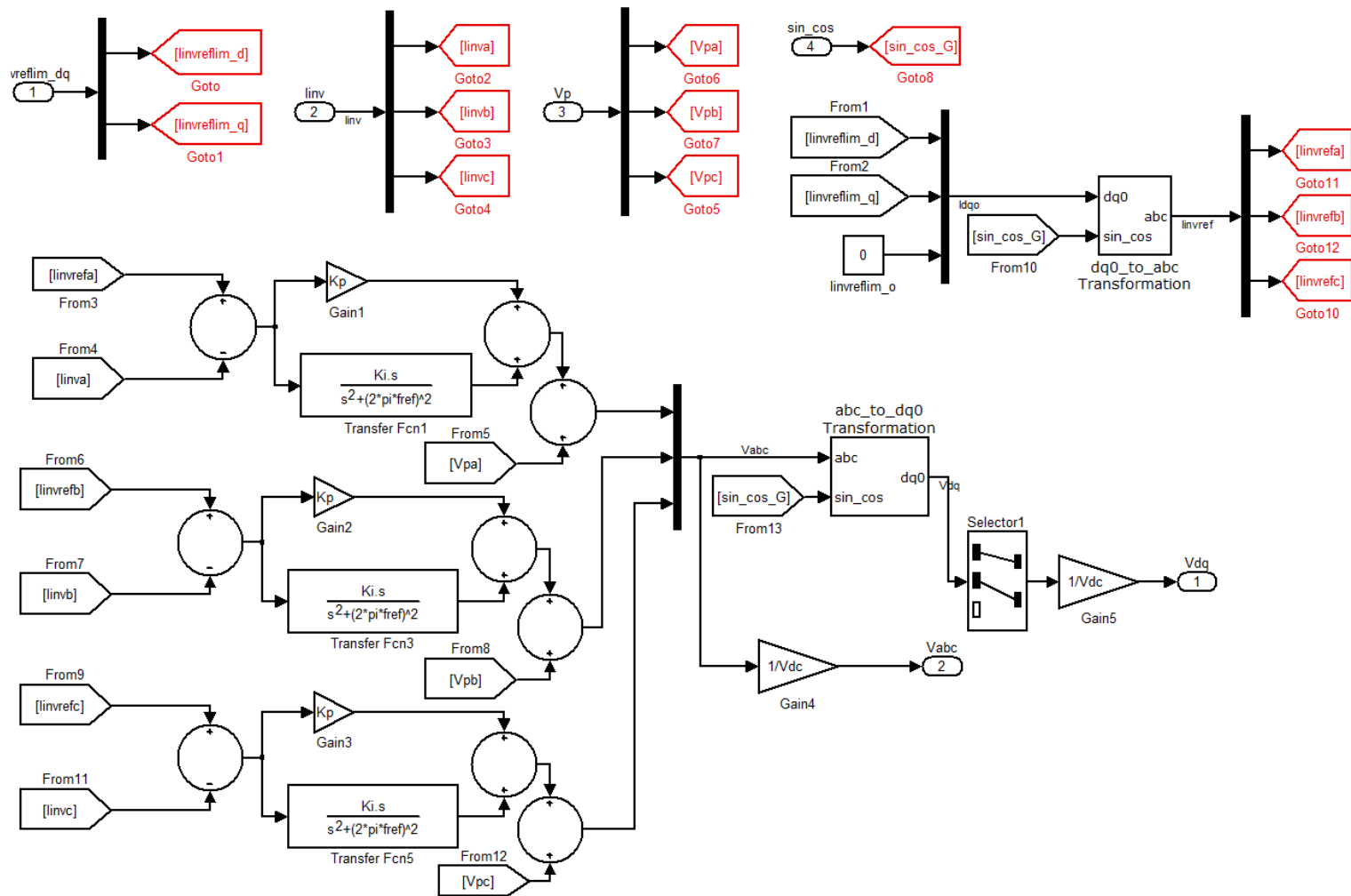
Figure B.6 Inside the Current controller block
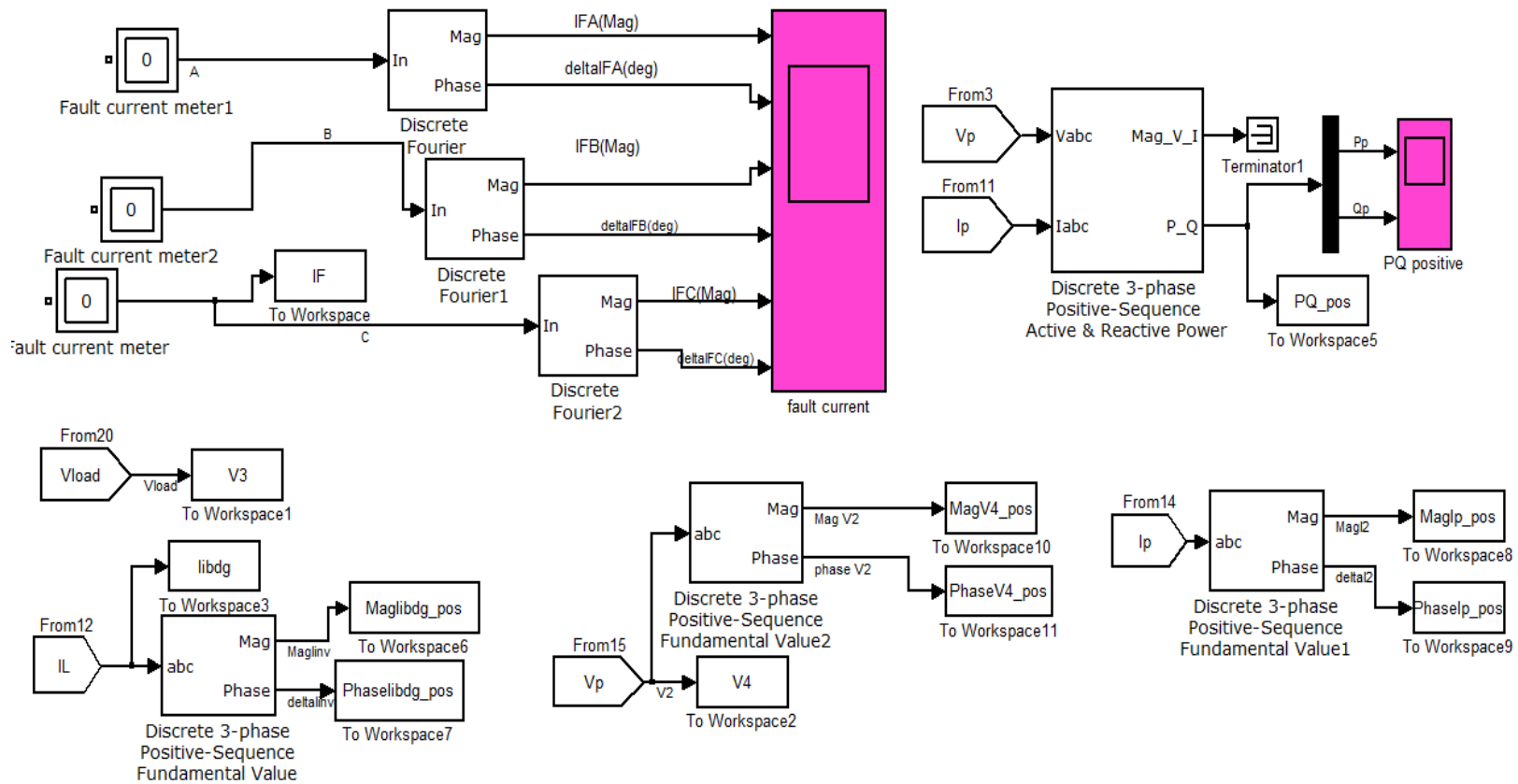
Figure B.7 Measurement and Export block

APPENDIX C
IEEE 34 NODE TEST FEEDER DATA

C.1 Practical Simplification for Fault Calculation

The IEEE 34 node test feeder is simplified with the following assumptions:

1. Neglect the two voltage regulator for load flow and fault calculation.
2. All 1 phase laterals are replaced by the three phase laterals with the same lengths and the configuration code is 301.
3. The three phase sections are assumed to be transposed by taking the self and mutual impedances respectively.
4. The unbalanced phase loads in each three phase sections are summed up and taken as three phase balanced loads. The loads on laterals are replaced by the spot three phase load at the end of the lateral with the same power in total.

C.1.1 The First Two Assumptions

The simplified feeder is presented on one phase basis as in Figure C.1. All the nodes are renumbered from 1 to 34.
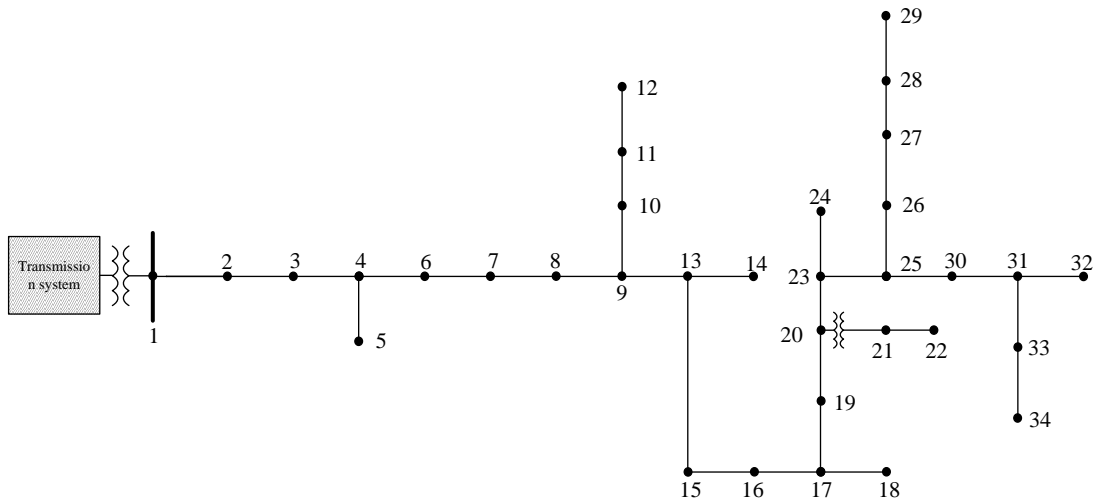
Figure C. 1 The simplified IEEE 34 Node Test Feeder

C.1.2 The Third Assumption

The third assumption is to calculate sequence impedance of three phase lines [59]. The symmetrical component transformation matrix A_s can be used to convert the phase impedance matrix Z_{abc} into the symmetrical component impedance matrix Z_{012} as (C.1)

$$Z_{abc} = \begin{bmatrix} Z_{aa} & Z_{ab} & Z_{ac} \\ Z_{ba} & Z_{bb} & Z_{bc} \\ Z_{ca} & Z_{cb} & Z_{cc} \end{bmatrix} \quad A_s = \begin{bmatrix} 1 & 1 & 1 \\ 1 & a^2 & a \\ 1 & a & a^2 \end{bmatrix} \quad A_s^{-1} = \frac{1}{3}\begin{bmatrix} 1 & 1 & 1 \\ 1 & a & a^2 \\ 1 & a^2 & a \end{bmatrix}$$

$$a = e^{-j2\pi/3}$$

$$Z_{012} = A_s^{-1} * Z_{abc} * A_s = \begin{bmatrix} Z_{00} & Z_{01} & Z_{02} \\ Z_{10} & Z_{11} & Z_{12} \\ Z_{20} & Z_{21} & Z_{22} \end{bmatrix} \tag{C.1}$$

The diagonal terms of Z_{012} are the sequence impedances of the line such that $Z_{00} =$ zero sequence impedance, $Z_{11} =$ positive sequence impedance, and $Z_{22} =$ negative sequence impedance.

The off-diagonal terms represent the mutual coupling between sequences. Because all lines are assumed to be transposed, the phase impedance matrix Z_{abc} is modified with the following notes:

  - The three diagonal terms are identical.
  - The mutual couplings between phases (off-diagonal terms of Z_{abc}) are identical. Consequently, the off-diagonal terms of the sequence impedance matrix Z_{012} become zero from (C.1).

The usual procedure is to set the three diagonal terms of Z_{abc} equal to the average of the diagonal terms of the original phase impedance matrix. A similar way is applied to determine the off-diagonal terms. Thus, the self and mutual impedances, Z_s and Z_m, are defined as (C.2)

$$Z_s = \frac{1}{3}\left(Z_{aa} + Z_{bb} + Z_{cc}\right) \qquad Z_m = \frac{1}{3}\left(Z_{ab} + Z_{bc} + Z_{ca}\right) \tag{C.2}$$

The phase impedance matrix is now defined as (C.3).

$$Z_{abc} = \begin{bmatrix} Z_s & Z_m & Z_m \\ Z_m & Z_s & Z_m \\ Z_m & Z_m & Z_s \end{bmatrix} \tag{C.3}$$

Then the sequence impedances can be determined directly from (C.3) as shown in (C.4).

$$Z_{00} = Z_s + 2Z_m \qquad Z_{11} = Z_{22} = Z_s - Z_m \tag{C.4}$$

All the off-diagonal terms are zero.

Configuration code 300 has the original parameters as shown in Table C.1.

Table C.1 Line configuration Code 300 – Z & B matrices before changes

Z (R +jX) in ohms per mile							B in micro Siemens per mile	
1.3368	1.3343	0.2101	0.5779	0.2130	0.5015	5.3350	- 1.5313	- 0.9943
		1.3238	1.3569	0.2066	0.4591		5.0979	- 0.6212
				1.3294	1.3471			4.8880

The self impedance is computed by averaging three diagonal terms in Z matrix:

$$z_s = \frac{1}{3}\left(Z_{aa} + Z_{bb} + Z_{cc}\right) = \frac{1}{3}\left(1.3368 + j1.3343 + 1.3238 + j1.3569 + 1.3294 + j1.3471\right)$$
$$= 1.33 + j1.3461$$

The mutual impedance is computed by averaging three off-diagonal terms in Z matrix:

$$z_m = \frac{1}{3}\left(Z_{ab} + Z_{bc} + Z_{ca}\right) = \frac{1}{3}(0.2101 + j0.5779 + 0.2130 + j0.5015 + 0.2066 + j0.4591)$$
$$= 0.2099 + j0.51283$$

Thus, the sequence impedances are:

$$z_0 = z_s + 2z_m = 1.7498 + j2.3718$$
$$z_1 = z_2 = z_s - z_m = 1.1201 + j0.83327$$

Ω/mile

Configuration code 301 has the original parameters as shown in Table C.2.

Table C.2 Line configuration Code 301 – Z & B matrices before changes

Z (R +jX) in ohms per mile							B in micro Siemens per mile	
1.9300	1.4115	0.2327	0.6442	0.2359	0.5691	5.1207	- 1.4364	- 0.9402
		1.9157	1.4281	0.2288	0.5238		4.9055	- 0.5951
				1.9219	1.4209			4.7154

The corresponding sequence impedances are:

$$z_0 = 2.3875+j2.5782$$
$$z_1 = z_2 = 1.6901+j0.8411$$

Ω/mile

Thus, sequence impedances of all lines in the system can be determined and shown in Table C.3.

Table C.3 Line sequence impedances in Ohm

Line Segment Data					Sequence components (Ω)					
			Config.	Simp.	Z_0		Z_1		Z_2	
Node A	Node B	Length(ft.)	code	Config.	R_0	X_0	R_1	X_1	R_2	X_2
800	802	2580	300	300	0.8550	1.1589	0.5473	0.4072	0.5473	0.4072
802	806	1730	300	300	0.5733	0.7771	0.3670	0.2730	0.3670	0.2730
806	808	32230	300	300	10.6811	14.4779	6.8373	5.0864	6.8373	5.0864
808	810	5804	303	301	2.6244	2.8341	1.8578	0.9246	1.8578	0.9246
808	812	37500	300	300	12.4276	16.8452	7.9553	5.9181	7.9553	5.9181
812	814	29730	300	300	9.8526	13.3549	6.3069	4.6919	6.3069	4.6919
814	850	10	301	301	0.0045	0.0049	0.0032	0.0016	0.0032	0.0016
816	818	1710	302	301	0.7732	0.8350	0.5474	0.2724	0.5474	0.2724
816	824	10210	301	301	4.6167	4.9855	3.2682	1.6264	3.2682	1.6264
818	820	48150	302	301	21.7724	23.5114	15.4126	7.6703	15.4126	7.6703
820	822	13740	302	301	6.2129	6.7092	4.3981	2.1888	4.3981	2.1888
824	826	3030	303	301	1.3701	1.4795	0.9699	0.4827	0.9699	0.4827
824	828	840	301	301	0.3798	0.4102	0.2689	0.1338	0.2689	0.1338
828	830	20440	301	301	9.2425	9.9808	6.5427	3.2561	6.5427	3.2561
830	854	520	301	301	0.2351	0.2539	0.1664	0.0828	0.1664	0.0828
832	858	4900	301	301	2.2157	2.3926	1.5685	0.7806	1.5685	0.7806
832	888	0	XFM-1	XFM-1	0.0000	0.0000	0.0000	0.0000	0.0000	0.0000
834	860	2020	301	301	0.9134	0.9864	0.6466	0.3218	0.6466	0.3218
834	842	280	301	301	0.1266	0.1367	0.0896	0.0446	0.0896	0.0446

	Line Segment Data				Sequence components (Ω)					
					Z_0		Z_1		Z_2	
Node A	Node B	Length(ft.)	Config. code	Simp. Config.	R_0	X_0	R_1	R_0	X_0	R_1
836	840	860	301	301	0.3889	0.4199	0.2753	0.1370	0.2753	0.1370
836	862	280	301	301	0.1266	0.1367	0.0896	0.0446	0.0896	0.0446
842	844	1350	301	301	0.6104	0.6592	0.4321	0.2151	0.4321	0.2151
844	846	3640	301	301	1.6459	1.7774	1.1651	0.5798	1.1651	0.5798
846	848	530	301	301	0.2397	0.2588	0.1697	0.0844	0.1697	0.0844
850	816	310	301	301	0.1402	0.1514	0.0992	0.0494	0.0992	0.0494
852	832	10	301	301	0.0045	0.0049	0.0032	0.0016	0.0032	0.0016
854	856	23330	303	301	10.5493	11.3919	7.4678	3.7165	7.4678	3.7165
854	852	36830	301	301	16.6537	17.9839	11.7891	5.8670	11.7891	5.8670
858	864	1620	302	301	0.7325	0.7910	0.5186	0.2581	0.5186	0.2581
858	834	5830	301	301	2.6362	2.8468	1.8662	0.9287	1.8662	0.9287
860	836	2680	301	301	1.2118	1.3086	0.8579	0.4269	0.8579	0.4269
862	838	4860	304	301	2.1976	2.3731	1.5557	0.7742	1.5557	0.7742
888	890	10560	300	300	3.4996	4.7436	2.2402	1.6665	2.2402	1.6665

The data in medium voltage system are converted into per unit system with the *baseMVA*=2.5 and the *basekV*=24.9. Results are shown in Table C.4 with the renumbered buses.

$$Z_{baseMV1} = \frac{24.9^2}{2.5} = 248 \ \Omega$$

The data of line 888-890 (Line 21-22 in the renumbered bus system) are converted into the per unit system with the baseMVA=2.5, *basekV*=4.16.

$$Z_{baseMV2} = \frac{4.16^2}{2.5} = 6.9222 \ \Omega$$

Table C.4 Line sequence impedances in per unit

Line Segment		Sequence components (Conf. 300, 301), pu. $Z_{baseMV1} = 248.004\ \Omega$					
Node A	Node B	R_0	X_0	R_1	X_1	R_2	X_2
1	2	0.003448	0.004673	0.002207	0.001642	0.002207	0.001642
2	3	0.002312	0.003134	0.00148	0.001101	0.00148	0.001101
3	4	0.043068	0.058378	0.027569	0.020509	0.027569	0.020509
4	5	0.010582	0.011428	0.007491	0.003728	0.007491	0.003728
4	6	0.05011	0.067923	0.032077	0.023863	0.032077	0.023863
6	7	0.039727	0.053849	0.025431	0.018919	0.025431	0.018919
7	8	1.82E-05	1.97E-05	1.29E-05	6.42E-06	1.29E-05	6.42E-06
9	10	0.003118	0.003367	0.002207	0.001098	0.002207	0.001098
9	13	0.018616	0.020102	0.013178	0.006558	0.013178	0.006558
10	11	0.08779	0.094803	0.062146	0.030928	0.062146	0.030928
11	12	0.025052	0.027053	0.017734	0.008826	0.017734	0.008826
13	14	0.005525	0.005966	0.003911	0.001946	0.003911	0.001946
13	15	0.001532	0.001654	0.001084	0.00054	0.001084	0.00054
15	16	0.037268	0.040244	0.026382	0.013129	0.026382	0.013129
16	17	0.000948	0.001024	0.000671	0.000334	0.000671	0.000334
20	23	0.008934	0.009648	0.006324	0.003147	0.006324	0.003147
20	21	0	0	0	0	0	0
25	30	0.003683	0.003977	0.002607	0.001297	0.002607	0.001297
25	26	0.000511	0.000551	0.000361	0.00018	0.000361	0.00018
31	32	0.001568	0.001693	0.00111	0.000552	0.00111	0.000552
31	33	0.000511	0.000551	0.000361	0.00018	0.000361	0.00018

Line Segment		Sequence components (Conf. 300, 301), pu. $Z_{baseMV1} = 248.004\ \Omega$					
Node A	Node B	Node A	Node B	Node A	Node B	Node A	Node B
26	27	0.002461	0.002658	0.001742	0.000867	0.001742	0.000867
27	28	0.006637	0.007167	0.004698	0.002338	0.004698	0.002338
28	29	0.000966	0.001044	0.000684	0.00034	0.000684	0.00034
8	9	0.000565	0.00061	0.0004	0.000199	0.0004	0.000199
19	20	1.82E-05	1.97E-05	1.29E-05	6.42E-06	1.29E-05	6.42E-06
17	18	0.042537	0.045934	0.030112	0.014985	0.030112	0.014985
17	19	0.067151	0.072515	0.047536	0.023657	0.047536	0.023657
23	24	0.002954	0.00319	0.002091	0.001041	0.002091	0.001041
23	25	0.01063	0.011479	0.007525	0.003745	0.007525	0.003745
30	31	0.004886	0.005277	0.003459	0.001721	0.003459	0.001721
33	34	0.008861	0.009569	0.006273	0.003122	0.006273	0.003122
21	22	0.505562	0.685273	0.323625	0.240747	0.323625	0.240747

C.1.3 The Fourth Assumption for Distributed Loads

The load data of the original test feeder includes uniformly distributed loads in some phases. Simplifying such loads to "spot" loads can be performed by assuming that the main feeder of the distribution system is balanced and fully transposed in three phases with distributed, single/two phase loads being lumped at the end of each section. Thus all loads are replaced by their equivalent balanced three phase loads as in Table C.5.

Table C.5 Lumped model of loads

		Spot Loads							Lumped Model (balanced three phase)		
Node	Load Model	Ph-1 kW	Ph-1 kVAr	Ph-2 kW	Ph-2 kVAr	Ph-3 kW	Ph-3 kVAr	Node	New node	kW	kVAr
860	Y-PQ	20	16	20	16	20	16	860	**30**	60	48
840	Y-I	9	7	9	7	9	7	840	**32**	27	21
844	Y-Z	135	105	135	105	135	105	844	**27**	405	315
848	D-PQ	20	16	20	16	20	16	848	**28**	60	48
890	D-I	150	75	150	75	150	75	890	**22**	450	225
830	D-Z	10	5	10	5	25	10	830	**16**	45	20
Total		**344**	**224**	**344**	**224**	**359**	**229**	**Total**		**1047**	**677**

		Distributed Loads							Lumped model (3 phase)		
Node A	Node B	Load Model	Ph-1 kW	Ph-1 kVAr	Ph-2 kW	Ph-2 kVAr	Ph-3 kW	Ph-3 kVAr	End Node	New node	Lumped kW	Load kVAr
802	806	Y-PQ	0	0	30	15	25	14	806	**3**	55	29
808	810	Y-I	0	0	16	8	0	0	810	**5**	16	8
818	820	Y-Z	34	17	0	0	0	0	820	**11**	34	17
820	822	Y-PQ	135	70	0	0	0	0	822	**12**	135	70
816	824	D-I	0	0	5	2	0	0	824	**13**	5	2
824	826	Y-I	0	0	40	20	0	0	826	**14**	40	20
824	828	Y-PQ	0	0	0	0	4	2	828	**15**	4	2
828	830	Y-PQ	7	3	0	0	0	0	830	**16**	7	3
854	856	Y-PQ	0	0	4	2	0	0	856	**18**	4	2
832	858	D-Z	7	3	2	1	6	3	858	**23**	15	7
858	864	Y-PQ	2	1	0	0	0	0	864	**24**	2	1
858	834	D-PQ	4	2	15	8	13	7	834	**25**	32	17

	Distributed Loads								Lumped model (3 phase)			
Node	Node	Node	Node	Node	Node	Node	Node	Node	Node	Node	Node	Node
A	B	A	B	A	B	A	B	A	B	A	B	A
834	860	D-Z	16	8	20	10	110	55	860	**30**	146	73
860	836	D-PQ	30	15	10	6	42	22	836	**31**	82	43
836	840	D-I	18	9	22	11	0	0	840	**32**	40	20
862	838	Y-PQ	0	0	28	14	0	0	838	**34**	28	14
842	844	Y-PQ	9	5	0	0	0	0	844	**27**	9	5
844	846	Y-PQ	0	0	25	12	20	11	846	**28**	45	23
846	848	Y-PQ	0	0	23	11	0	0	848	**29**	23	11
Total			**262**	**133**	**240**	**120**	**220**	**114**	**Total**		**722**	**367**

Load data in simplified system are summarized in Table C.6.

Table C.6 Load data in IEEE 34 Node Test Feeder

Node	kW	kVAr
3	55	29
5	16	8
11	34	17
12	135	70
13	5	2
14	40	20
15	4	2
16	7+45=52	3+20=23
18	4	2
23	15	7
24	2	1

Node	kW	kVAr
25	32	17
30	146+60=206	73+48=121
31	82	43
32	40+27=67	20+21=41
34	28	14
27	9+405=414	5+315=320
28	45+60=105	23+48=71
29	23	11
22	450	225
Total	**1769**	**1044**

The symmetrical components of equivalent load impedances are determined by using the symmetrical component transformation matrix. In case of balanced load:

$$Z_m = 0 \rightarrow Z_0 = Z_1 = Z_2 = Z_{load}$$

where Z_{load} can be obtained by converting the constant power into constant impedance at the nominal voltage.

C.2 Other Data for Fault Analysis

C.2.1 Shunt Capacitors

Node	Ph-A kVAr	Ph-B kVAr	Ph-C kVAr	New node	Total kVAr	S=P+jQ kVA
844	100	100	100	27	300	-j300
848	150	150	150	29	450	-j450
Total	**250**	**250**	**250**		**750**	**-j750**

The impedance of capacitors:

$$Z_C^{844} = \frac{\sqrt{3}V^2}{\hat{S}} = \frac{24.9^2\,kV}{j300kVA} = -j2066.7\ \Omega \rightarrow Z_C^{844} = \frac{-j2066.7}{248} = -j8.333\ pu$$

$$Z_C^{848} = \frac{\sqrt{3}V^2}{\hat{S}} = \frac{24.9^2\,kV}{j450kVA} = -j2386.4\ \Omega \rightarrow Z_C^{848} = \frac{-j2386.4}{248} = -j5.555\ pu$$

However, in load flow program (such as MATPOWER), a capacitor is modeled as a shunt element whose admittance at bus *i* is given as:

$$y_{sh}^i = g_{sh}^i + jb_{sh}^i$$

g_{sh} is in MW (consumed) and b_{sh} is in MVAr (injected) at a nominal voltage magnitude of 1.0 p.u and angle of zero. Thus, the first capacitor is modeled at bus 27 with *Bs*=0.3 (MVAr). The second capacitor is modeled at bus 29 with *Bs*=0.45 (MVAr).

C.2.2 System Source

C.2.2.1 Transmission system

The three-phase short circuit MVA on the 69 kV bus of the substation is 1000 MVA at an angle of 85 degrees. The positive and negative sequence impedance of the source:

$$Z_{S1} = Z_{S2} = \left.\left(\frac{V^2}{\hat{S}_{sc}}\right)\middle/\frac{V^2}{\hat{S}_{base}}\right. = \frac{2.5MVA}{1000\left(\cos 85^0 - i\sin 85^0\right)MVA} = 0.0002 + 0.0025i\ \ p.u.$$

Due to the delta winding, the system zero sequence impedance is not seen from the low side transformer terminal.

C.2.2.2 Synchronous machine based distributed generator

Power factor = 0.9 = constant

P = 0 ÷ 10 MW

V = 480 V $\qquad\qquad$ X$_d$´ = 0.2 pu $\qquad\qquad\qquad$ X$_0$ = 0.05 pu

Convert to new system base: *baseMVA*=2.5, *basekV*=24.9

$$X_d' = 0.2\,pu \times \left(\frac{V_{baseDG}}{V_{basesystem}}\right)^2 \times \frac{S_{basesystem}^*}{S_{baseDG}^*} = \frac{0.0001858}{S_{DG}^*}$$

$$X_0 = 0.05\,pu \times \left(\frac{V_{baseDG}}{V_{basesystem}}\right)^2 \times \frac{S_{basesystem}^*}{S_{baseDG}^*} = \frac{4.6451\text{e-}005}{S_{DG}^*}$$

C.2.2.3 Transformer

Substation transformer

The positive, negative and zero-sequence impedance of the substation transformer (69 kV base, 2.5 MVA base):

$$Z_1 = Z_2 = Z_0 = 0.01 + j0.08 \text{ p.u}$$

DG transformer

The rating of DG transformer is determined in depending on DG rating with the step of 0.25 MVA

The positive, negative and zero-sequence impedances of DG transformer are assumed to be (1.5% + 1i*8%). They must be converted into system base.

XFM-1 transformer

The positive, negative and zero-sequence impedance of the substation transformer:

$$Z_1 = Z_2 = Z_0 = (0.019 + j0.0408) \times \left(\frac{24.9}{24.9}\right)^2 \times \left(\frac{2.5}{0.5}\right) = 0.0950 + j0.2040$$

BIOGRAPHY

Dao Van Tu was born in Vietnam, on December 12, 1984. He studied electrical engineering and received his Engineer and Master degrees at Hanoi University of Science and Technology, Vietnam, in 2007 and 2009, respectively.

In 2010, Dao Van Tu received a scholarship from ASEAN University Network / Southeast Asia Engineering Education Development Network (AUN/SEED-Net) Program of Japan International Cooperation Agency (JICA) to study in Chulalongkorn University, Thailand for a Ph.D. degree in Electrical Engineering. He had 8 months training in The University of Tokyo, Japan in the same field from August 2012 to March 2013. He received his PhD degree in 2013 at Chulalongkorn University, Thailand.